Verisk Crop Hail Model for the United States

Publication Date: June 2022

Revision History

Date	Description
June, 2022	Original document release.

Table of Contents

List of Figures

List of Tables

1 Facts at a Glance

1.1 Verisk Crop Hail Model for the United States: Model Abstract

The Verisk Crop Hail Model for the United States has been developed to meet the hail risk management needs of the agriculture insurance industry. It supports standard crop hail and production plan hail policies and is based on a variety of policies as summarized by the National Crop Insurance Services (NCIS).

The Verisk Crop Hail Model for the United States explicitly models the effects of hail in the contiguous United States excluding the six New England states (Connecticut, Maine, Massachusetts, New Hampshire, Rhode Island and Vermont) for eight crops: barley, corn, cotton, rice and soybeans, and durum, spring and winter wheat. Hail damage to additional crops is estimated statistically based on how damage to non-modeled crops is related to damage to the explicitly modeled crops. The model uses the simulated hail events and straight-line winds[1] from the 10,000-year all-events stochastic hazard catalog of the Verisk Severe Thunderstorm Model for the United States. Hail events are simulated from atmospheric reanalysis data and a suite of hail report data. Crop damage is calculated as a function of hail impact energy – a measure of the total kinetic energy (horizontal and vertical) of hail – and unique damage functions for each crop type and crop developmental stage. To account for green snap and wind endorsements, in a subset of states loss associated with wind-induced crop damage is calculated and included in the model based on the frequency of severe wind events. This model applies policy condition distributions for each state to calculate losses to both the crop hail and production plan lines of business.[2]

For each simulated event, the model uses Verisk's all-events 10,000-year stochastic catalog to determine

- location
- track direction
- length
- width
- maximum simulated hail diameter
- hail impact energy (representing local intensity, derived from the maximum hail diameter)
- storm date

Damage to crops in a given location is calculated using the above parameters on an 8-km resolution exposure grid.

---

[1] The wind module processes the straight-line wind hazard data for the following states: Arkansas, Iowa, Illinois, Indiana, Kansas, Kentucky, Louisiana, Minnesota, Missouri, North Dakota, Nebraska, South Dakota

[2] Production plan policies are available in Colorado, Iowa, Idaho, Illinois, Indiana, Kansas, Minnesota, Missouri, North Dakota, Nebraska, Ohio, South Dakota, Texas and Wisconsin.

All model components, as well as overall model performance, have been validated using published research on hail damage to crops and resultant financial losses.

1.2 Model Facts

Model Name	Verisk Crop Hail Model for the United States
Release Date	June 2022
Software System	Touchstone Re 2022 (10.0)
Model Domain	42 states (the contiguous United States excluding the six New England states: Connecticut, Maine, Massachusetts, New Hampshire, Rhode Island, and Vermont).
Modeled Perils	Hail for the entire model domain; straight-line winds for the following states: Arkansas, Iowa, Illinois, Indiana, Kansas, Kentucky, Louisiana, Minnesota, Missouri, North Dakota, Nebraska, South Dakota
Intensity Parameters	• Hail – Hail impact energy (J/m^2) • Convective straight-line winds – Average maximum wind speed (3-sec gust; mph)

1.3 United States Country Facts

The following table provides population and gross domestic product (GDP) statistics for the United States of America.[3]

Population	337.3 million (2022 estimate)
GDP	19.85 trillion USD (2020 estimate)
Per capita GDP	60,200 USD (2020 estimate)

The population density map shown in Figure 1 below shows the location of population centers across the United States.

[3] Data from the CIA World Factbook

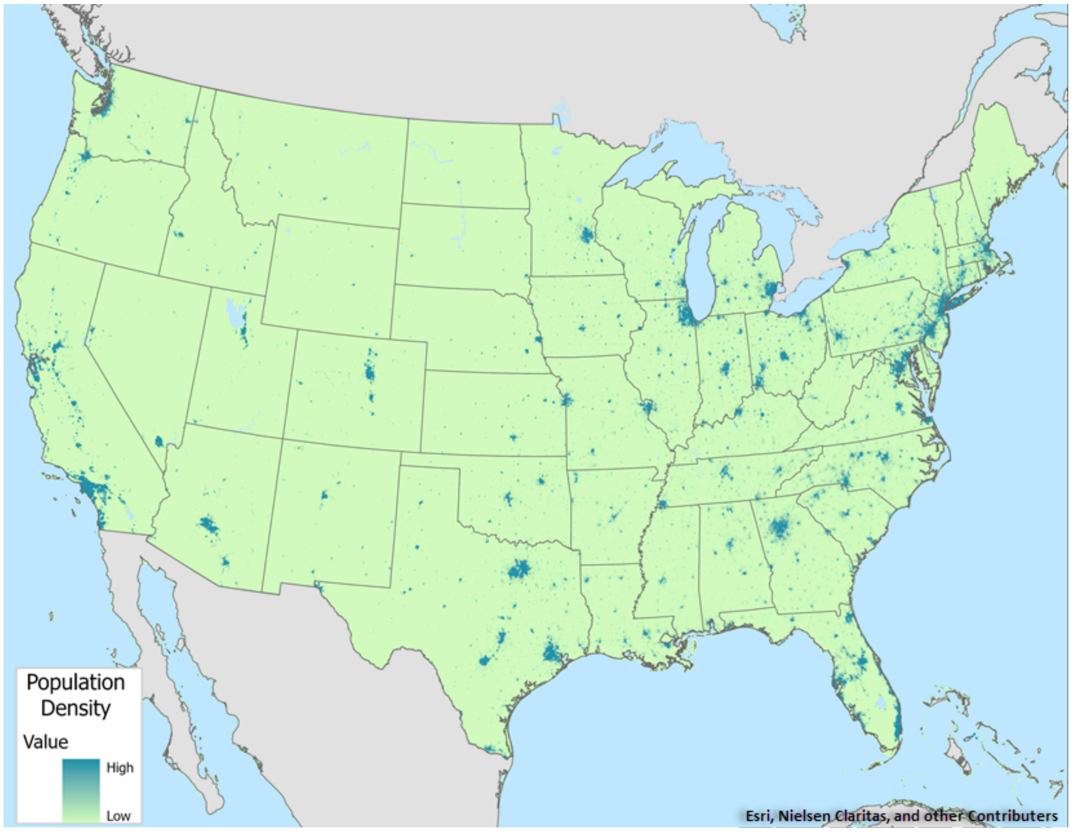

Figure 1. Population density in the continental United States

1.4 United States - Agriculture Facts

Facts at a Glance

Farmland and Farms (2021 Est.)

Statistics for Farms and Farmland were obtained from the United States Department of Agriculture (February 2022) *Farms and Land in Farms 2021 Summary*[4]

Farms	2,012,050 (down 6,950 farms from 2020)
Total farmland	895,300,000 acres (down 1,300,000 acres from 2020)
Average area per farm	445 acres (up 1 acre from 2020)

4 National Agriculture Statistics Service, USDA (February 2022). Farms and Land in Farms 2021 Summary https://www.nass.usda.gov/Statistics_by_Subject/Demographics/index.php

Crop value indicators

	2017	2018	2019	2020	2021 (Forecast)
All commodity cash receipts: crop, animals & products (USD billion) [5]	370.4	371.2	367	363.8	432.6
Crops (USD billion)[6]	194.9	194.9	191.6	198.8	236.6
Livestock (USD billion)[7]	175.6	176.3	175.4	165.0	195.9
Direct government payments (USD billion)[8]	11.5	13.7	22.4	45.7	27.1
Gross cash income (USD billion)[9]	413.1	414.0	424.2	443.8	492.4
Net cash income (USD billion)[10]	101.3	102.6	106.9	117.2	134.2
Net value added by agricultural sector (USD billion)[11]	141.7	145.3	145	163.1	190.2
Farm equity (USD billion)[12]	2,615.5	2,624.7	2,655.5	2,733.4	2,816.0
Farm debt-asset ratio[13]	13.0	13.3	13.6	13.9	13.9
Farm sector assets (USD billion)[14]	3,006.0	3,026.7	3,075.2	3,174.6	3,270.3
Average farm household income from farming (USD)[15]	N/A	18,425	21,730	25,603	29,981
Average farm household income (USD) [16]	N/A	112,210	123,368	122,291	131,030
Cropland harvested (million acres)[17]	319	317	303	309	N/A

5 USDA Economic Research Service- Farm Income and Wealth Statistics: Net Cash Income https://data.ers.usda.gov/reports.aspx?ID=17831
6 Ibid
7 Ibid
8 Ibid
9 Ibid
10 Ibid
11 USDA Economic Research Service- Value Added https://data.ers.usda.gov/reports.aspx?ID=17830
12 USDA Economic Research Service- Farm Income and Wealth Statistics Balance Sheet https://data.ers.usda.gov/reports.aspx?ID=17835
13 Ibid
14 Ibid
15 USDA, ERS, Farm Household Income and Characteristics, https://www.ers.usda.gov/data-products/farm-household-income-and-characteristics/
16 Ibid
17 USDA Economic Research Service- Major Land Uses, Summary Table 3: Cropland used for crops: cropland harvested (including double-cropped), crop failure, and cultivated summer fallow for the United States, annual, 1910-2020 https://www.ers.usda.gov/data-products/major-land-uses/major-land-uses/#Cropland

1.5 Data Sources for the Verisk Crop Hail Model for the United States

The Verisk Crop Hail Model for the United States uses wind and hail in Verisk's all-events 10,000-year stochastic hazard catalog. Data sources used to generate the events in this catalog include but are not limited to: the National Oceanic and Atmospheric Administration's (NOAA)'s Storm Prediction Center (SPC), Climate Forecast System Reanalysis (CFSR), and Next Generation Radar (NEXRAD) level III dataset.

See Also

Data Sources for Event Generation
Verisk Industry Exposure Database
Historical Trends

1.6 Industry Exposure Database

Industry Exposure Database
• Crop Data Layers – 2017-2020 • Premium Rates – 2020 • Policy Conditions – 2020 • Resolution – County, State (the underlying industry exposure database resolution is 8 km)

See Also

Verisk Industry Exposure Database

1.7 Stochastic Hazard Catalog

The Verisk Crop Hail Model for the United States uses the 10,000-year all-events stochastic hazard catalog of the Verisk Severe Thunderstorm Model for the United States. The catalog has 77,005,148 simulated hail microevents and 47,423,952 straight-line wind microevents; the peril-specific microevents leveraged by the Verisk Crop Hail Model for the United States are specific to the model domain.[18]

In the catalog, events are categorized as *microevents* or *macroevents*. A microevent is a single simulated convective straight-line wind or hail event (a single "swath" or "footprint") and is modeled as a discrete ellipse object with no artificial grid. A macroevent represents a large-scale atmospheric system that causes outbreaks of severe weather. The Verisk Crop Hail Model for the United States uses the hail and straight-line wind *microevents* from the 10,000-year all-events stochastic hazard catalog.

[18] The wind module processes the straight-line wind hazard data for the following states only: Arkansas, Iowa, Illinois, Indiana, Kansas, Kentucky, Louisiana, Minnesota, Missouri, North Dakota, Nebraska, South Dakota.

Figure 2 and Figure 3 show the monthly relative frequencies of stochastically-generated wind and hail microevents.

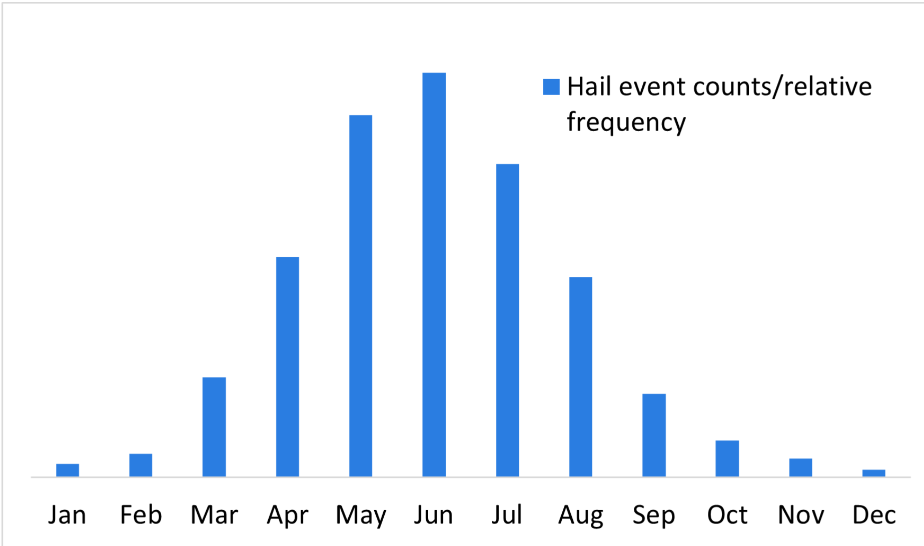

Figure 2. Hail monthly relative frequency

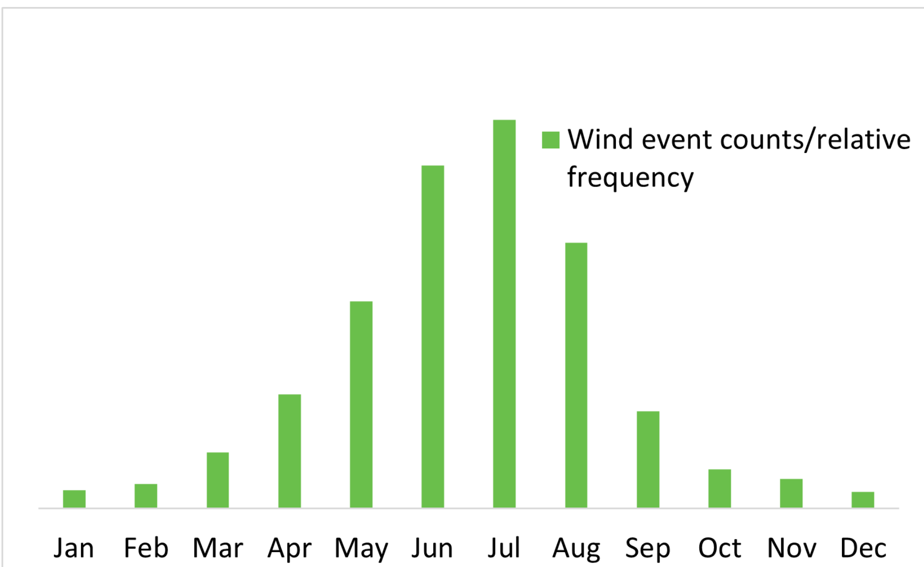

Figure 3. Wind monthly relative frequency

See Also
Event Generation
Available Catalogs in Touchstone Re

1.8 Model Resolution

General

Hail module grid resolution	8 km
Wind module grid resolution	State[19]

Touchstone Re

Industry exposure loss files	County and State
Input	County and State
Output (losses)	County and State

- **Losses throughout a model year are aggregated to a single event per year.**
- **Crop damage and associated losses are calculated at the model grid resolution and then aggregated to the county and state levels in Touchstone Re**

See Also
Crop Hail Loss Calculation
Loss Calculation in the Wind Module
Calculating Crop Areas Damaged by Hail
Verisk Industry Exposure Database

1.9 Covered Crops

The Verisk Crop Hail Model for the United States explicitly models the effects of hail in the contiguous United States excluding the six New England states (Connecticut, Maine, Massachusetts, New Hampshire, Rhode Island and Vermont) for eight crops:

- barley
- corn
- cotton
- rice
- soybeans
- wheat (durum)
- wheat (spring)
- wheat (winter)

Hail damage to additional crops is estimated statistically based on how damage to non-modeled crops is related to damage to the explicitly modeled crops.

[19] The model's wind module includes losses in Arkansas, Iowa, Illinois, Indiana, Kansas, Kentucky, Louisiana, Minnesota, Missouri, North Dakota, Nebraska, South Dakota

See Also
Damage Estimation

1.10 Supported Lines of Business

The Verisk Crop Hail Model for the United States supports two lines of business for reporting modeled losses: crop hail and, for the subset of states listed below, production plan. These lines of business correspond to two distinct groups of insurance policy types.

Crop hail policies issue payments at the time when a loss occurs based on an adjustor's loss estimate following a hail event, regardless of the final production outcome at harvest. In contrast, production plan policies have a yield-based guarantee; payments are therefore issued when the yield at harvest is below that guarantee.

The Verisk Crop Hail Model for the United States supports production plan policies in the following states:

- Colorado
- Iowa
- Idaho
- Illinois
- Indiana
- Kansas
- Minnesota
- Missouri
- North Dakota
- Nebraska
- Ohio
- South Dakota
- Texas
- Wisconsin

See Also
General Structure of Loss Estimation
Supported Lines of Business for Reporting Modeled Losses

1.11 Modeled Industry Losses

Insurable exposure	Total value of production cost and planted area (risk count) that is eligible for insurance.

Insured exposure	Although planted areas may be eligible for insurance, "take-up" (i.e., purchase of insurance coverage for eligible planted areas) varies by crop and region. For example, due to the voluntary nature of crop insurance, take-up rates may be in single-digit percentage values in some locales. In other areas where crop insurance has been well established, take-up rates may be closer to 100%.
Insurable loss	Estimated losses to insurable exposure (as though the take-up rate is 100%).
Insured loss	Estimated losses to insured exposures

See Also

Policy Condition Assumptions

Insurable Occurrence/Aggregate Losses

In the Verisk Crop Hail Model for the United States, the losses for all crops in a given year of the stochastic catalog are aggregated to a single annual event. **Therefore, occurrence losses are equivalent to aggregate losses for this model.**

Table 1 shows the modeled insurable loss estimates for 50%, 10% and 2% exceedance probabilities (2-yr, 10-yr, and 50-yr return periods) for the entire model domain and separately for selected states.

In the Verisk Crop Hail Model for the United States, insurance take-up rate is set at 100%; therefore, only insurable losses are provided, not insured losses.

Table 1. Insurable losses (USD millions)

	Return Period	Crop Hail	Production Plan
42-state Model Domain	2-year (50% EP)	1,125.0	1,735.8
	10-year (10% EP)	1,463.2	2,443.3
	50-year (2% EP)	1,832.2	3,251.1
Colorado	2-year (50% EP)	87.1	47.5
	10-year (10% EP)	137.6	86.4
	50-year (2% EP)	177.4	114.7
Iowa	2-year (50% EP)	68.8	152.8
	10-year (10% EP)	102.7	265.3
	50-year (2% EP)	131.2	537.7
Illinois	2-year (50% EP)	22.0	152.0
	10-year (10% EP)	44.6	293.8
	50-year (2% EP)	63.0	433.5
Kansas	2-year (50% EP)	12.0	129.2
	10-year (10% EP)	35.2	205.7
	50-year (2% EP)	57.8	262.0
Minnesota	2-year (50% EP)	10.7	196.5

	Return Period	Crop Hail	Production Plan
	10-year (10% EP)	28.3	344.0
	50-year (2% EP)	45.1	678.5
Missouri	2-year (50% EP)	14.9	158.4
	10-year (10% EP)	28.6	303.1
	50-year (2% EP)	40.4	411.3
North Dakota	2-year (50% EP)	11.8	126.5
	10-year (10% EP)	19.5	232.8
	50-year (2% EP)	26.7	319.3
Nebraska	2-year (50% EP)	8.5	348.3
	10-year (10% EP)	15.8	536.8
	50-year (2% EP)	22.1	960.5
South Dakota	2-year (50% EP)	0.7	119.8
	10-year (10% EP)	3.9	211.0
	50-year (2% EP)	8.3	425.6
Texas	2-year (50% EP)	0.2	135.9
	10-year (10% EP)	2.5	327.2
	50-year (2% EP)	6.4	491.0

Figure 4 shows the insurable average annual aggregate losses for the 5 states exhibiting the highest losses to crops from hail damage, plus loss for the entire 42-state model domain (USA)

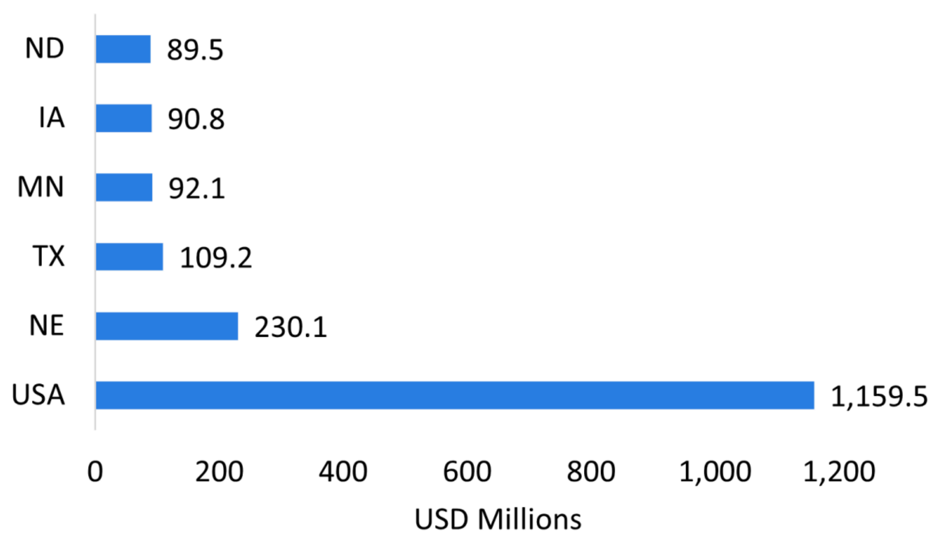

Figure 4. Insurable Aggregate Average Annual Losses for crop hail for the 5 states with the highest AAL losses, and for the model domain

Figure 5 is a map showing the loss cost, by county, for the explicitly modeled crops in the Verisk Crop Hail Model for the United States (loss cost for crops that were modeled statistically are not shown).

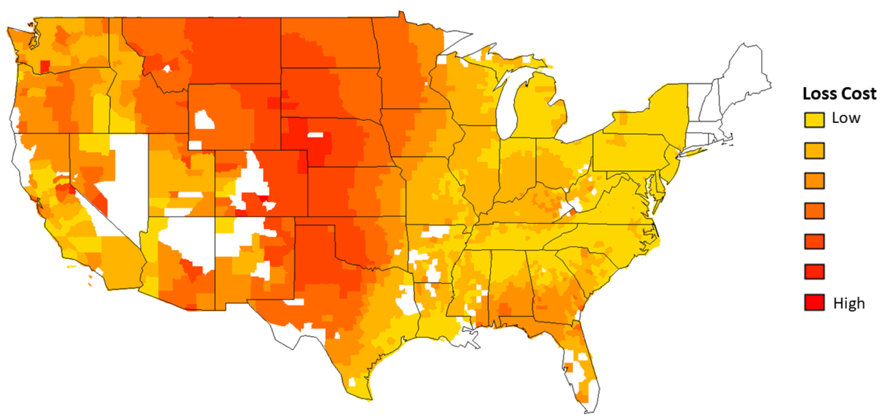

Figure 5. Verisk Crop Hail Model for the United States loss cost map for explicitly modeled crops: barley, corn, cotton, rice and soybeans, and durum, spring and winter wheat

1.12 Navigating the Document

Figure 6 illustrates the components of the Verisk model and how they are related.

Figure 6. Components of the Verisk model

2 Hail and Crop Exposure to Hail in the US

2.1 Hailstorms

A hailstone forms when an existing ice particle collides with supercooled liquid water within a thunderstorm. As the hailstone is repeatedly lifted and dropped by updrafts within the storm clouds, water collects and freezes on the hailstone, and the hailstone grows. When the hailstone becomes too heavy to be suspended aloft by the storm updraft, it will fall to the ground, partially melting as it passes through warmer layers of the atmosphere. Larger hailstones can also form by collisions of two smaller hailstones, which create odd, non-spherical shapes sometimes observed.

Table 2 compares hail size to the size of common objects and demonstrates damage potential at a variety of hail sizes. Note that due to these objects being used for reference, 1.75- and 2.5-inch hail reports are more common than 2-inch reports, a bias that must be accounted for using non-parametric smoothing in the local intensity calculation. Hail measuring at least one inch in diameter is associated with severe thunderstorms.

Table 2. Estimating hailstone size and damage potential

Hailstone Diameter (in)	Object for Comparison	Damage Potential
0.25	Pea	Very Light
0.5	Marble	Light
0.75	Penny	Moderate
0.875	Nickel	Moderate
1.0	Quarter	Moderate (severe thunderstorm definition threshold)
1.5	Ping-Pong Ball	Considerable
1.75	Golf Ball	Considerable
2.5	Tennis Ball	Severe
2.75	Baseball	Severe
3.0	Teacup	Devastating
4.0	Softball	Incredible
4.5	Grapefruit	Incredible

Usually, the largest observed hailstone is recorded from a given thunderstorm, but that alone does not determine hail damage potential. Other factors, such as the size distribution of all hailstones that fall, hailfall duration, and horizontal wind speed, help determine hail damage potential. High winds can increase the kinetic energy of hailstones and blow them at angles significantly off the vertical, thus increasing the likelihood of damage. Larger hailstones generally create more damage than smaller stones because they can fall at higher speeds (up to 100 mph).

The heaviest and largest authenticated hailstone to fall in the U.S. was found in Vivian, South Dakota on July 23, 2010. The stone weighed nearly 2 pounds (1 pound 15 ounces), was 8.0 inches in diameter, and had a circumference of 18.625 inches. The previous record for the heaviest documented hailstone was 1.67 pounds for a stone that fell in Coffeyville, Kansas on September 3, 1970. The previous record for hailstone diameter was 7 inches, which was found in Aurora, Nebraska on June 22, 2003. Note that this Aurora hailstone still holds the record for largest circumference at 18.75 inches.[20]

Thunderstorms that produce hail occur throughout the United States, but severe activity is particularly common in the Great Plains, Midwest, and Southeast. This activity is in part due to the proximity of these regions to the Atlantic Ocean and the Gulf of Mexico. Also, a lack of major east-west mountain ranges allows the cool continental air mass to funnel down the Rocky Mountains and collide with moist air from the Gulf of Mexico, which facilitates severe thunderstorm formation. Florida also has a high rate of severe storms; portions of central and southern Florida experience violent storms almost daily during the summer months.

With an average frequency of about 160 days per year with crop-damaging hail in the U.S., hailstorms pose a significant threat to domestic agricultural products; for comparison, the average annual frequency of hail days that cause property damage in the U.S. is about 120 days per year (Changnon et al, 2009). In the United States, storms producing hail occur most frequently in Colorado, Nebraska, and Wyoming . This "hail alley" region experiences, on average, seven to nine hail days[21] per year.

See Also

SPC Storm Reports

2.2 Effects of Hail on Crops

See Also

Damage Estimation

Variables Affecting Hail Damage

Studies of observed and simulated hail effects on crops reveal several variables that are associated with crop damage from hailstorms.

For many crops, an adequate water supply confers some resistance to hail damage by making crop stems or stalks more elastic and able to deform without breaking. Conversely, after a very heavy hailstorm, crops can become waterlogged after the hailstones melt.

[20] National Oceanic and Atmospheric Administration (NOAA) National Weather Service Aberdeen, SD Weather Forecast Office. *Record Setting Hail Event in Vivian, South Dakota on July 23, 2010.* https://www.weather.gov/abr/vivianhailstone

[21] Since the 1890s, the National Weather Service of the United States has defined "hail days" as those days when hail was observed, regardless of whether damage was inflicted.

This excess water encourages root rot and fungal diseases. However, the most important variables affecting damage to crops due to hail is the kinetic energy of the hail impacting the crop and the crop type and its developmental stage at the time of impact.

Total Kinetic Energy and Hailstone Size

Total kinetic energy is a function of the hailstone diameter and speed; when hailstones are accompanied by high winds the total kinetic energy of the hailstones and the damage they cause increase.[22, 23] However, for each type of crop, there is a threshold hailstone size below which no damage will be inflicted; for most crops this is about ~0.2 inches (and damage to crops is most frequently caused by hail in the range of about ~0.2 inches to ~0.8 inches).[24]

Crop Type

For a given hail kinetic energy, damage depends on the crop type. Small hailstones (~0.25 inches in diameter) can cause serious damage to crops with delicate leaves, such as tea, soybeans, and tobacco. Hailstones of small-to-medium (~0.25 - ~0.75 inches in diameter) size can bruise apples, peaches, and other fruits, greatly decreasing the overall value of the harvest. Medium-sized hailstones (~0.5 inches in diameter) can also bend or break wheat stems or corn stalks, causing serious damage.[25] Corn crops may suffer significant yield losses if the plants experience stalk bruising, as bruised stalks render the corn plants more susceptible to fungal infections and rotting.[26] The following sections describe in more detail how hail can damage the eight explicitly modeled crops.

See Also

[Damage Functions by Crop Type](#)

Effects of Hail on the Explicitly Modeled Crops

The following crop descriptions were prepared using information from the Agricultural Resource Center,[27] the Environmental Protection Agency (EPA) National Agriculture Center[28] and the United States Department of Agriculture.

22 Towery, N. G., G. M. Morgan Jr., S. A. Changnon Jr. 1976, "Examples of the wind factor in crop-hail damage," Journal of Applied Meteorology 15, 1116-1120.
23 Morgan, G. M. Jr., and N. G. Towery 1976, "On the role of strong winds in damage to crops by hail and its estimation with a simple instrument," Journal of Applied Meteorology 15, 891-898.
24 Sanchez, J. L., R. Fraile, J. L. de la Madrid, M. T. de la Fuente, P. Rodriguez, and A. Castro 1996, "Crop damage: the hail size factor," Journal of Applied Meteorology 35, 1535-1541.
25 Changnon, S. A., D. Changnon, and S. D. Hilberg 2009, Hailstorms Across the Nation: An Atlas about Hail and Its Damages, Illinois State Water Survey, Contract Report 2009-12.
26 Lauer, J. "Hail Damage on Corn." Wisconsin Corn Agronomy. N.p., 23 Feb. 2014. Web. 08 June 2017. http://corn.agronomy.wisc.edu/Management/L039.aspx.
27 Agricultural Marketing Resource Center. N.p., n.d. Web. 14 June 2017. The Agricultural Resource Center is a research cooperative formed by several universities, including the University of Iowa, funded in part by a United States Department of Agriculture (USDA) Rural Development grant. http://www.agmrc.org/.
28 Agriculture. Environmental Protection Agency, 08 June 2017. Web. 13 June 2017. http://www.epa.gov/oecaagct/ag101/cropmajor.html.

Corn

More than 85 million acres of corn were harvested in 2021 in the United States.[29] Currently, about half of the crop is the main food source for livestock feed; other uses include human consumption (sweetcorn, popcorn, sweeteners, oil, beverage and alcohol industries) and fuel ethanol.[30]

Corn plants are warm weather annuals with deep, broad root systems that require abundant moisture to produce a high quality crop. Most corn in the United States is planted in April or May and the crop is harvested by October or November.

Although corn is produced in Kansas, northern Texas, and along the Atlantic coast, production is concentrated in Illinois, Iowa, Indiana, eastern South Dakota and Nebraska, western Kentucky and Ohio, and most of northern Missouri.[31]

Corn Crops and Hail

Hailstorms can reduce corn yields by decreasing the number of corn plants per unit area (thereby lowering the field's yield per acre), harming the plants' stems and leaves, inhibiting the growth of normal, healthy ears of corn, and directly damaging the ears of corn.[32] When the growing point of the corn plants is still below the soil surface (ISU V6 developmental stage, or 8-leaf stage), corn is highly resistant to hail. And, early in the growing season surviving plants can compensate by developing a second ear or increasing potential kernel numbers.[33] However, after the corn emerges from the soil—and especially as the corn approaches its tasseling and pollination developmental stages—its susceptibility to hail damage increases because the greatest reduction in corn yields is caused by defoliation .[34, 35] Therefore, the percentage of destroyed leaf area of hail-damaged corn, rather than the number of corn plants destroyed per acre, is used to estimate yield loss.[36, 37]

Corn developmental stages are assessed using two different techniques. The most common is the Iowa State University (ISU) leaf collar method of counting the number of visible leaf collars (i.e., places where the corn leaves meet and wrap around the plant's stem). The second method, which is frequently used by the crop insurance industry, consists of counting the number of visible leaves that are bent over.[38]

---

29 USDA National Agricultural Statistics Service https://www.nass.usda.gov/Statistics_by_Subject/
30 USDA Economic Research Service https://www.ers.usda.gov/topics/crops/corn-and-other-feedgrains/feedgrains-sector-at-a-glance//
31 USDA Economic Research Service https://www.ers.usda.gov/topics/crops/corn-and-other-feedgrains/feedgrains-sector-at-a-glance/
32 Klein, R. N. and C. A. Shapiro 2011a, Evaluating Hail Damage to Corn, University of Nebraska-Lincoln Extension, Report EC-126. http://www.ianrpubs.unl.edu/live/ec126/build/ec126.pdf
33 Nielsen, R. L. 2012, Recovery From Hail Damage to Young Corn, Agronomy Department, Purdue University. Available online: http://www.agry.purdue.edu/ext/corn/news/timeless/HailDamageYoungCorn.html.
34 Lee, C. 2007, Estimating Hail Damage in Corn, University of Kentucky, College of Agriculture Extension Service. Available online: http://www2.ca.uky.edu/agc/pubs/agr/agr194/agr194.pdf
35 Ibid
36 Ibid
37 Lee, C. 2007, Estimating Hail Damage in Corn, University of Kentucky, College of Agriculture Extension Service. Available online: http://www2.ca.uky.edu/agc/pubs/agr/agr194/agr194.pdf
38 Ibid

Soybeans

More than 86 million acres of soybeans were harvested in 2021.[39] The US is the world's leading soybean producer and the second-leading exporter.

Soybeans are usually planted in May and early June. The young plants produce pods between July and August, and are harvested between late September and early November.

Although soybeans are a popular food crop in most of the world, they are primarily used to make high protein animal feed and vegetable oil in the U.S.

In 2020, 81% of US soybean acreage was in the upper Midwest; the top soybean producing states are Illinois, Iowa, and Minnesota (accounting for 35.2 percent of total U.S. production).[40]

Soybean Crops and Hail

Hailstorms can reduce soybean yields directly by killing a portion of the plants in a field, or damaging the seed pods, and/or indirectly, by destroying some of the plants' leaves. Soybeans can recover from hail damage inflicted during the early vegetative developmental stages (VE-V6) as long as the plants' stems are not cut off below the cotyledons (i.e., seed leaves). The reduction of the number of live plants per acre causes yield loss, and if hail damage has removed all leaf material from the stem, the plant will not survive. [41, 42]

Wheat

Wheat is the most common food grain and third most commonly harvested crop in the US after corn and soybeans with more than 37 million acres harvested in 2021.[43,44] Varieties include winter wheat, spring wheat, and durum wheat. In 2021, 10 million acres of spring wheat (excluding durum), 1.5 million acres of durum wheat, and 25.5 million acres of winter wheat were harvested in the United States.[45] Wheat is planted in the winter or spring, depending on the variety.

Winter wheat (hard red and soft red) was projected to be about 67% of the total wheat bushels harvested in the in 2021/22 growing season.[46] Winter wheat is planted in the fall and harvested the following summer after experiencing a dormancy period during the winter months. Because in many regions winter wheat emerges in the autumn when rainfall is often abundant, it is able to grow well even if the following spring and summer are relatively dry. However, winter wheat does not thrive in regions where the average daily temperature in January and February drops below 10° Fahrenheit. In such locations, spring wheat is planted instead.

39 USDA National Agriculture Statistics Service https://www.nass.usda.gov/Statistics_by_Subject/
40 USDA Economic Research Service https://www.ers.usda.gov/topics/crops/soybeans-oil-crops/oil-crops-sector-at-a-glance/
41 Staton, Mike. "Assessing hail damage to soybeans in the early vegetative stages." MSU Extension. Michigan State University, 21 June 2013. Web. 11 June 2017. https://www.canr.msu.edu/news/assessing_hail_damage_to_soybeans_in_the_early_vegetative_stages .
42 Thelen, Marilyn. "When to assess hail damage to crops." MSU Extension. Michigan State University, 21 June 2013. Web. 11 June 2017. http://msue.anr.msu.edu/news/when_to_assess_hail_damage_to_crops.
43 https://www.ers.usda.gov/topics/crops/corn-and-other-feedgrains/feedgrains-sector-at-a-glance//
44 USDA National Agricultural Statistics Service https://www.nass.usda.gov/Statistics_by_Subject/
45 USDA. N.p., n.d. Web. 13 June 2017. https://www.usda.gov/
46 USDA Economic Research Service, Wheat Data https://www.ers.usda.gov/data-products/wheat-data/

Hard red winter wheat is grown throughout the Great Plains states—Montana, South Dakota, Nebraska, Kansas, and Oklahoma—as well as in Colorado and Texas. Soft red winter wheat is primarily sown in Indiana, Illinois, Ohio, Arkansas, and Tennessee. Several states along the East Coast also produce winter wheat, primarily North Carolina and Georgia. White winter wheat is mostly grown in the Pacific Northwest (Washington, Oregon, and Idaho). Both of the spring wheat varieties raised in the U.S.—hard red spring wheat and durum wheat—are grown in North Dakota, South Dakota, and Montana.

Wheat Crops and Hail

In spite of its economic importance, there are relatively few published studies available that quantitatively assess the effects of hail on wheat yields. Studies of simulated hail damage on hard spring wheat suggest that, at all developmental stages, stem injuries closer to the wheat head (where the kernels are housed) reduce yields more than stem damage closer to the ground. Damage lower on the stem still reduces yields, perhaps by lowering the plants' heads below the height of the combine cutter bar and preventing their harvest. In addition, the quality of the harvest—as measured by kernel weight—was most severely reduced by simulated hail damage during the milk stage.[47]

Katz and Garcia have quantified hail damage to wheat during four developmental stages of this crop: just headed (or earlier), milk, soft dough, and hard dough.[48] To accomplish this goal, hailstone kinetic energy, momentum, mass, and count of hailstones greater than 12.7 mm (0.5 in) in diameter were all considered. While all of these variables exhibited a significant correlation with reduction in crop yields at each developmental stage, wheat was most sensitive to hail damage at the milk and hard dough stages. Similarly, Schiesser found a robust relationship between radar-derived hailstone kinetic energy and damage to wheat.[49]

Cotton

The US accounts for one-third of global trade in raw cotton and is the world's third-largest cotton producer.[50] In 2021, the US harvested almost 10 million acres of cotton, producing 17.6 million bales.[51]

By far, the bulk of the cotton crop in the United States is comprised of upland cotton grown in western Texas. Smaller amounts of upland cotton are grown in other southern states such as Georgia, Arkansas, North Carolina, Mississippi, and Virginia. The less common variety, pima cotton, is generally cultivated in southern California.

Although nearly 90% of the global cotton crop is used to make textiles, cotton is also used to make important products such as cottonseed oil (for cooking) and high protein feed for livestock.

47 Busch, R. H. 1969, "Simulated Hail Damage on Spring Wheat," Farm Research 26, 8-9.
48 Katz, R. W. and R. R. Garcia 1981, "Statistical relationships between hailfall and damage to wheat," Agricultural Meteorology 24, 29-43.
49 Schiesser, H. H. "Hailfall: the relationship between radar measurements and crop damage." Atmospheric Research. Science Direct, 01 Jan. 1990. Web. 23 May 2017. http://adsabs.harvard.edu/abs/1990AtmRe..25..559S.
50 USDA Economic Research Service https://www.ers.usda.gov/topics/crops/cotton-wool/
51 USDA National Agricultural Statistics Service https://www.nass.usda.gov/Statistics_by_Subject/

Cotton is a perennial shrub that is native to tropical and sub-tropical areas; however, it is successfully grown as an annual in the southern United States. Between 60 and 80 days after sprouting, cotton plants begin to bloom. Soon after the flowers are pollinated, they form fruits, also termed cotton bolls, which contain the cotton fibers that are processed to form cloth. Although cotton plants are bred for drought resistance, sufficient water is critical during the fruiting phase. If water is limited when the bolls form, the bolls will be smaller and the fibers they contain will be weaker and shorter, yielding a poorer-quality cloth.

Cotton Crops and Hail

Unlike many crops, cotton plants produce seeds while the plant continues to grow. This indeterminate growth habit means that, at all developmental stages, cotton possesses some ability to recover from hail damage, depending on the severity of the damage.[52] However, although cotton seedlings can recover from leaf damage and largely regrow lost leaves as they mature, even mild defoliation at early developmental stages is enough to reduce subsequent yields.[53] For example, Table 3 shows the relationship between average yield and simulated hail damage for cotton fields over a three year period, compared to control undamaged fields.[54]

Table 3. Effect of simulated hail damage at different developmental stages on cotton yields

Location of Damage / Developmental Stage*	Average Yield (% of control)**
C5/R5	75%
C7/R5	75%
C5/R7	69%
C7/R7	84%

* C denotes the leaf node just below the damaged region of the plant; R denotes the plant's developmental stage when the damage was inflicted.

** The control yields (from undamaged plants) are 100%.

Stem damage from hail, including stem bruising, can also be a serious source of reduced cotton yields. For example, if a plant's stem is broken below its cotyledons, the plant will not recover and should be considered completely destroyed.[55]

Hail damage can also reduce the quality of the cotton bolls produced by recovered plants. The fibers produced by severely injured plants were notably finer in texture (but no shorter or weaker) than those from uninjured plants.[56] However, simulated studies of hail damage to

52 Smith, C. W. and J. J. Varvil Jr. 1981, "Recoverability of cotton following simulated hail damage," Agronomy Journal 73, 597-600. https://dl.sciencesocieties.org/publications/aj/abstracts/73/4/AJ0730040597?access=0&view=pdf.

53 Longer, D. E. and D. M. Oosterhuis 1999, "Cotton regrowth and recovery from early season leaf loss," Environmental and Experimental Botany 41, 67-73.

54 Smith, C. W. and J. J. Varvil Jr. 1981, "Recoverability of cotton following simulated hail damage," Agronomy Journal 73, 597-600.

55 Ibid

56 Peacock, H. A. and B. S. Hawkins 1974, "Hail damage to upland cotton," *Agronomy Journal* 66, 100-104.

cotton plants suggest that these finer fibers do not significantly affect the overall quality of the harvested bolls.[57]

Rice

Rice is a primary staple for more than half of the world's population and the US is a major exporter.

The US accounts for less than 2 percent of global rice production, but provides around 6 percent of the global exports; as of 2021 the US is the fifth largest exporter of rice globally.[58] Almost 2.5 million acres of rice were harvested in the United States in 2021.[59]

Four regions in the US produce almost the entire rice crop: Arkansas, the Mississippi Delta, the Gulf Coast and the Sacramento Valley; each region specializes in different types of rice. For example, the Mississippi Delta states (including Arkansas) and the Gulf Coast states (such as Texas) generally produce long grain rice as well as smaller amounts of aromatic or medium grain rice. In contrast, most rice grown in the Sacramento Valley is medium grain, short grain, or specialty rice (such as basmati).

Successful rice cultivation requires pooled water between 2 and 3 inches deep across all fields during the growing season. Clay-rich soils that are poorly suited for most crops are excellent for rice due to their ability to retain water. When the rice plants are fully mature, the fields are drained and combines are used to harvest the rice crop, separating the grains from the stalks. After harvesting, the rice is milled to remove the inedible hull around each grain. Some of the crop may be milled further to produce white, or polished, rice.

Rice Crops and Hail

The effect of hail damage on rice yields is most pronounced when hail strikes during the plants' reproductive developmental stages (i.e., after the small branch that will support the grain head has begun to form). Studies of simulated hail damage to rice plants show that leaf removal causes a larger reduction in yield than stem bending or stem severing at all points in the rice life cycle.[60] The impact of leaf removal on rice yields is strongest when the rice plants are in the heading developmental stage, as shown in Table 4. At about two weeks after the rice plants have formed grain heads, severing the stems of the plants is nearly as damaging to yields as leaf removal at that same developmental stage.[61]

57 Smith, C. W. and J. J. Varvil Jr. 1981, "Recoverability of cotton following simulated hail damage," Agronomy Journal 73, 597-600.
58 USDA Economic Research Service https://www.ers.usda.gov/topics/crops/rice/
59 USDA National Agricultural Statistics Service https://www.nass.usda.gov/Statistics_by_Subject/
60 Counce, P. A., B. R. Wells, R. J. Norman, and J. Leong 1994, "Simulated hail damage to rice: II. Effects during four reproductive growth stages," Agronomy Journal 86, 1113-1118.
61 Ibid

Table 4. Rice yields at different developmental stages in plants with leaf damage (control yields are 100%)*

	Grain yield of rice at different reproductive developmental stages**			
Leaves Removed	**Panicle Initiation**	**Booting**	**Heading**	**Two Weeks After Heading**
1	93.6%	87.4%	85.3%	94.4%
2	87.4%	71.1%	65.1%	76.8%
3	84.0%	61.2%	58.8%	75.5%

*** Ibid**

**** Panicle initiation means that the branchlets (panicles) that will support the rice grains have begun to grow. This is facilitated by the transition of the terminal cells of the rice shoot (apical meristem) from vegetative cells to reproductive cells, allowing them to produce flowers and eventually rice grains. During booting, the panicles continue to develop. Heading means that at least some of the panicle is visible outside the main stem.**

Barley

In 2021, almost 2 million acres of barley were harvested in the US. For comparison, almost 12 million acres were harvested in 1986.[62]

Similar to wheat, barley is a two-season grain crop that can be planted in the spring or the late fall; however, barley matures more rapidly than wheat and can generally be grown in colder climatic conditions.

The majority of the U.S. barley crop is grown in North Dakota; South Dakota, Montana, Idaho, and Washington are also major barley producers.

Barley is used for livestock feed, malt production, and human food, with different varieties of barley being more appropriate for each. Specifically, high protein barley is best for feed, while lower protein varieties are superior for the malting process.

Barley Crops and Hail

Simulated studies of hail damage to barley suggest that hail reduces yields most dramatically when it strikes barley plants at the soft dough period of development. Regrowth after hail damage is more likely if the hail damage is near heading time rather than ~1-2 weeks after heading; lower yields are more likely when the hail damage occurs after heading time.[63]

2.3 2019 Crop Exposure to Hail in the United States

The Verisk Crop Hail Model for the United States estimates losses for barley, corn, cotton, rice and soybeans, and durum, spring and winter wheat using crop data obtained from the National Agricultural Statistics Service (NASS). In 2020, these crops accounted for 92.7% of the industry insured liability for the crop hail line of business and 96.3% of industry

[62] USDA National Agricultural Statistics Servicehttps://www.nass.usda.gov/Statistics_by_Subject/
[63] Gilbertson K. M. and E. A. Hockett 1979, "The effect of hail damage on barley," Canadian Journal of Plant Science 59, 1147-1152.

insured liability for the production plan line of business. The figures in this section show the geographic distribution of the harvested acres for each of these crops, for 2019. Note that losses from crops that are not explicitly modeled are calculated using statistical relationships between the non-modeled and explicitly modeled crops.

See Also

Verisk Insurable Crop Industry Exposure Database Maps

Average Harvested Acres of Barley for Selected Counties, 2019

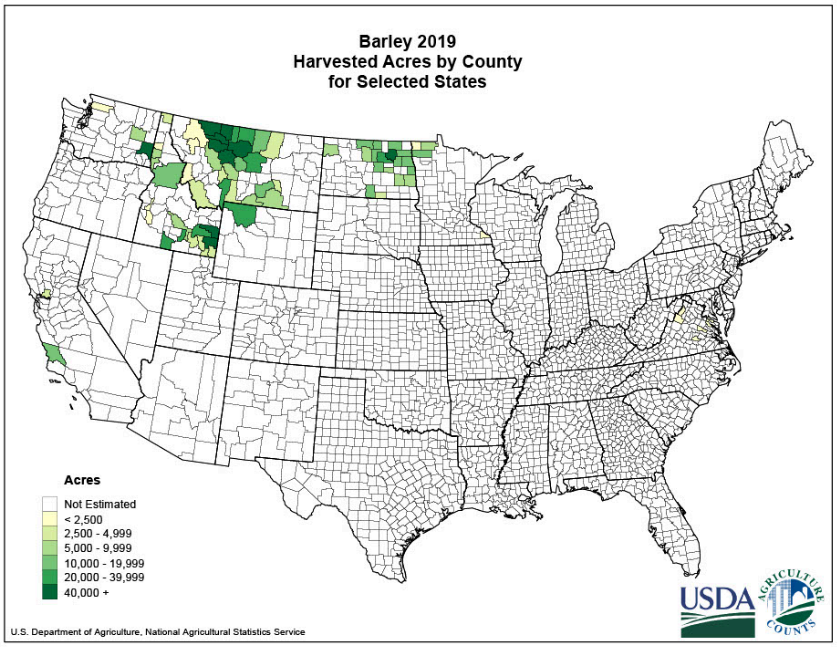

Figure 7. Barley Exposure

Average Harvested Acres of Corn for Selected Counties, 2019

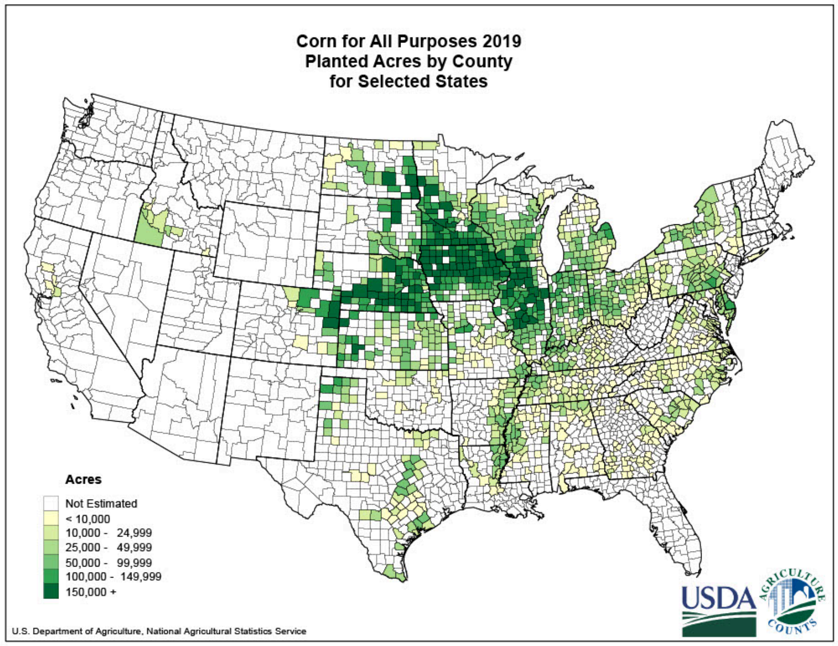

Figure 8. Corn Exposure

Average Harvested Acres of Cotton for Selected Counties, 2019

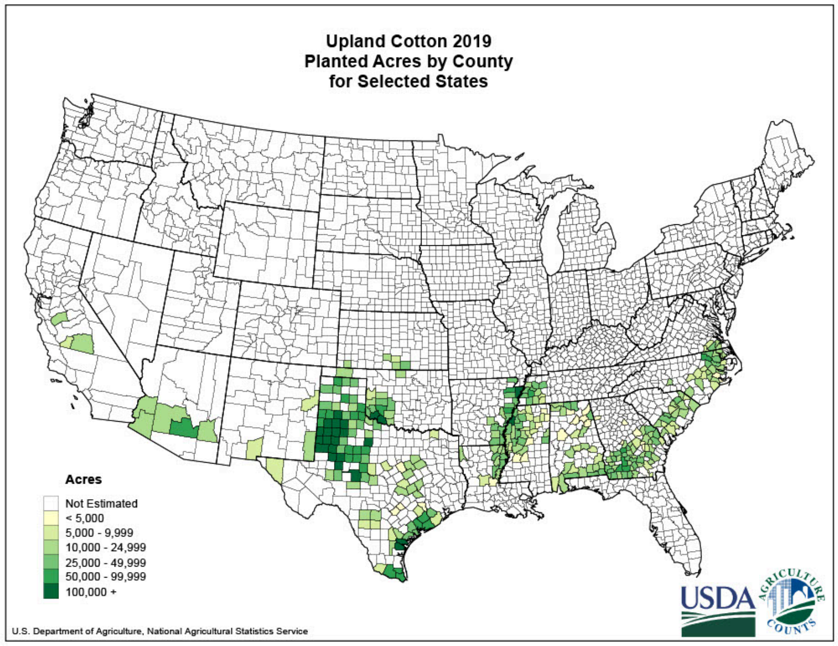

Figure 9. Cotton Exposure

Harvested Acres of Rice for Selected Counties, 2019

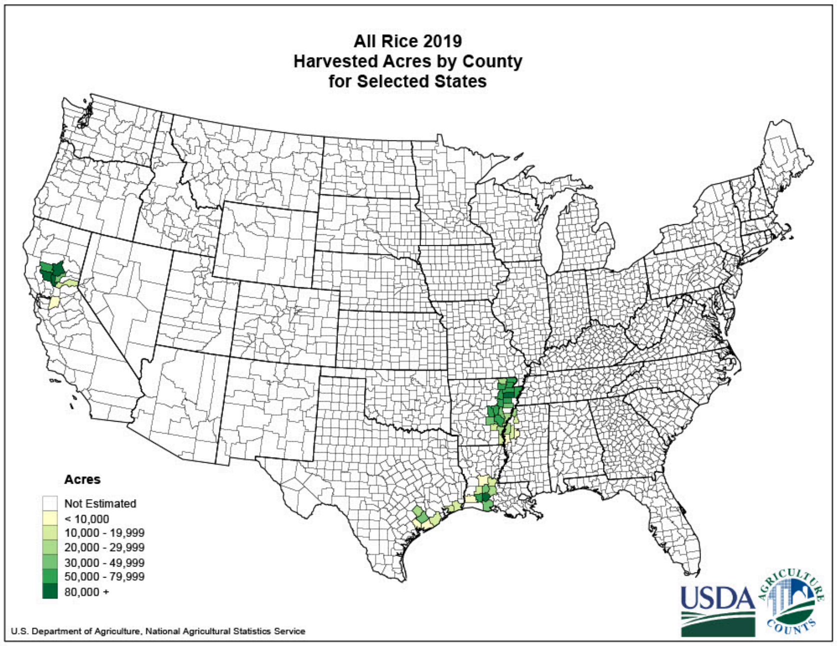

Figure 10. Rice Exposure

Average Harvested Acres of Soybeans for Selected Counties, 2019

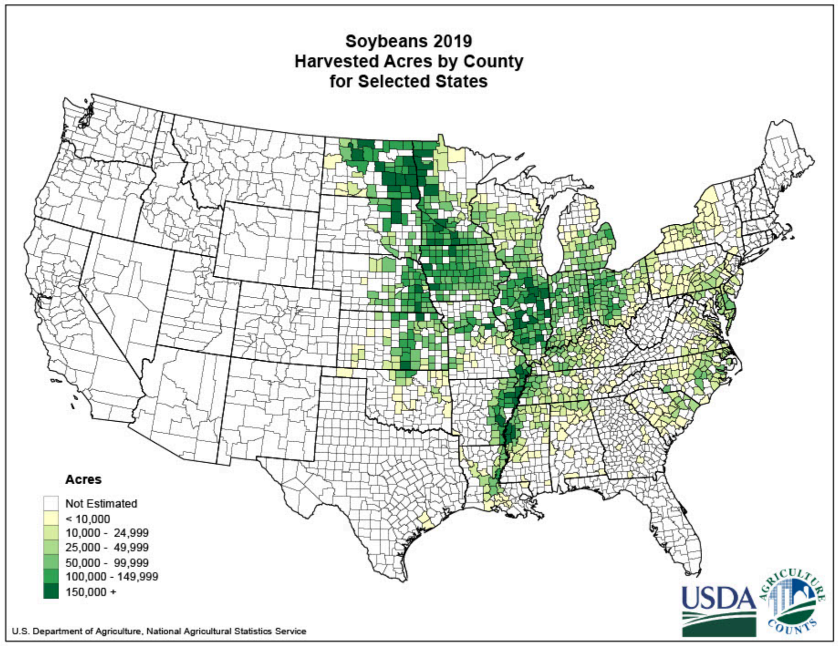

Figure 11. Soybean Exposure

Average Harvested Acres of Winter Wheat for Selected Counties, 2019

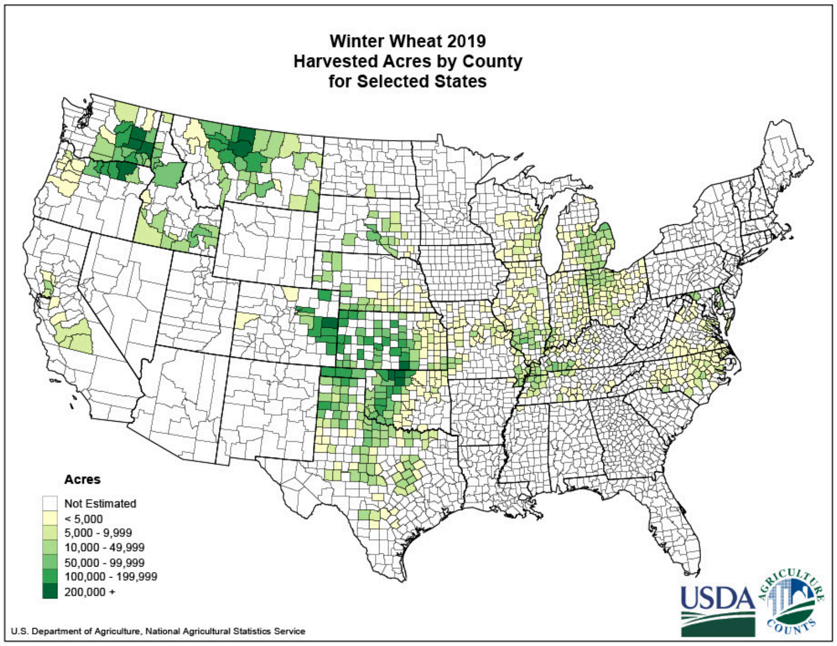

Figure 12. Winter Wheat Exposure

Average Harvested Acres of Spring Wheat for Selected Counties, 2019

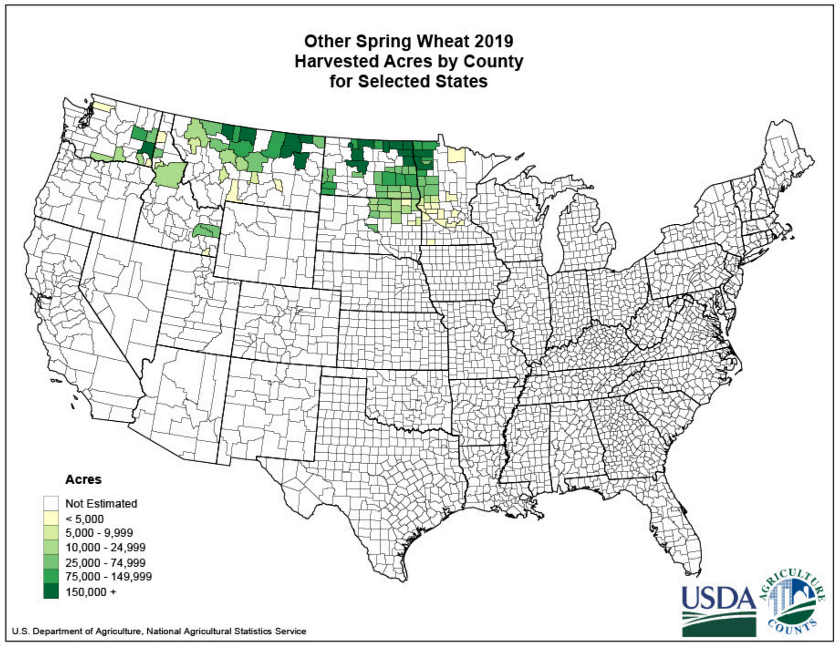

Figure 13. Spring Wheat Exposure

Average Harvested Acres of Durum Wheat for Selected Counties, 2019

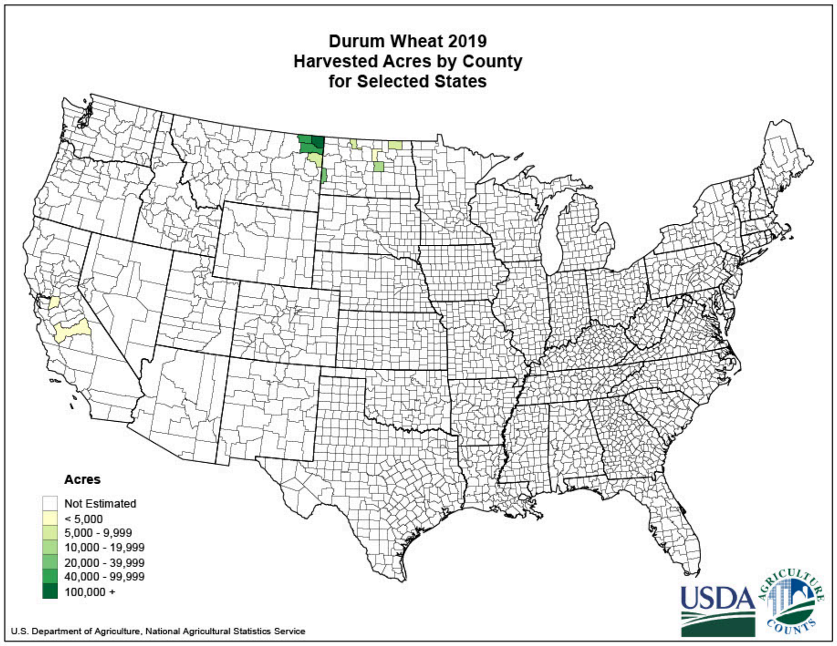

Figure 14. Durum Wheat Exposure

2.4 Significant Historical Crop Hail Events in the United States

Selected historical hail events are described in the section that follows. [64]

It is also important to recognize that many crop-damaging hailstorms are comparatively isolated events and many small, localized hailstorms have caused damage that are not described in this section.

Southeastern Iowa/Western Illinois Hailstorm, August 18, 1925

Starting in southeastern Iowa and progressing into western Illinois, a significant hailstorm cut a path of destruction 6–10 miles wide and 75 miles long on August 18, 1925. According to contemporary reports, fields of corn up to 75 acres in size were completely flattened by hailstones. Some of the largest hailstones of this outbreak measured nearly 4 inches across. Farmers also suffered the loss of chickens and other livestock killed by falling hail. The storm

[64] For additional descriptions of severe thunderstorms—including hail events—that inflicted serious property damage on exposures in the United States, see the document *Verisk Severe Thunderstorm Model for the United States*, which is available on the Client Portal.

caused serious property damage as well, with broken windows and pierced roofs common throughout the storm's footprint.

Central Midwest Hailstorm, July 21-24, 1962

This complex and long-lived storm system produced massive hail damage to crops in many Midwestern states, including Minnesota, Iowa, Missouri, Illinois, Wisconsin, Indiana, Ohio, and Kentucky. However, states as far to the east as North Carolina also reported storm damage, with high winds of up to 90 mph. In all, 31 states experienced damaging hail during this event.

Starting on July 21, the collision of a cold front from the northeast and a squall line to the south generated a large and severe storm system over North Dakota and Minnesota. Over its four-day lifespan, this system progressed to the south and spawned numerous hailstorms that generated enormous crop losses throughout the Midwest. On July 21, hailstones two and three inches in diameter fell in northwestern Minnesota; hail losses were also reported that day in Nebraska and western Iowa. Hail damage occurred the following day in Minnesota, Iowa, northern Illinois, and Kentucky.

Northern Iowa/Southern Minnesota Hailstorm, June 23, 1981

An extremely destructive hailstorm inflicted major crop damage in northern Iowa and southern Minnesota on June 23, 1981, prompting disaster declarations in 23 counties. Hailstones the size of tennis balls pounded crops at the height of the growing season. In Blue Earth County, Minnesota, nearly 100,000 acres of soybeans and corn were completely flattened. High winds associated with the storm also destroyed a grandstand and lofted a parked airplane into a field in Buchanan County, Iowa.

Denver, Colorado Hailstorm, July 11, 1990

On July 11, 1990, one of the costliest hailstorms in United States history struck the Front Range of Colorado, pummeling the Denver metropolitan area from Estes Park to Colorado Springs with marble-to-tennis-ball-sized hailstones. Thousands of homes, commercial buildings, and automobiles were heavily damaged by this hailstorm, with punctured and dented roofs and broken windows being common. Thousands of trees were defoliated as well. However, because the majority of the hail fell over urban and suburban locations, significant crop damage was not associated with this event.

Southern Kansas Thunderstorms, June 19, 1992

Two severe thunderstorms ripped through south-central Kansas within six hours of each other on June 19, 1992, dropping hailstones more than 4 inches in diameter at Sedgwick and surrounding counties. With 10,000 homes affected, the storms caused millions of dollars of property damage. Crops in Kansas were also devastated, with wheat crops suffering the heaviest damage. Many wheat fields in the affected region were totally destroyed.

Midwest Supercell Event, April 10, 2001

Some hailstorms, despite being major and costly events, do not cause significant damage to crops.

During the afternoon and evening of April 10, 2001, a long-lived and devastating supercell spawned nine tornadoes; hail fell over an area that stretched from Kansas City to St. Louis. Termed the "Tristate Hailstorm," (although the storm covered much of the Midwest) this event produced large hailstones (between 1 and 3 inches in diameter) nearly continuously during its eight-hour lifetime. Propelled by high winds, these golf ball-to-baseball-sized hailstones wreaked massive property damage throughout a 292-mile long and 20-mile wide area. Many buildings suffered serious damage to roofs, windows, and siding. Vehicles were also badly damaged, including several airplanes parked at Lambert St. Louis International Airport. This was one of the costliest hail events in United States history in terms of damage to insured properties.

However, due to its occurrence early in the growing season, crop damage was minimal.

Central Midwest Hailstorm, April 13-14, 2006

Spawned by the interaction of an unseasonably warm, moist air mass and a cold front, a long-lasting supercell thunderstorm developed on April 13, 2006, over Iowa. Over a 30-hour period, hail from this storm fell in three distinct areas, each of which extended more than 200 miles in length. Most losses were inflicted in the metropolitan areas of Chicago, Indianapolis, and Milwaukee.

Due to the storm's occurrence in mid-spring, however, crop damage was minimal.

Northern Iowa Hailstorms, July 24 and August 9, 2009

On July 24, 2009, a major hailstorm caused severe crop damage in northeastern Iowa. More than 400,000 acres — mostly corn and soybeans — were seriously damaged in Allamakee, Clayton, Buchanan, Fayette and Winneshiek counties. Of this hail-damaged acreage, about 10% experienced a total loss.

Less than a month later, on August 9, 2009, supercell thunderstorms producing high winds and hail caused widespread crop damage across five counties in north central and northeastern Iowa. The 25-mile long, 5-mile wide area impacted by hail stretched across Webster, Calhoun, Hamilton, Hardin and Grundy counties. Occurring at the height of the growing season, when corn crops are in the highly vulnerable tasseling stage, the storm heavily damaged corn and soybean fields. By some reports, the August 9 storm caused the worst hail damage to crops seen in Iowa for decades.

Other, smaller hail events occurred across Iowa in July and August 2009 as well, causing pockets of serious crop damage that in some cases overlapped with the regions affected by the July 24 and August 9 storms. The additive effect of this series of hailstorms made it more difficult for farmers and insurance adjusters to decide how to respond to hail-damaged fields.

Nebraska, Western Iowa, Kansas, and Missouri Hail, August 18, 2011

A particularly damaging event occurred on August 18, 2011, triggered by the collision of a warm, humid air mass with a cooler, drier air mass across a broad region of the Midwest. With scattered supercell thunderstorms developing across Nebraska, western Iowa, Kansas, and Missouri, high winds and hail caused significant crop damage throughout this region. The corn crop was particularly hard hit. In fact, 2011 in general was an extreme year for hail damage to crops.

Eastern Nebraska, June 3, 2014

The crop hail insurance program experienced its largest single-year hail losses in the program's history in 2014. There were several hail outbreaks throughout the Midwestern states during the growing season, making 2014 only the third year since 1948 to have a countrywide loss ratio above 100%. On June 3, 2014, severe thunderstorms formed throughout Nebraska and into Iowa, bringing severe straight-line winds, floods, and baseball-sized hail. Bands of severe hail up to 4 miles wide, trending northwest to southeast, flattened corn and soybean crops in the greater Omaha region and eastern Nebraska in general.

Colorado, Kansas, and Nebraska Hail Outbreak, June 18-19, 2018

The combination of a stalled cold front across Colorado and a cutoff low — a closed upper-level low pressure system that has been completely cut off from westerly currents, moves independently of the jet stream, and can remain stationary for days — created a favorable environment for severe thunderstorm development in northeastern Colorado, western Kansas, and southern Nebraska in June, 2018. Large hailstones of up to 3 inches in diameter (slightly larger than a baseball) were reported in Boulder, Arapahoe and Logan counties in Colorado, and hailstones as large as 2.75 inches in diameter were reported in Harlan County, Nebraska. A tornado was spawned northeast of Denver. On June 19, winds reached 80 mph in Cheyenne County, Kansas, and 71 mph in Red Willow and Thayer counties in Nebraska.

In Boulder County, Colorado, many vegetable crops at small farms were destroyed, and cornfields were decimated. Hail in Scott County, Colorado caused minor damage to corn. Winter wheat was also damaged by hail throughout the region.

In Kansas, damage to wheat and corn crops were minor (some leaves were stripped from stems).

The storms in Nebraska had a larger impact on winter wheat. Nebraska’s winter wheat crop was about 10 days from harvest, making this is a particularly bad time for storms of this severity; some fields nearing harvest north of Alma were destroyed. Corn and soybean crops were also damaged in Nebraska, but were in earlier developmental stages than winter wheat.

3 Event Generation

The event generation module combines statistical and physical methods to determine the annual frequency, intensity, and location of simulated severe thunderstorms. The motivation for employing both methods in the model is to (1) apply the large amount of meteorological research that suggests that parameters (index values) can be used to determine when conditions are favorable for severe thunderstorm formation, and (2) address the significant reporting biases that exist in the SPC data. The approach Verisk researchers followed to evaluate historical data, develop damage footprints, augment the data, and validate the catalog are all discussed in this chapter.

Although the Verisk Severe Thunderstorm Model for the United States includes three sub-perils—straight-line wind, tornado, and hail—the Verisk Crop Hail Model for the United States uses only the simulated straight-line wind and hail events from this catalog. The model domain, shown in Figure 15, includes the conterminous United States and most of Canada's southernmost provinces. Note that events are not generated over the Atlantic or Pacific Oceans.

The Verisk Crop Hail Model for the United States reports losses for U.S. crop exposures only. Specifically, the model explicitly reports losses to barley, corn, cotton, rice and soybeans, and durum, spring and winter wheat for the 42 states shown in green in the figure below.

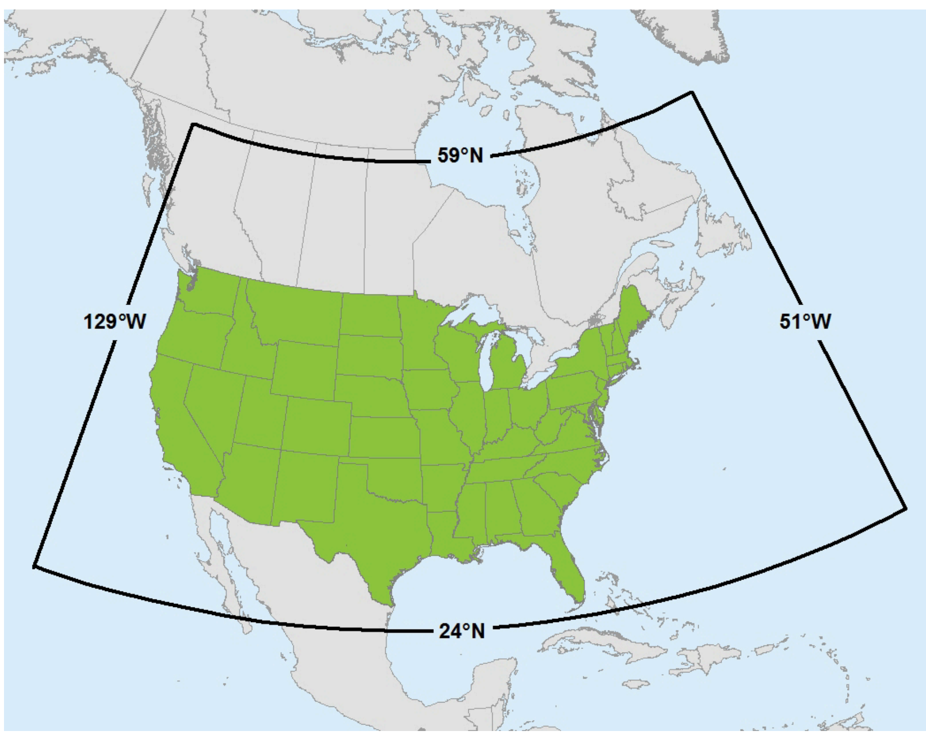

Figure 15. Model domain of the event generation module

See Also
Stochastic Hazard Catalog

3.1 Event Definition

Verisk's event generation module captures both the highly-localized effects of individual hailstorms and convective straight-line windstorms, as well as the effects of large severe thunderstorm events.

Events are categorized as *microevents* or *macroevents*; the Crop Hail Model for the US leverages *microevents*.

A microevent is a single simulated convective straight-line wind or hail event (a single "swath" or "footprint") and is modeled as a discrete ellipse object with no artificial grid. Each microevent has the following properties:

- Starting/"Touchdown" location
- Spatial extent
- Orientation/Direction
- Date of occurrence
- Intensity

A location is impacted by a microevent if it is inside the ellipse and missed if it is outside the ellipse. This modeling approach best represents the binary nature of severe thunderstorm damage footprints, as there is often an abrupt change from little or no damage to severe damage over a short distance.

See Also

Hail Impact Energy
Straight-Line Wind Speeds

3.2 Data Sources for Event Generation

The Verisk Crop Hail Model for the United States uses wind and hail in Verisk's all-events 10,000-year stochastic hazard catalog.

To thoroughly analyze risk throughout the model domain, Verisk researchers used information from:

NOAA's Storm Prediction Center (SPC) and National Centers for Environmental Information (NCEI) Storm Reports	Historical hail, convective straight-line windpoint data https://www.spc.noaa.gov/wcm/#data Dates: 1979 to 2018
Community Collaborative Rain, Hail, and Snow (CoCoRaHS) Network	Historical hail point data https://www.cocorahs.org/ViewData/ Dates: 1998 to 2018

Severe Hazards Analysis and Verification (SHAVE) Project	Historical severe weather point data https://www.nssl.noaa.gov/projects/shave/ Dates: Mid-spring through late summer, 2006 to 2015
Climate Forecast System Reanalysis (CFSR)	Various meteorological variables combined into composite severe weather indices https://climatedataguide.ucar.edu/climate-data/climate-forecast-system-reanalysis-cfsr Dates: 1979 to 2018 Resolution: 0.5° latitude x 0.5° longitude; 6-hr time intervals
NOAA's Next Generation Radar (NEXRAD) Level III Data	Individual radar site reflectivity data, storm cell ID, predicted probability of hail, predicted probability of severe hail, predicted maximum hail size, and hail index overlay products https://www.ncdc.noaa.gov/nexradinv/ Dates: 1996 to 2017 Resolution: 2-km grid spacing; 10-min time intervals
National Lightning Detection Network (NLDN)	Daily cloud-to-ground lightning flash counts https://www.ncei.noaa.gov/maps/swdi/ Dates: 1992 to 2017 Resolution: 0.10-degree

The sections that follow contain additional details on data sources and data analysis techniques.

See Also

Data Sources for the Verisk Crop Hail Model for the United States
Historical Trends
Accounting for Current Climate in the Model and Catalog Development
Available Catalogs in Touchstone Re

SPC Storm Reports

Historical point data on hailstorms and straight-line windstorms are available in a severe thunderstorm database maintained by NOAA's SPC and the NCEI known as the SPC Storm Reports. This extensive database includes information on more than 345,000 hailstorms, and 366,000 convective straight-line windstorms from 1955 to the present. The SPC maintains this database by collecting storm event reports from local authorities, trained weather spotters, the media, and local citizens.

The SPC Storm Reports contain valuable information about the frequency, geographical distribution, and intensity of individual microevents that are a crucial part of evaluating severe thunderstorm risk across the United States. However, there are several reporting biases in the SPC data that must be corrected by the model. These biases include:

- Population - Since someone must witness an event to report it, reports are more common in and around population centers. In addition, as the population grows over time, so does the event reporting frequency.
- Location - Some areas within the U.S. have a more robust trained spotter network and data collection methods than others and, therefore, receive more reports than other areas.

- Intensity estimation - There can be significant uncertainty in reported hail size and wind speed because these measurements are frequently estimated by the person reporting the event. For example, individuals often compare hailstones to common objects (e.g., golf balls). As a result, diameters associated with common objects appear more frequently in the report databases than in reality, causing large peaks and valleys in the reported intensity distribution. Finally, most straight-line wind reports in the SPC data include estimated, rather than measured, wind speeds. These estimated wind speeds are typically biased high compared to actual wind speeds.
- Event classification - Wind reports can include wind speeds from various types of weather systems (e.g., extratropical cyclones) and not just severe thunderstorm-produced convective straight-line winds. These wind reports must be filtered to eliminate non-convective straight-line wind events.

Verisk researchers determined that reporting biases were most severe between 1955 and the early 1970s when no formal reporting system existed. For this reason, and the lack of CFSR data (discussed in a subsequent section) prior to 1979, Verisk researchers did not directly include any SPC data collected prior to 1979. However, the Verisk model uses hundreds of thousands of SPC reports from 1979 to 2018.

Severe thunderstorm event reporting rose beginning in the 1970s due to several reasons. First, the NWS launched a campaign in the 1970s to recruit volunteers to report spot observations. This campaign consisted of the establishment of a formal training program known as SKYWARN®. This program greatly improved the quality of event reporting by providing severe weather spotters with essential information for identifying and describing local storms.

Further increases in reports ensued in the 1980s because the NWS started issuing severe thunderstorm warnings, which increased event awareness and interest among the general public. Also, the installation of Doppler radar systems at local and regional weather forecast offices in the 1990s dramatically expanded the coverage density and observance of events. There were further increases in event reporting in the 1990s and 2000s due to advances in technology (including the expansion of cell phone networks, making it easier to report severe weather), social media, and the blockbuster 1996 movie "Twister," which resulted in a greater interest in severe weather and storm reporting. Lastly, there were increases over the entire time period due to population growth (i.e., the number of reports increased as the population grew).

Verisk researchers employ a combination of statistical and physical methods to correct for all these reporting biases to ensure full spatial coverage of storm potential, including in locations where no severe weather events have been observed in the past, and generate a stochastic catalog. In addition, hail and wind reports are spatially clustered on a daily resolution to combine reports that were likely from the same storm. A hierarchical clustering algorithm is used with single linkage and cut heights of 0.3 and 0.5 for hail and wind, respectively. Minimum bounding ellipses are computed for each cluster of reports to estimate swath dimensions. Swath intensities are based on the maximum reported hail size and the average wind gust.

See Also
Hailstorms
Wind Event Placement: Hybrid Smoothing

Additional Observational Datasets

Additional historical observational data are obtained from the Community Collaborative Rain, Hail, and Snow (CoCoRaHS) network and the Severe Hazards Analysis and Verification (SHAVE) project. The CoCoRaHS network began in 1998 and is comprised of volunteer weather enthusiasts who measure and report precipitation (i.e., rain, hail, and snow) in their local communities. As a result, these data are limited to static locations. In addition, the density of this network varies throughout the country, with higher density in the High Plains region, particularly Colorado. The amount of information that accompanies each observation is typically greater than SPC Storm Reports, but there are much fewer CoCoRaHS reports overall.

The SHAVE project was an effort to collect additional targeted storm reports through phone surveys and blend these reports with radar data. This project collected thousands of additional storm reports while it ran (from mid-spring through late summer, 2006-2015). Both the CoCoRaHS network and SHAVE project provide additional but limited data for use in Verisk-model validation.

Climate Forecast System Reanalysis

In 2010, NOAA's NCEP completed a climate study that provided a high-resolution coupling of the atmosphere, ocean, land surface, and sea ice systems around the globe. The goal of the project, called the Climate Forecast System Reanalysis (CFSR) Project, is to provide the best currently available estimate of the state of these connected systems over a historical period at a higher spatial and temporal resolution than had been done in past climate studies.[65] Version 1 CFSR data (also known as CFSv1) are available from 1979 to 2011. This dataset has been extended to the present using the same climate model run with real-time observations and is known as CFS, version 2 (i.e., CFSv2).

Reanalyses, which produce datasets for climate research, use dynamical models and observation data to produce best estimates of the state of the atmosphere at regular time intervals (usually every 6-12 hours). The raw data used as input come from various sources including satellite, radiosonde (i.e., weather balloon), and reported observations from sea vessels, aircraft, and land-based stations. These data vary, as would be expected, but the amount of data input and thorough validation has shown reanalysis data to be extremely valuable.

CFSR data (i.e., CFSv1 and CFSv2) are available on a global grid at a resolution of 0.5° latitude x 0.5° longitude, four times a day, and at six-hour time intervals. Thus, these datasets provide a higher spatial and temporal resolution than previous well-known and established reanalyses (e.g., NCEP/NCAR Reanalysis). They are widely believed to provide the best available state of

[65] "Climate Forecast System Reanalysis (CFSR)." Climate Data Guide. NCAR/UCAR, 2017. Web. 08 Nov. 2017. https://climatedataguide.ucar.edu/climate-data/climate-forecast-system-reanalysis-cfsr

the interaction between the ocean and the atmosphere for use in climate research. They are used by NCEP's Climate Prediction Center (CPC) to calibrate operational climate forecasts and to provide estimates and evaluations of the Earth's climate. In addition, a large amount of meteorological research suggests that composite indices calculated from the CFSR data can be used to determine when historical atmospheric conditions were favorable for the occurrence of hail and/or straight-line wind events.

To supplement the SPC data, Verisk researchers extract 6-hourly meteorological variables from the CFSR dataset over the domain from 1979 to 2018. These variables are combined into composite severe weather indices known to be correlated with severe thunderstorm activity at each 0.5° latitude x 0.5° longitude grid cell and include:

- Convective Available Potential Energy (CAPE)
- Vertical wind shear
- Mid-level lapse rate
- 500 mb temperature
- Significant Hail Parameter (SHiP)
- Energy Helicity Index (EHI)

Finally, these indices are aggregated to represent daily (maximum, minimum, or mean, depending on the index) values, which are used to inform the stochastic microevent locations.

Atmospheric Indices

There is extensive research showing that meteorological parameter values can indicate whether atmospheric conditions are favorable for severe thunderstorm activity. For example, historically lower parameter values over mountainous terrain and the leeward side of the Great Lakes is consistent with lower levels of severe thunderstorm activity in those regions. Variations in parameter values within an air mass are also indicative of differences in the stability of the air mass, which sometimes explains why some locales experience more severe thunderstorm activity than others even though both locales are influenced by the same air mass. In other cases, the lack of severe thunderstorm activity is due to an insufficient storm initiation mechanism.

In the Verisk Severe Thunderstorm Model for the United States, parameter values are an integral part of enabling the model to (1) account for risk in regions that have not experienced major severe thunderstorm activity in the brief historical record, and (2) simulate major outbreaks similar to those that occurred outside the historical record used in model development.

The Verisk Crop Hail Model for the United States uses the following parameters:

- Significant Hail Parameter (SHiP) for hail,[66]
- and the Energy Helicity Index (EHI) for straight-line winds.[67]

[66] http://www.spc.noaa.gov/exper/soundings/help/ship.html
[67] http://www.stormtrack.org/library/forecast/ehi.htm

These parameter values are known as composite indices because they are composed of meteorological variables (i.e., Convective Available Potential Energy (CAPE), lapse rates, moisture content, and wind shear, amongst others) that are considered ingredients for severe thunderstorm formation. The equations for these parameters are as follows:

$$SHiP = \left[\left(CAPE_{MU}\ J/kg\right) \times \left(Mixing\ Ratio\ of\ MU\ PARCEL\ g/kg\right) \times \left(LAPSE\ RATE_{700\text{-}500\,mb}\ ^{\circ}C/km\right) \times \left(-TEMP_{500\,mb}\ ^{\circ}C\right) \times \left(Shear_{0\text{-}6\,km}\ m/s\right)\right] \div 44,000,000$$

$$EHI = \left(CAPE_{SB} \times SRH_{0\text{-}1km}\right) - 160,000$$

- "MU," "ML," and "SB" denote the type of air parcels used to calculate CAPE or Lifting Condensation Level (LCL). "MU" refers to the "Most Unstable" parcel found in the lowest 300 mb of the atmosphere, "ML" refers to the "Mean Layer" conditions in the lowest 100 mb of the atmosphere, and "SB" (i.e., "Surface Based") refers to a parcel found at the surface. Note that for the EHI calculations, Verisk researchers substituted a surface-based ("SB") parcel for all instances of "MU" or "ML" to simplify the calculation of the composite indices.
- "SRH" represents Storm Relative Helicity.

Data for these variables are available in the form of the CFSR data for the period of 1979 to the present. For those variables that were not present in the data, Verisk researchers made the appropriate substitutions. Verisk researchers used these data to calculate maximum daily values (06 UTC – 06 UTC) for each of the chosen parameters for the entire historical record used in model development.

See Also

Wind Event Placement: Hybrid Smoothing

Radar Reflectivity

Additional historical data are obtained from 22 years of raw NEXRAD Level III radar data from individual radar sites across the contiguous United States from 1996 to 2017. These data are combined into gridded composite radar reflectivity data at 2-km grid spacing and 10-min time intervals. The reflectivity value in each mosaic grid cell is determined using the maximum reflectivity from the nearest neighbor of each contributing radar.

Verisk researchers use these data to identify thunderstorms and to characterize these storms. Radar measures the strength of reflected microwave pulses, which depend, in part, on the average size and state of the precipitation particles. Hail is a better reflector of microwaves than liquid water primarily because hail particles have larger diameters than raindrops but also because water-coated ice particles have a very high reflectivity as compared to liquid water. As a result, hail is usually measured on a radar scan as an anomalously high area of reflectivity. Thus, Verisk researchers developed a storm tracking algorithm that tracks these areas of high reflectivity, which represent the severe portion of the storm's precipitation and often coincide with hail reports and claims that are overlaid.

The Verisk-developed storm tracking algorithm identifies thunderstorms with the potential for large hail as contiguous grid cells with reflectivity values exceeding a 50-dBZ threshold. The algorithm calculates each storm's centroid and then predicts each storm's position for the next timestep based on the current centroid position, movement direction, and speed (new storms are assigned a speed of zero for this timestep).

At the next timestep, storms are again identified and then matched between timesteps. A storm identified at the second timestep is considered to be the same storm identified at the first timestep if: 1) its centroid is the closest to its predicted location, and 2) it has traveled a realistic distance from one timestep to another. Storm movement direction and speed are updated based on the difference in centroids between the first and second timesteps. Storms identified during the first timestep that do not match a storm at the second timestep are terminated. Likewise, storms identified during the second timestep that do not match a storm from the first timestep are initiated as new. This process is repeated every 10 minutes for every day. At the end of each day, all grid cells that were affected ("hit") by a storm are saved. From these data, storm footprints are created by computing the minimum bounding ellipse around the grid cells hit by each storm. Several radar maximum reflectivity statistics (e.g., mean, median) at each grid cell in a footprint are saved. In addition, various other parameters are attached to each footprint such that appropriate filter analyses can be performed by Verisk researchers, including:

- Several meteorological indices (e.g., CAPE, freezing level, SHiP, shear) extracted from CFSR data
- National Lightning Detection Network (NLDN) cloud-to-ground lightning flashes
- NEXRAD Level III hail signatures (e.g., probability of hail, probability of severe hail, maximum hail size)
- SPC, CoCoRaHS, and SHAVE storm report summaries

The full set of radar-based storm swaths is filtered to retain only those that 1) have a predicted maximum hail size of at least 1.75 in. and occur in an environment with a freezing level less than 4,000 m above ground level, or 2) have a reported (SPC, CoCoRaHS, or SHAVE) maximum hail size of at least 0.75-in. The 1.75-in. threshold is based on Verisk's analysis of predicted and observed hail sizes in populated areas where most severe hail would likely be reported. This 1.75-in. hail size threshold is the best discriminator that maximizes the probability of detection and minimizes the false positive rate when predicting whether a radar-based swath contains severe hail. In addition, radar-based storm swath widths are divided by two before generating distributions based on Verisk's internal analysis and results from various field studies that have found actual hail swaths are narrower than radar-based storm swaths (e.g., Changnon, 1970; Giammanco and DeCiampa, 2018; Nisi et al., 2018).

See Also

Hail

3.3 Microevents

During Verisk's microevent-generation process, both the frequency and location of severe thunderstorm events are determined based on historical years 1979 - 2017. In addition, SPC's storm reports are augmented for underreporting, the false linear time trend, and frequency discontinuities present in the data using statistical detrending, hybrid smoothing, and Generalized Additive Models (GAMs). This microevent-generation process is discussed in further detail in the following subsections.

Event Frequency

Generation

The microevent-generation process begins with randomly selecting a historical seed year to represent a base year at the start of each stochastic year. Both the frequency and locations of simulated events are based on days of the randomly-selected historical seed year, with noise to avoid being too constrained by the historical record.

Next, each stochastic day is simulated separately, based on the corresponding day of that historical seed year. For example, if historical year 2005 is randomly selected as the seed year for stochastic year 1, then 1 January of stochastic year 1 will be based on 1 January 2005, 2 January of stochastic year 1 will be based on 2 January 2005, and so forth.

The simulated number of microevents is calculated from the modified historical count plus noise to account for variability. About 30% of the simulated years are skewed, meaning that there is an additional factor applied to daily counts that further inflates or deflates all days in the year. Skewing some simulated years produces a more comprehensive stochastic catalog that allows the model to include years that experience more or less severe thunderstorms than average. The annual skew factors are based on historical clustered SPC Storm Report counts on the date of interest in each seed year. Modifications are made to these storm report counts and include adjustments to account for the lack of severe storm reports in neighboring Canada and detrending to account for growth in the number of severe days and reports over time.

Statistical Detrending of SPC Storm Reports

Prior to simulating microevent frequency, Verisk researchers statistically detrend the annual severe hail and convective straight-line wind days and clustered reports in the SPC data to remove the false linear time trend present in the earlier years of this dataset. The detrending process for hail and wind reports is accomplished using a piecewise model fit to the data that assumes a positive linear trend in the early years and no trend in the later years. In addition, adjustments are made to account for known deficiencies in the database.

For example, Figure 16 shows a time series of the annual number of reported hail days in the SPC Storm Reports database from 1979 to 2017. It is evident that there is a general increase in reported hail days with time from 1979, which levels off around 1998 (green line). If this false trend is not corrected, then simulated years based on the 1979-1997 historical years would have fewer severe days than post-1997 years because the daily count is based on what was reported. These earlier years likely had more severe weather days, but the severe weather was never reported. After statistically detrending these data, the false linear trend is significantly reduced (blue line).

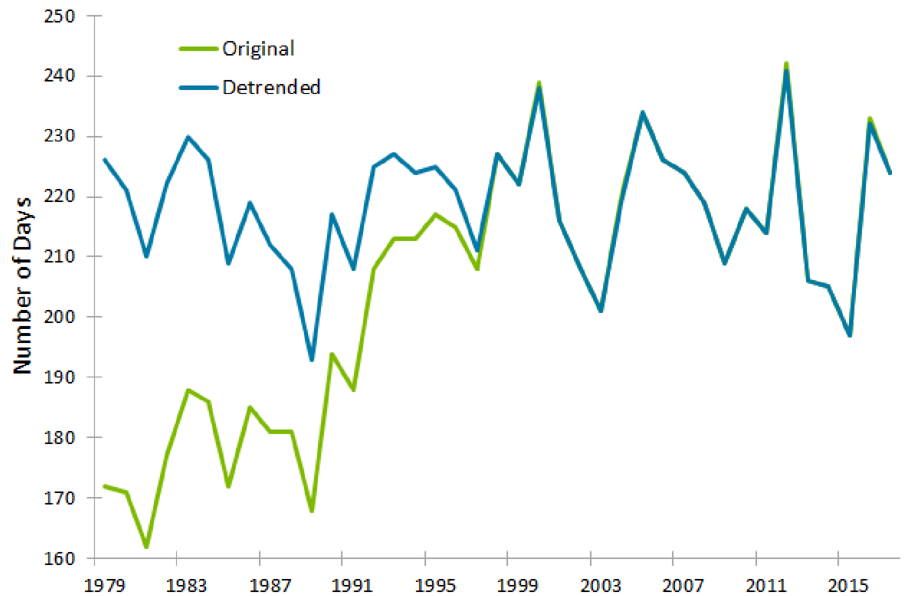

Figure 16. Historical (green line) and detrended (blue line) annual reported number of hail days from SPC's Storm Reports database from 1979 to 2017

As seen in Figure 16, even with adding severe days to the early years, there is still a positive trend in the number of severe hail reports with time. To correct for this false positive trend, Verisk researchers perform the following additional processing steps to the data. First, as seen in Figure 17, hail reports are added to the raw annual number of clustered severe hail reports (green line) to produce the "adjusted" light blue line. This step is performed to account for days that were added during the previous detrending step and to compensate for the lack of data in neighboring Canada. Next, the "adjusted" time series is detrended by using the same piecewise model fit to the data where early years are explained by a linear increase, and no trend is assumed after 2010. The dark blue line in the figure represents this resulting "detrended" time series. Finally, this "detrended" time series is multiplied by two for hail (no inflation factor is used for wind) and represents the "final" model hail count (orange line). This final step is performed because clustered hail reports and radar data often combine two or more actual separate narrow hail swaths into one swath. If not corrected, a low bias in hail swath frequency would exist in the Verisk model.

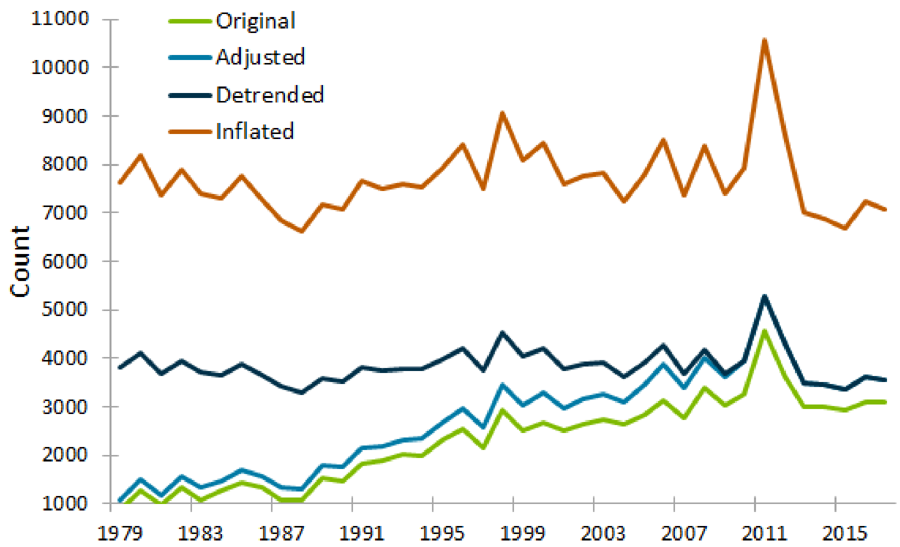

Figure 17. Example of the Verisk statistical detrending methodology used for SPC hail reports.
Plotted in this time series include historical raw annual number of clustered severe hail reports (green line), annual clustered hail reports plus detrended days added (light blue line), detrended version of the light blue line (dark blue line), and the inflated version of the dark blue line (orange line) that accounts for the difference between the actual hail swath shape and what clustered storm reports and radar data indicate. Raw data are from SPC's Storm Reports from 1979 to 2017.

The resulting dataset produces an average number of microevents used to simulate for each historical date and sub-peril. Each time a historical date is used as a seed for a simulated date, this average number is determined, and some noise is added for variability in the dataset. The detrending process ensures that simulated years that use earlier historical years as their seeds do not suffer from lower frequencies than recent years of data would indicate is the true frequency.

See Also

Hazard Footprints for Historical Events

Event Placement

Similar to microevent frequency, microevent locations are based on where historical storms occurred. For each historical seed date, Verisk researchers use atmospheric reanalysis data to identify severe storm environments. In addition, Verisk researchers use hybrid smoothing of SPC reports and environmental conditions derived from CFSR (for wind) and hybrid smoothing of SPC reports and environmental conditions captured by Generalized Additive Models (GAMs; for hail) to account for the geographical differences in sub-peril frequency and variability across the U.S. From these resulting data, the model creates gridded probability surfaces representing possible locations where severe thunderstorms could have occurred. These surfaces are sampled hundreds of times (for a 10K catalog) to generate events that are realistic but have not occurred in the relatively short historical record.

Wind Event Placement: Hybrid Smoothing

To address the observed discontinuities in historical straight-line windstorm frequency among neighboring grid cells in some regions, Verisk researchers statistically smooth the data using high-resolution CFSR-based meteorological parameter indices (i.e., EHI and STP, respectively) in a process that can aptly be called "hybrid statistical-meteorological smoothing" to produce a probability surface. This surface represents the chance that a randomly simulated microevent will occur within a 0.5-degree grid cell. This statistical smoothing (via kernel density estimation) allows historical storms to occur in areas where they were meteorologically plausible but not recorded, while the parameter values ensure that the storms are smoothed to physically realistic locations. Since probability surfaces are based on historical storm reports and meteorological variables, the grid cells with the highest probability are locations where storms were observed or where the atmospheric conditions were conducive for storms.

Verisk researchers chose to use the EHI and STP indices for microevent placement location after performing extensive research including analyzing 40 years of CFSR data alongside SPC data for the same time period. They concluded that, on a given day, when the chosen parameters were above certain threshold values, there was a high number of SPC reports for the respective sub-perils. However, when the parameter values were below certain threshold values, there could still be SPC reports for the respective sub-perils. Similarly, there were often areas that seemed favorable for severe storm development according to the indices, but storms never formed. For these and other reasons (e.g., CAPE values tend to inflate the indices over warm bodies of water, like the Gulf of Mexico, leading to final results that were not physically realistic), Verisk researchers concluded that the stochastic catalog should be built using a combination of index values and SPC data.

A probability surface for a specific sub-peril is created by first taking the storm reports from a historical date of interest and summing the number that occur within each grid cell. Based on extensive meteorological research, Verisk researchers chose both minimum and maximum cutoff values for the EHI and STP indices to compare against the calculated daily maximum values for each of the indices as follows:

- If the maximum daily value at a location falls below the minimum cutoff point, Verisk researchers do not smooth the historical reports into that area.
- If the maximum daily value at a location falls below the minimum cutoff point **and** there are historical reports in that area, Verisk researchers spatially smooth the historical reports into that area. This smoothing is performed because low index values do not necessarily indicate that severe thunderstorm activity is not possible.
- If the maximum daily value at a location is greater than the maximum cutoff point **and** there are no historical reports in that area, Verisk researchers allow the probability of events to generate in that location. The amount of probability added is proportional to the difference between the cutoff value and maximum daily value at that location. These gridded data are then smoothed spatially.

The resulting probability surface allows for the generation of plausible, physically realistic, alternative scenarios that did not actually happen, but could have, had conditions been slightly different.

See Also
SPC Storm Reports
Atmospheric Indices

Hail Event Placement Using Generalized Additive Models

While the "hybrid statistical-meteorological smoothing" technique for determining probable straight-line wind event locations on a given day validates well, this technique's dependence on a single threshold atmospheric value (i.e., SHiP) for probable hailstorm locations has limited success. This dependence ignores the fact that SHiP is a better indicator of hail in certain regions of the U.S. (e.g., the Great Plains) than others (e.g., the Northeast and the Rocky foothills) because many of its constituent components (e.g., CAPE, shear, lapse rate, and 500-mb temperature) are more important in specific regions and/or elevations than others.

To address both reporting discontinuities in hailstorm events and the varying appropriateness of using a single SHiP threshold value as an indicator of hail activity across the U.S., Verisk researchers use spatially-varying Generalized Additive Models (GAMs) trained separately for each month with equally-weighted observational data and individual SHiP parameters to generate daily hail probability surfaces across the U.S. GAMs allow Verisk researchers to fit a relationship between hail occurrence and environmental parameters while maintaining the flexibility of accounting for regional differences, term interactions, and non-linear relationships. Observational data includes SPC Storm Reports, CoCoRaHS, SHAVE, various claims, and radar data. The individual SHiP parameters are obtained from the maximum and minimum CFSR values for their respective variables on a given day and include:

- CAPE
- Temperature lapse rate (700 - 500 mb)
- 500 mb temperature
- Vertical wind shear
- Elevation
- CAPE-elevation interaction
- Shear-elevation interaction
- CAPE-shear interaction

All data are preprocessed on a 0.5-degree grid, which aligns with the native CFSR grid. The GAMs' results are processed through a sigmoid transform function to produce a grid point-specific probability of hail occurrence on a given day for every day from 1979 to 2017 and for every grid cell in the model domain. These hail probability surfaces were blended with smoothed observational surfaces using a method similar to that for straight-line wind , but with more equal weights given to each dataset for hail. The results were further calibrated to correct state frequency biases in the data. The final resulting daily hail probability surfaces more accurately capture the hail frequency and variability across the U.S. than using a single SHiP threshold value alone.

Adaptive Clustering Sampling

To create realistic, spatially-grouped severe thunderstorm events that would not be possible using random sampling alone, the model employs a method called adaptive clustering sampling. This method determines a microevent's location by randomly selecting a grid cell from the appropriate probability surface and seed date. It also ensures that subsequently-placed microevents are likely to fall near that first microevent.

Adaptive clustering sampling was introduced and developed by Steven K. Thompson in 1990 (Thompson, 1990) as a method of sampling for rare events. This sampling strategy is often used by botanists to sample for rare plant species suspected of forming clusters within the larger population. For botanists, the strategy involves searching for a rare plant until one is found and then focusing the search near the discovered plant, as one would expect that there would be more of this plant species nearby. This sampling strategy is considered adaptive because the design is not completely predictable but rather adapts to the search as it happens.

Adaptive cluster sampling can be applied to severe thunderstorm microevents because, like rare plants, microevents often occur in clusters. That is, a localized area favorable for severe convection will likely generate multiple severe weather-producing cells. The cluster sampling strategy is implemented using the model's daily smoothed and augmented probability distributions as the seeds for stochastic events. First, a point is drawn at random from the distribution and placed according to the original probability surface. Areas immediately surrounding the "touchdown" location of the first stochastic microevent then have an increased probability of hosting a subsequent microevent. Each sub-peril uses separate clustering parameters, which were based on comparisons of modeled results with storm reports. The procedure continues, each time increasing the probability around each placed microevent.

The combination of using meteorological and statistical smoothing with adaptive cluster sampling allows meteorologically plausible, yet unrecorded, outbreaks to occur.

As an example, Figure 18 shows four stochastic simulations. The black dots show the locations of the microevents for each simulation. The simulation shown on the bottom right is possible because meteorological and statistical smoothing created the probability of generating events in eastern and central Texas and adaptive cluster sampling allowed for realistic outbreak patterns.

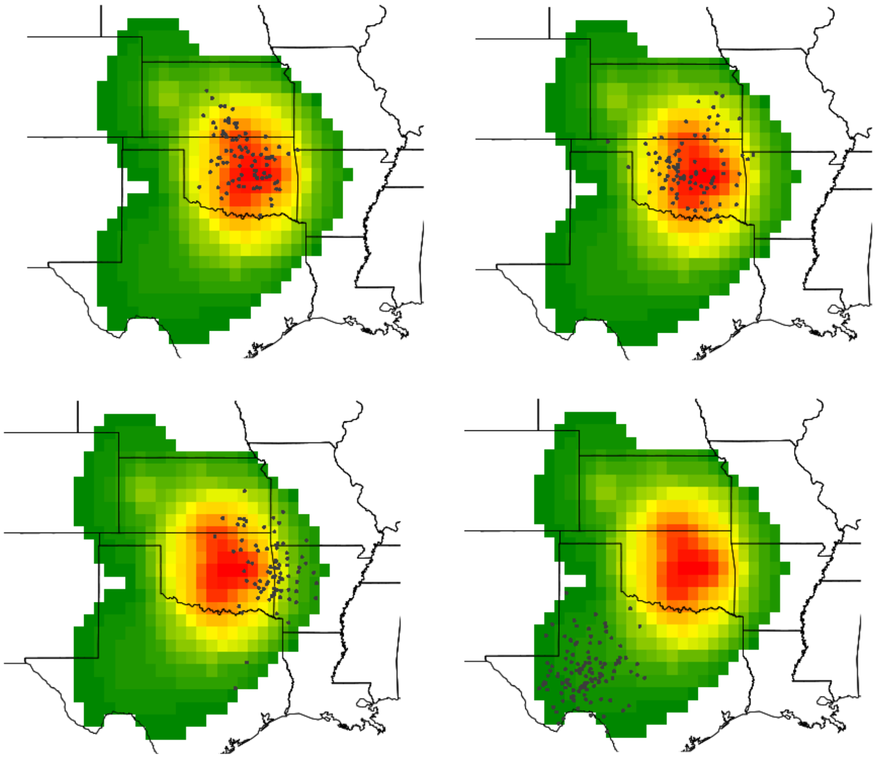

Figure 18. Four stochastic tornado simulations based on the May 10, 2010 seed date.

Note that the stochastic events generated in Figure 18 constitute samples from the smoothed distributions for this particular historical day. As the number of simulation years increases, the spatial distribution of simulated microevents will approach the distribution shown in the background of the figure.

Storm-track Direction

The direction of each microevent depends on its starting location. Daily predicted storm motion vectors are calculated from CFSR data using the right-moving supercell motion equation from Bunkers et al. (2000). Since CFSR data is available on a 6-hourly time resolution, the daily average of each vector component (x and y) is calculated, and the direction is calculated from the average components. The model assumes that the most likely direction is similar to that of the storm motion vector at the microevent's starting location. This direction given by the reanalysis is then perturbed slightly to obtain each microevent's unique simulated storm track direction.

3.4 Modeled Storm Variables

Verisk's stochastic catalog is built based on detailed historical frequency and storm track information. Attributes (length, width, direction, and intensity) for all microevents are randomly drawn from distributions developed from the historical data (for hail, these data include radar data) to create a complete range of possible scenarios. The simulated microevents are then clustered to create macroevents. Each event in Verisk's resulting stochastic catalog contains storm parameters and includes a starting location, storm track direction, storm length and width, and intensity.

See Also

Local Intensity Calculation

Hazard Footprints for Historical Events

Hazard footprints, or swath sizes, are derived from the dimensions of historical severe thunderstorm microevents. For wind these dimensions were derived from clustered SPC reports; for hail, the radar dataset was used.

See Also

Statistical Detrending of SPC Storm Reports

Footprint Length and Width

Footprint length is the distance along the axis of storm motion, and footprint width is the cross-swath distance. They are determined through empirically fit cumulative distribution functions (CDFs) developed using historical observed swaths and vary by sub-peril, location, and season. Unlike microevent frequency and location, these distributions are not specific to the historical seed date, but some vary seasonally and spatially, which allows for realistic variation in microevent attributes.

See Also

Swath Length
Swath Width

Hail

To define hail microevent footprint length, width, and intensity, Verisk researchers create empirical CDFs from filtered radar-based swaths for each 0.5-degree grid cell in the model domain and for each month of the year. These filtered radar-based swaths are generated using 2-km national gridded composite radar reflectivity imagery from 1996-2017 along with SPC reports, as discussed earlier. This Cumulative Distribution Function-generation (CDF-generation) process involves both spatial and temporal smoothing as well as additional inverse distance weighted (IDW) interpolation to further spatially-smooth the CDFs.

Specifically, for a given grid cell during a given month, radar-based swaths that occurred within 2 degrees of the grid cell and within plus or minus one month of the selected month are used to create empirical CDFs if the number of swaths exceeds 250. This process allows for a higher number of hail swaths to be sampled for creating the microevent attribute CDFs than using a single 0.5-degree grid cell alone. An example is shown in Figure 19 below.

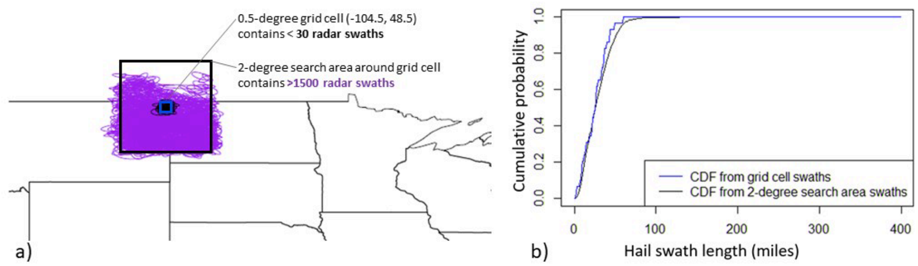

Figure 19. Example showing how using a 2-degree search area around a sample grid cell instead of a single 0.5-degree grid cell alone allows a much higher number of hail swaths to be sampled for creating the microevent attribute CDFs
a) A single 0.5-degree grid cell may contain too few radar swaths to create smooth hail swath length, width, and intensity CDFs. By adding a 2-degree search window around each grid cell, many more radar swaths are available to create hail swath length, width, and intensity CDFs. b) Hail microevent attribute CDFs are much smoother when they are created from many swaths (black) pulled from the 2-degree search area than from few swaths (blue) pulled from the grid cell alone.

If fewer than 250 swaths are identified in a given grid cell, then that grid cell's CDF is temporarily assigned as "NA" but later filled in using IDW interpolation of the surrounding grid cells' distributions. Verisk researchers determined the appropriate swath threshold number (N = 250) to use by dividing the hail swath length, width, and intensity standard error by the mean for each month according to:

$$N = \left(\frac{stdev}{0.05 \times mean}\right)^2$$

For hail swath, width, and intensity in each month, N ranges from 200 to 300 swaths. As a result, a 250-swath target was selected.

For grid cells that contain greater than 250 swaths, radar-based swaths are first used to compute kernel density estimates of the probability density function (PDF) for hail length, width, and intensity for the given grid cell. Then, these PDFs are cumulatively summed to result in monthly CDFs for each hail attribute for each grid cell in the model domain. The smooth CDFs created closely follow the observational data but avoid introducing biases due to data scarcity.

For grid cells that contain fewer than 250 swaths, empirical CDFs are created by spatially smoothing each bin of the monthly CDFs in the surrounding grid cells using IDW interpolation. The resulting hail swath length, width, and intensity empirical CDFs for each month and grid cell in the model domain are uncontaminated by biases due to small sample sizes and reflect both seasonal and spatial variation.

Since hail swath length and width are correlated, Verisk researchers use a Gaussian copula method to simulate them in a three-step process. First, random correlated variables are generated from standard normal distributions by generating a random standard normal. Then, a second, correlated random standard normal is generated using the equation:

$$x_2 = r \times x_1 + \sqrt{(1 - r^2)} \times N(0, 1),$$

where x_1 and x_2 are the correlated standard normal variables, r is the correlation coefficient, and N(0,1) is a random standard normal. The correlation coefficient used is 0.585 and was determined by calculating the Spearman correlation coefficient from the radar-based storm swath lengths and widths. Once these correlated standard normals are generated, their probabilities are calculated using the standard normal cumulative distribution function. Finally, the empirical marginal CDFs created from the radar-based swaths are used as quantile functions to transform probability to the length and width of a hail swath.

See Also

Radar Reflectivity

Straight-line Winds

To define convective straight-line wind footprint length and width, Verisk researchers create empirical CDFs from clustered storm reports. These distributions are created by kernel density smoothing the observed lengths and widths for each month for non-derecho dates, and for the whole year for derecho dates. The same method of simulating correlated hail length and width swaths is used for straight-line wind swath simulation. A correlation coefficient of 0.714 is used and was determined from clustered SPC reports' swaths.

Footprint Shape

While the rectangular swath shown in Figure 20 realistically captures the size of the historical microevents, the shape is not necessarily representative of a microevent's true hazard footprint. Therefore, when generating swath sizes for the simulated events, the model translates the rectangular dimensions into those of ellipses. As shown schematically in Figure 20, the length of the ellipse's minor axis is set equal to the length of the short side of the rectangle and the length between the ellipse's two foci (light blue dots) is set equal to the length of the long side of the rectangle.

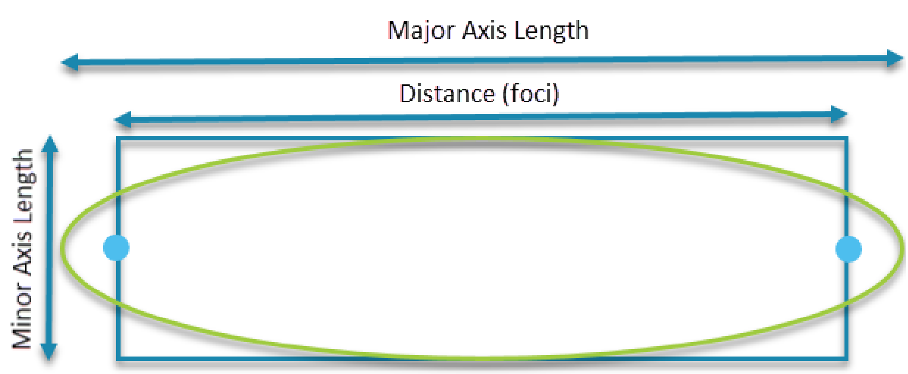

Figure 20. Schematic drawing of an ellipse placed around a microevent (Source: Verisk)

3.5 Validating Event Generation

The Verisk Crop Hail Model for the United States uses the 10-K all-events catalog from the Verisk Severe Thunderstorm Model for the United States. This catalog has been extensively validated against the available historical data. This section provides validation of the model's spatial event frequency distributions, seasonality, and microevent attribute correlations.

Spatial Frequency Distributions

Average Annual Days

A common method used to measure severe thunderstorm frequency is by days per year. By definition, a location or area experiences a severe day if there is at least one occurrence of severe weather on a given day. The number of days is then summed for the year to determine the annual count. This calculation is performed over a defined number of years to determine the average annual severe days for the defined time period.

Verisk researchers validate the Verisk Severe Thunderstorm Model for the United States by comparing the model-simulated average annual severe days by state and sub-peril to the number of severe days in the clustered SPC storm reports. Due to the stability in the reported number of severe days in the last couple decades, reports between 2000 and 2018 are used to create the observed severe days. Since it is very computationally intensive to compute the full ellipse to state polygon intersections, only the ellipse centroids are used to assign an ellipse to a state. This methodology leads to an underestimate in severe weather days assigned to a given state because an ellipse can intersect multiple states, but the centroid would only be inside one of these states. However, this underestimate is small for most states, and because the same method is used for both modeled and observed days, it is a fair comparison.

Figure 21, and Figure 22, below are scatter plots of model versus observed average annual severe hail, and straight-line wind, respectively, with each point in the plot representing a state. As evident in these figures, there is good agreement between Verisk-modeled and observed average annual severe days. In the hail plot (Figure 21), the blue dots represent model validation against a second set of observations derived from radar swaths for the periods 1996-2002 and 2005-2017 (2003 and 2004 are missing). Hail (Figure 21) average annual days show no clear bias, with all points distributed around the y=x (1:1) line. Average annual straight-line wind days (Figure 22) shows a small low bias, meaning the model simulates fewer days than observed. This behavior is expected because the observed SPC data has a noted high bias in estimated gusts and many wind reports may actually be less than severe intensity. Thus, the true severe wind frequency may actually be lower than what is reported.

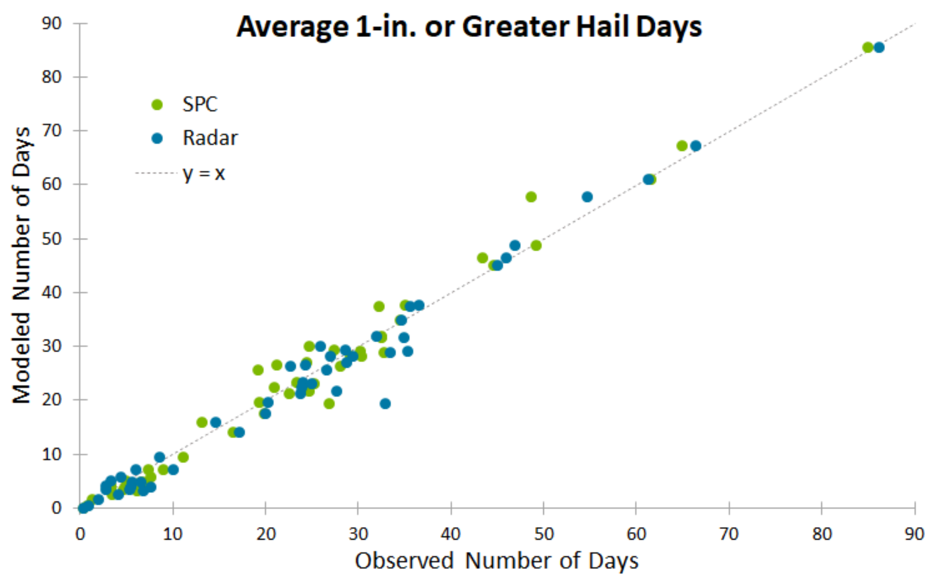

Figure 21. Verisk-Modeled versus observed average annual severe hail days (1-in. or greater) by state
Green dots represent model simulated versus 2000-2018 SPC observations. Blue dots represent model simulated versus 1996-2017 radar observations. Note: Each state's annual average value is represented by a dot.

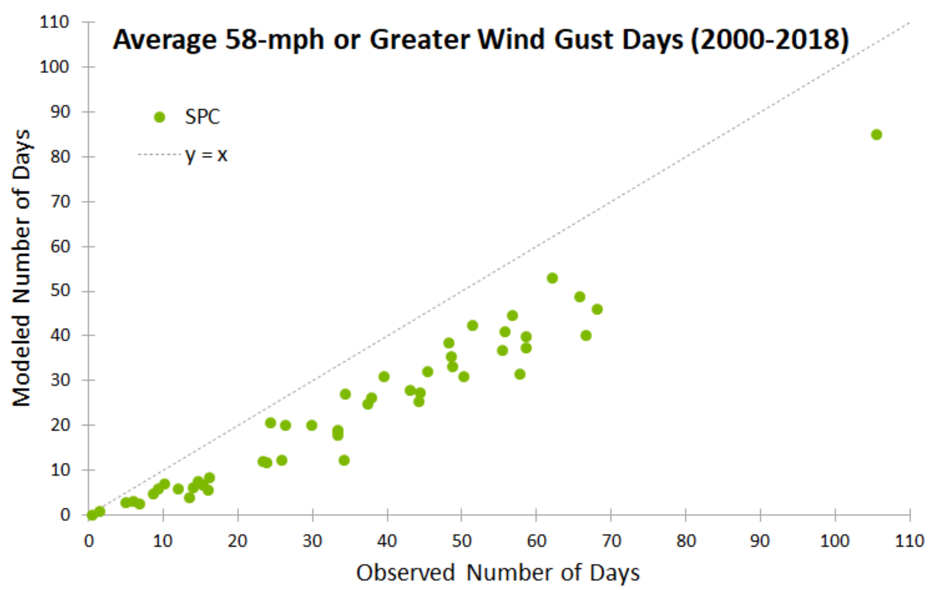

Figure 22. Verisk-modeled versus observed (SPC storm reports; 2000-2018) average annual severe straight-line wind days (58-mph or greater) by state
Note: Each state's annual average value is represented by a dot

Hits

The following set of images shows the spatial variation in average annual severe thunderstorm days by sub-peril on a regular 0.5-degree latitude/longitude grid ("hit" maps).

Verisk model simulated hit maps are based on the 10K stochastic catalog, and observed hits are based on SPC reports from 2000 to 2018. As a result, the observed maps are much noisier than the modeled maps and show the previously-described population biases. Overall, there is good agreement between these model-simulated and observed spatial frequency maps.

The Verisk model-simulated average annual severe hail (1-in. or greater) days (Figure 23) depicts an area of greatest hail activity that extends from Texas northward into the Dakotas, with a maximum in Kansas and Nebraska. A local maximum also exists in North and South Carolina, east of the Appalachian Mountains. Hail frequency rapidly decreases west of the Rocky Mountains and in the Northeast. The observed spatial pattern (Figure 24) looks very similar to the model but with magnitudes being notably lower. These lower magnitudes are a result of underreporting, particularly in many locations where hail occurs most frequently.

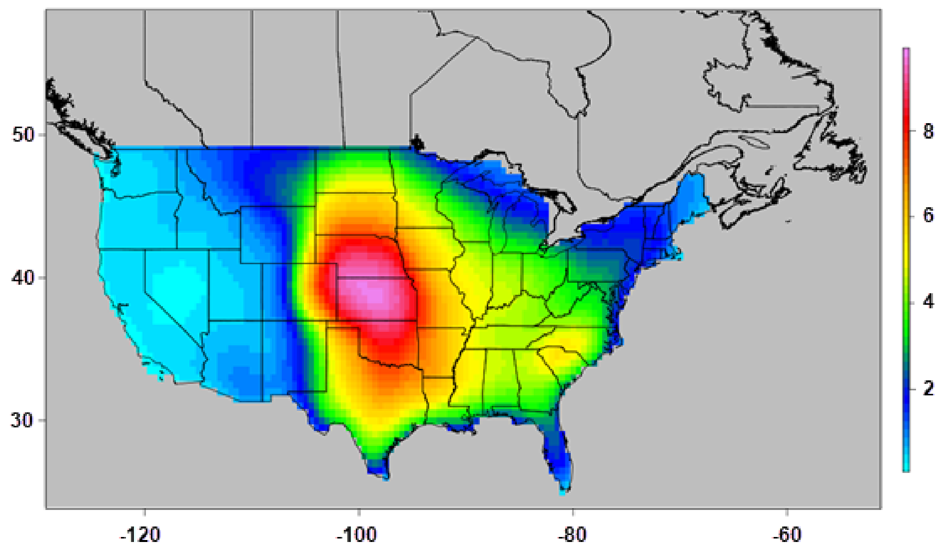

Figure 23. Verisk model-simulated average annual severe hail days (1-in. or greater) based on the 10,000-year stochastic catalog

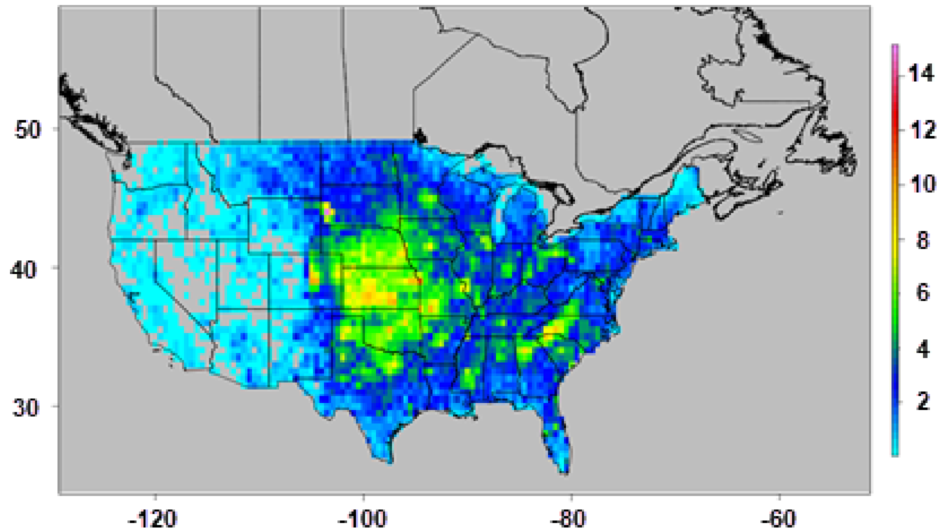

Figure 24. Observed average annual severe hail days (1-in. or greater) based on the SPC Storm Reports database from 2000 to 2018

The Verisk model-simulated average annual significant hail (2-in. or greater) days (Figure 25) has a very similar pattern as the modeled average annual severe hail frequency (Figure 23) but with lower magnitudes. The location of maximum frequency is shifted northwestward slightly toward the Kansas/Nebraska/Colorado intersection. The observed significant hail frequency spatial pattern (Figure 26) has its maximum farther south than the modeled significant hail frequency, but the magnitudes are similar in that area.

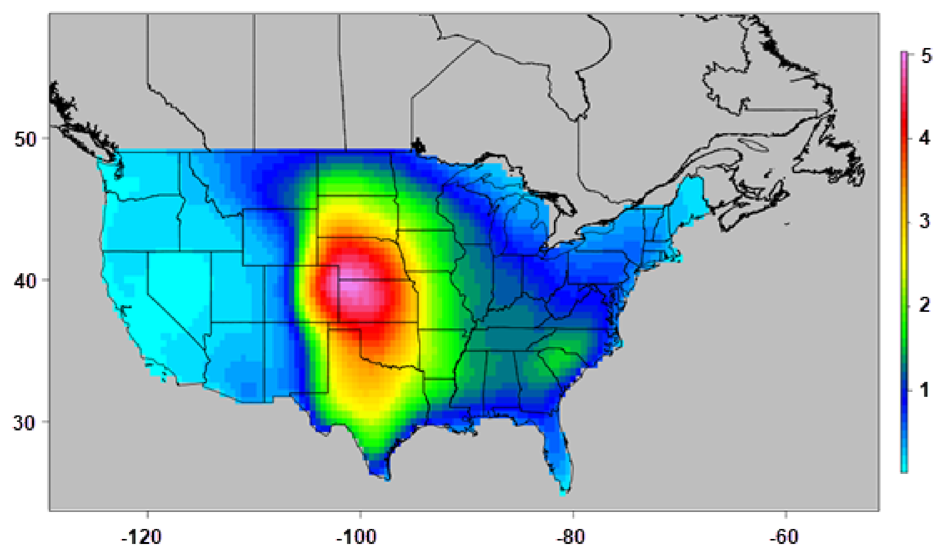

Figure 25. Verisk model-simulated average annual significant hail days (2-in. or greater) based on the 10,000-year stochastic catalog

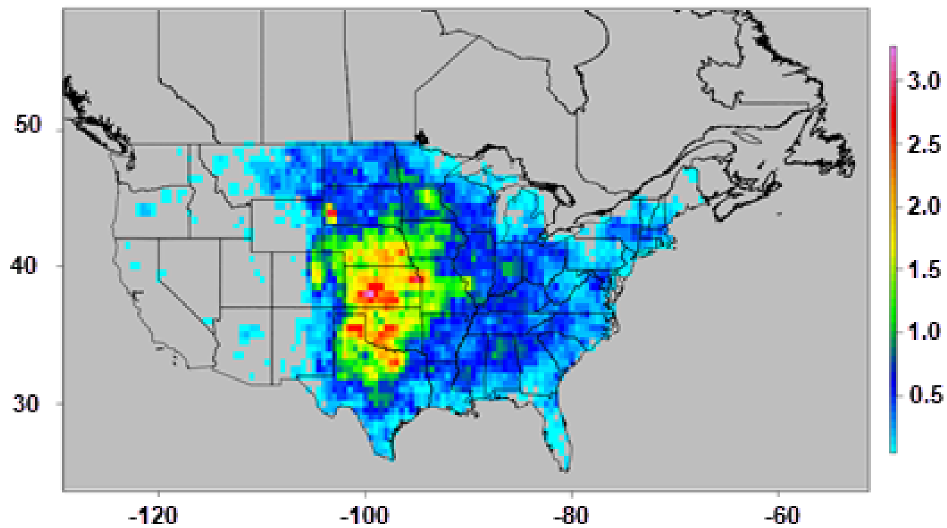

Figure 26. Observed average annual significant hail days (2-in. or greater) based on the SPC Storm Reports database from 2000 to 2018

The Verisk model-simulated average annual severe 58-mph or greater convective straight-line wind speed days (Figure 27) depicts a large area of greatest wind activity that encompasses much of the South and the southern portion of the Midwest. The observed 58-mph or greater wind speed frequency spatial pattern (Figure 28) also has a large area of maximum wind frequency across much of the South and southern portion of the Midwest, but with its maximum frequency expanded slightly farther north into the Mid-Atlantic.

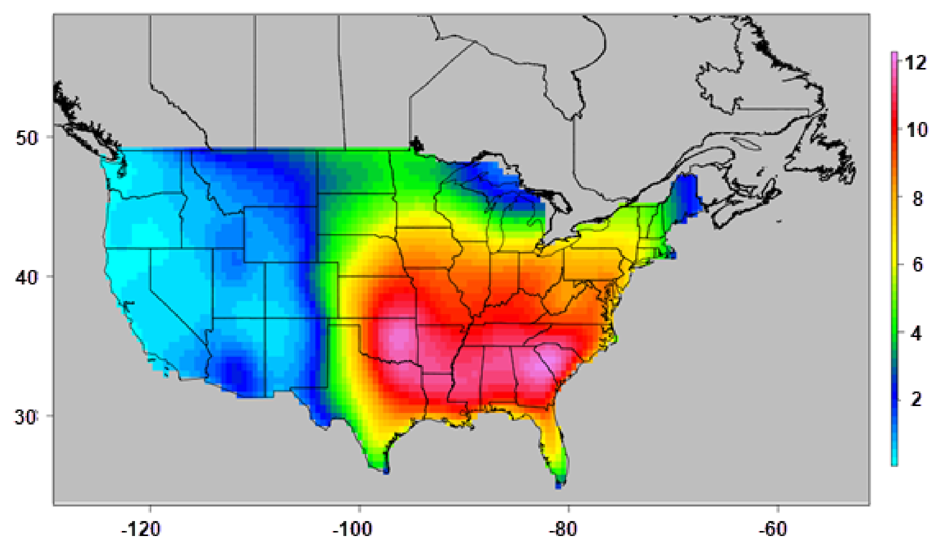

Figure 27. Verisk model-simulated average annual severe convective straight-line wind speed days (58 mph or greater) based on the 10,000-year stochastic catalog

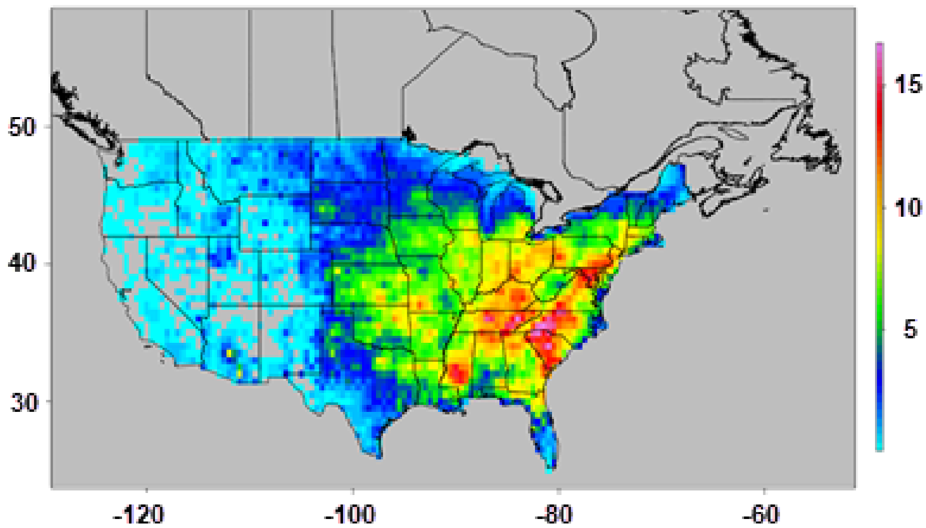

Figure 28. Observed average annual severe convective straight-line wind speed days (58 mph or greater) based on the SPC Storm Reports database from 2000 to 2018

The Verisk model-simulated average annual severe 75-mph or greater convective straight-line wind speed days (Figure 29) depicts an area of greatest wind activity that extends from Texas northward into the Dakotas, with a maximum in Kansas and northern Oklahoma. The observed 75-mph or greater wind speed frequency spatial pattern (Figure 30) shows a similar area of high wind frequency but with maxima over western Kansas (instead of central Kansas) and over Montana and North Dakota.

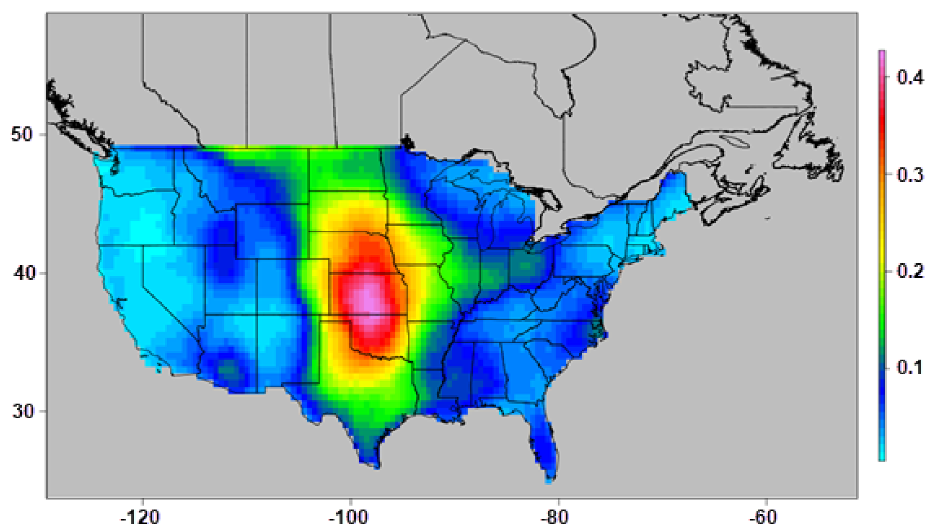

Figure 29. Verisk model-simulated average annual 75-mph or greater convective straight-line wind speed days based on the 10,000-year stochastic catalog

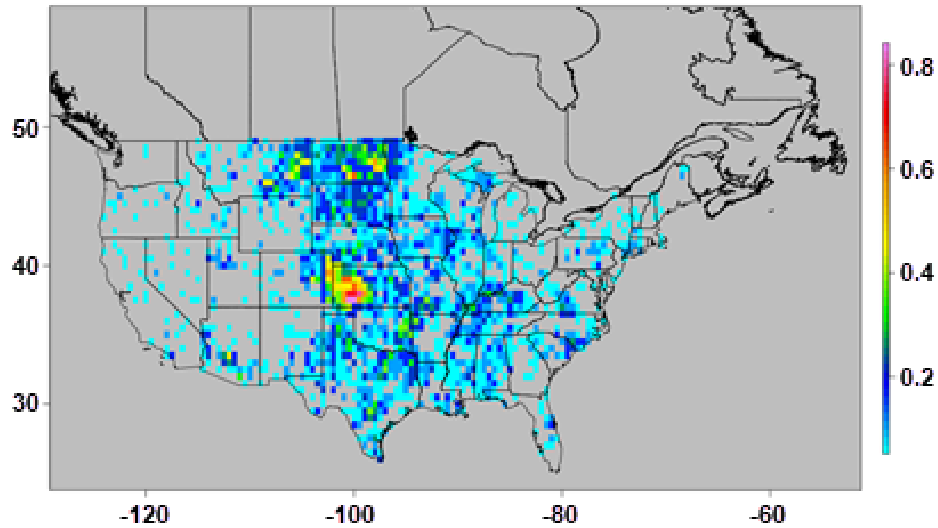

Figure 30. Observed average annual 75-mph or greater convective straight-line wind speed days based on the SPC Storm Reports database from 2000 to 2018

Seasonality

Verisk researchers validated Verisk model-simulated seasonality by comparing model-simulated to observed monthly relative occurrence frequencies. The observed monthly frequencies are based on SPC's Storm Reports database from 2000 to 2018, and the Verisk-modeled monthly frequencies are based on Verisk's 10K all-events catalog. In addition, a second set of observations derived from radar swaths for the periods 1996-2002 and 2005-2017 (2003 and 2004 are missing) is available for hail. The Verisk model, SPC's Storm Reports data, and radar-derived seasonality show similar frequencies in sub-peril activity throughout the year with 1-in. or greater diameter hail peaking in May and June (Figure 31) and 58-mph or greater convective straight-line wind activity peaking in June and July (Figure 32).

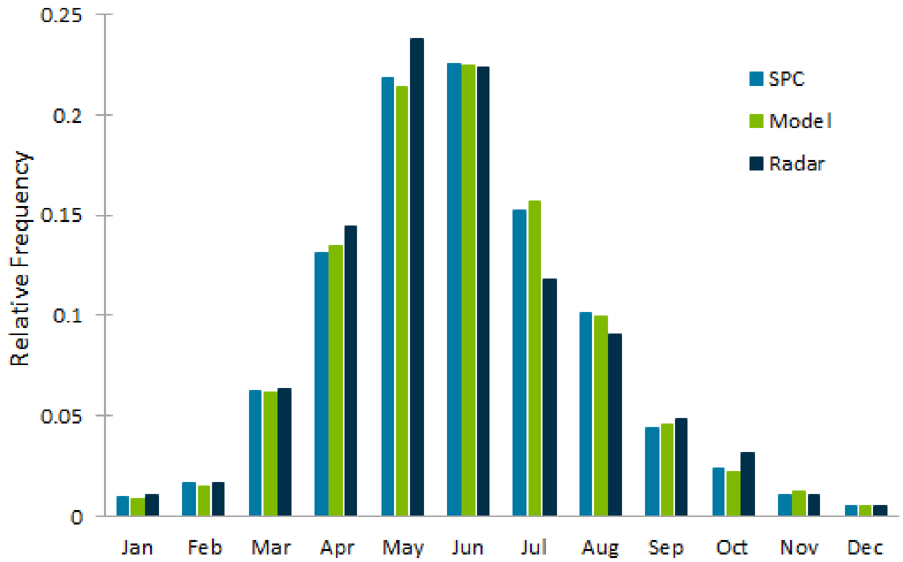

Figure 31. Seasonal distribution of 2000-2018 SPC-observed (light blue bars), 1996-2002 and 2005-2017 radar-derived (dark blue bars), and Verisk model-simulated (10K all-events catalog; green bars) 1-in. or greater hail counts

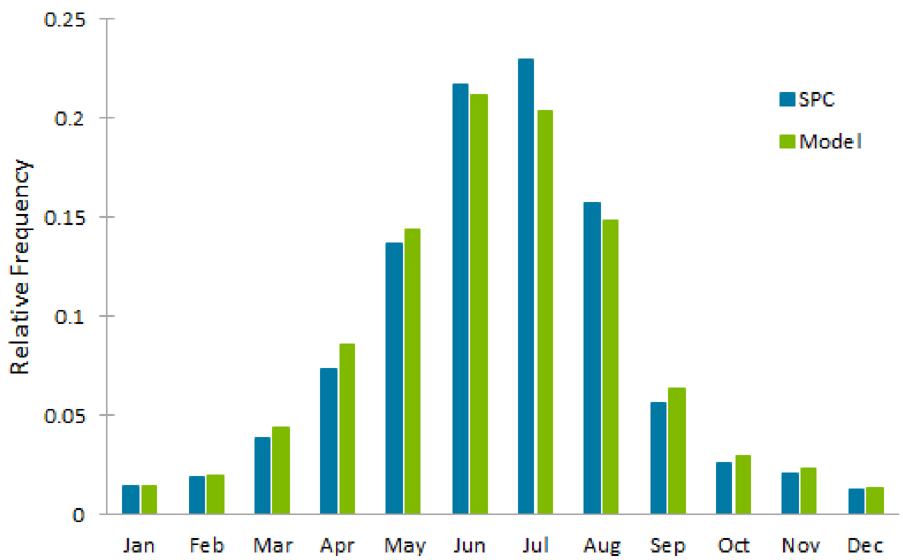

Figure 32. Seasonal distribution of 2000-2018 SPC-observed (light blue bars) and Verisk model-simulated (10K all-events catalog; green bars) 58-mph or greater convective straight-line wind counts

Swath Length

Verisk researchers validated Verisk model-simulated swath length by comparing model-simulated to observed swath length relative occurrence frequencies for the individual hail and straight-line wind sub-perils (Figure 33, Figure 34,). The observed frequencies are based on

SPC's Storm Reports database from 2000 to 2018, and the Verisk-modeled frequencies are based on Verisk's 10K all-events catalog. In addition, a second set of observations derived from radar swaths for the periods 1996-2002 and 2005-2017 (2003 and 2004 are missing) is available for the hail sub-peril. As seen in these figures, in general, the straight-line wind compare well to those in the historical record.

For hail , there are reasonable patterns among the Verisk-modeled, reported (SPC), and radar-derived hail swath lengths. Specifically, for hail swaths of moderate to long lengths (20-30 mi and longer), the modeled swath length relative frequency is lower than radar but higher than SPC reports. This relationship is expected because, in general, SPC-reported swath lengths may underestimate the true swath length (due to difficulty in resolving the ends of the swath where hailstones are sparse), while radar-derived swath lengths represent overestimates of the true swath dimensions (Giammanco and DeCiampa, 2018). In addition, the high relative frequency of shorter swath lengths (0-10 mi and 10-20 mi in length, specifically) in the SPC data reflect the fact that reported swath lengths are underestimates of the true swath lengths. It would be expected that some of the 'true' longer swath lengths (>20 mi) have had their length underestimated in the SPC data and are therefore reflected in a smaller bin than they would have been if the true swath length had been observed. Similarly, the overestimation of swath length relative frequencies present in the radar-derived data result in some of the 'true' shorter swath lengths (0-10 mi and 10-20 mi in length, specifically) being overestimated in the radar-derived data. Therefore, these 'true' shorter swath lengths are classified into a larger bin than they would have been if the true swath length had been derived.

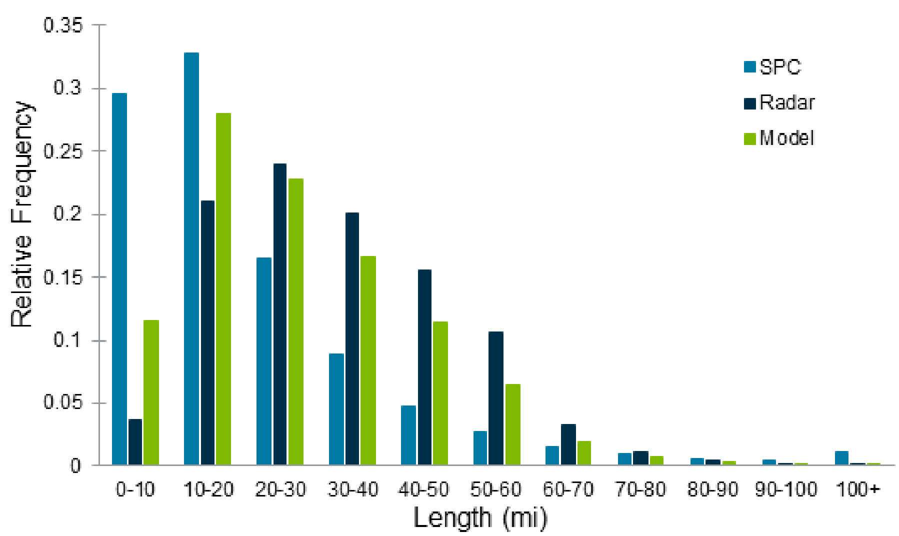

Figure 33. Comparison of the relative occurrence frequency of 1-in. or greater hail swath length distributions between Verisk model-simulated (10K all-events catalog; green bars), 2000-2018 SPC-observed (light blue bars), and 1996-2002 and 2005-2017 radar-derived (dark blue bars) events

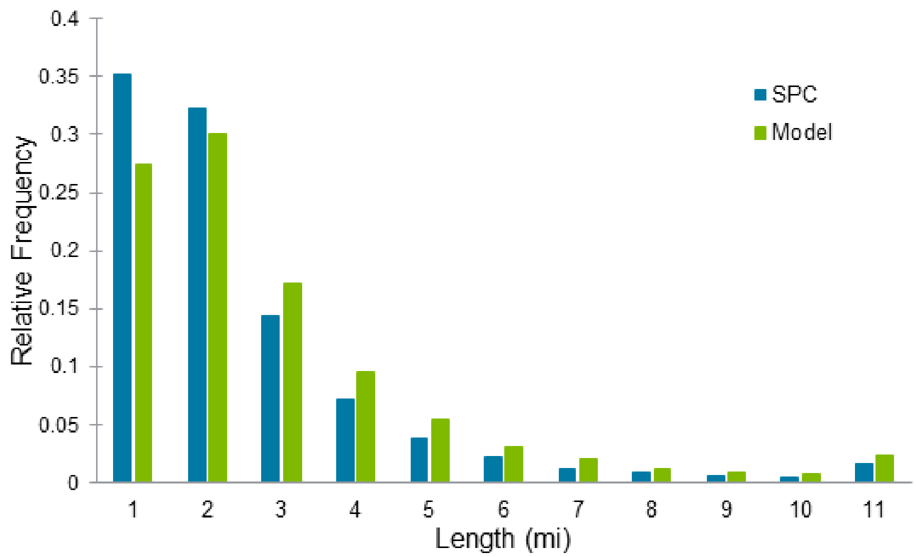

Figure 34. Comparison of the relative occurrence frequency of 58-mph or greater convective straight-line wind swath length distributions between Verisk model-simulated (10K all-events catalog; green bars) and 2000-2018 SPC-observed (light blue bars) events

See Also

Footprint Length and Width

Swath Width

Verisk researchers validated Verisk model-simulated swath width by comparing model-simulated to observed swath width relative occurrence frequencies for the individual hail and straight-line wind sub-perils (Figure 35, , and Figure 36, respectively). The observed frequencies are based on SPC's Storm Reports database from 2000 to 2018, and the Verisk-modeled frequencies are based on Verisk's 10K all-events catalog. In addition, a second set of observations derived from radar swaths for the periods 1996-2002 and 2005-2017 (2003 and 2004 are missing) is available for the hail sub-peril. As seen in these figures, overall, the values compare well to those in the historical record.

There are reasonable patterns among the Verisk-modeled, reported (SPC), and radar-derived hail swath widths. Specifically, for narrower hail swaths (≤10 mi), the modeled swath width relative frequency is higher than SPC reports whereas, for moderate to wide hail swath widths (>10 mi), the modeled swath width relative frequency is lower than SPC reports. This relationship is expected because, in general, swath widths derived from SPC reports may actually be a combination of more than one swath. As a result, some of the 'true' narrower swath widths (≤10 mi) have had their width overestimated in the SPC data and are therefore reflected in a larger bin than they would have been if the true swath width had been observed. While the Verisk-modeled and radar-derived hail swath width relative frequencies compare well overall, the radar-derived wide bias (i.e., actual hail swaths tend to be narrower than radar-based storm swaths) is evident when comparing the relative frequencies of the 0 - 5 mi bin to the 5 - 10 mi bin.

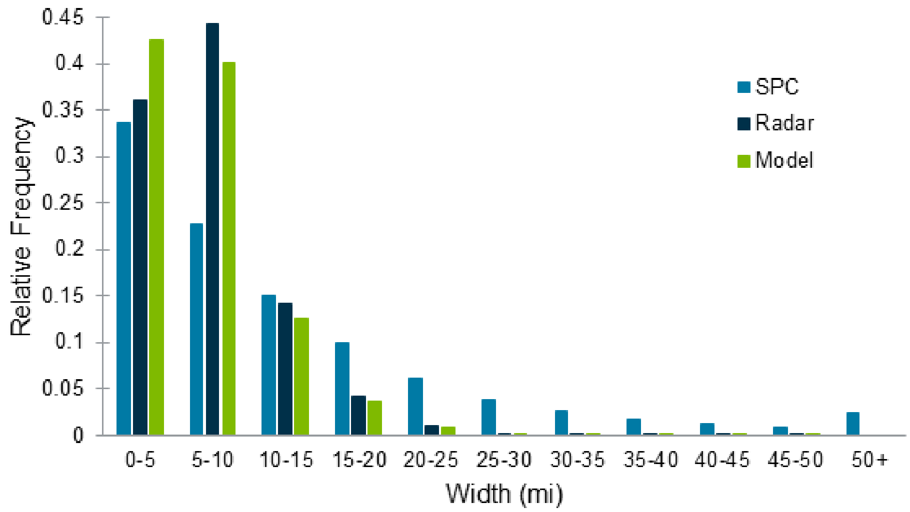

Figure 35. Comparison of the relative occurrence frequency of 1-in. or greater hail swath width distributions between Verisk model-simulated (10K all-events catalog; green bars), 2000-2018 SPC-observed (light blue bars), 1996-2002 and 2005-2017 radar-derived (dark blue bars) events

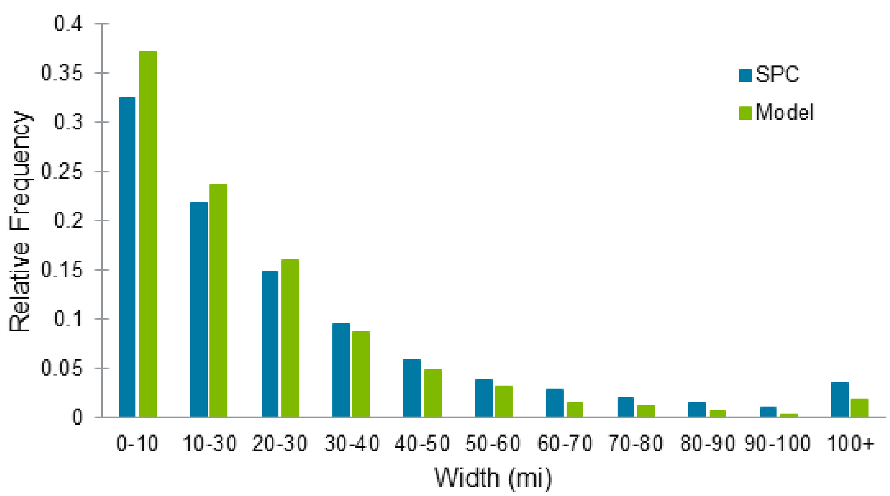

Figure 36. Comparison of the relative occurrence frequency of 58-mph or greater convective straight-line wind swath width distributions between Verisk model-simulated (10K all-events catalog; green bars) and 2000-2018 SPC-observed (light blue bars) events

See Also

Footprint Length and Width

4 Local Intensity Calculation

In the local intensity component of the Verisk model, hailstorm intensity is represented by hail impact energy (J/m^2) (a measure of total kinetic energy), derived from the maximum reported hail diameter. For convective straight-line winds, intensity is represented as an average 3-sec wind speed gust (mph), derived from the mean reported 3-sec gust from all the SPC reports within the footprint. An average wind speed is used because the clustered wind footprints tend to be quite large, but only a small fraction of the footprint experiences the highest of reported wind speeds. Using a 3-sec average gust allows the wind footprints to be reasonably large but still produce realistic loss estimates.

For each of these intensity parameters, cumulative distribution functions (CDFs) are fit on a moving 0.5° by 0.5° grid by season based on the clustered SPC reports and radar-based footprints. Note that to account for uncertainty around the reported values, kernel density estimation was used to smooth the clustered reports into other-sized bins using a 5° by 5° moving window. SPC hail reports, for example, are typically given in terms of objects more familiar to observers (e.g., baseballs, golf balls, quarters, etc.), which leads to inexact measurements.

To simulate events that are stronger or weaker than what is represented in the CDFs, correlation is imposed within outbreaks by making daily, yearly, and microevent adjustments to intensity and swath counts. These adjustments and the reasoning for each adjustment are as follows:

- Yearly adjustments are made because some years have a higher frequency of severe convective weather events than other years.
- Daily adjustments are made because, regardless of the seed day, a simulated day may be more or less convectively-active than expected.
- Microevent adjustments are made because individual microevents may occur in very convectively-favorable or convectively-unfavorable areas (according to the severe weather index values), and it is necessary to account for this behavior.
- Once a simulated event's intensity parameter is determined, the intensity at each location affected by the event is calculated as discussed below.

See Also

Modeled Storm Variables

4.1 Local Intensity Calculation Data Sources

To thoroughly analyze hail and convective straight-line wind intensity risk in the conterminous United States, Verisk researchers use information from several agencies, which are listed below.

NOAA's SPC and NCEI Storm Reports	Historical hail, convective straight-line wind https://www.spc.noaa.gov/wcm/#data Dates: 1979 to 2018
Community Collaborative Rain, Hail, and Snow (CoCoRaHS) Network	Historical hail point data https://www.cocorahs.org/ViewData/ Dates: 1998 to 2018
Severe Hazards Analysis and Verification (SHAVE) Project	Historical severe weather point data https://www.nssl.noaa.gov/projects/shave/ Dates: Mid-spring through late summer, 2006 to 2015
Insurance Institute for Business and Home Safety (IBHS) Severe Hail Field Study	Historical severe hail point data (e.g., maximum and mean hail size, duration, area impacted) in the Central Plains region https://ibhs.org/hail/hailstones/ Dates: Spring Season, 2015 to 2019
NOAA's Next Generation Radar (NEXRAD) Level III Data	Individual radar site reflectivity data, storm cell ID, predicted probability of hail, predicted probability of severe hail, predicted maximum hail size, and hail index overlay products https://www.ncdc.noaa.gov/nexradinv/ Dates: 1996 to 2017 Resolution: 2-km grid spacing; 10-min time intervals
Verisk Weather Solution's RESPOND® Hail Analysis	Near real-time radar-derived hail footprints https://www.verisk.com/insurance/products/respond/hail-analysis-precision/ Dates: 2010 to 2012 (corresponding to the dates of the marquee event set)

4.2 Hail Impact Energy

Verisk researchers have developed a formulation for hail impact energy that consists of a vertical component, which is the primary source of hail damage, and a horizontal component. Both components are defined in terms of kinetic energy flux density, which is the rate of energy transfer per unit area and is measured in J/m^{2}s. The vertical component is a result of the momentum of falling hailstones, while the horizontal component is due to the horizontal advection of hailstones by accompanying winds. The total kinetic energy flux density is, therefore, the sum of the horizontal and vertical components.

The general form of the equation used to calculate these components is given by Waldvogel et al. (1978) as follows:

$$KE = \frac{(\pi \times \rho_{hail})}{(12 \times 10^6)} \int_0^\infty n(D) \times D^3 \times (v(D))^3 \, dD \qquad (1)$$

where $n(D)$ is the concentration of hailstones of diameter, D, per unit volume, $v(D)$ is either the terminal fall speed or the maximum horizontal speed, and ρ_{hail} is the density of hail (900 kg/m^3). The terminal fall speed is given by Mason (1971) as follows:

$$v = v_o D^{1/2} \quad (2)$$

where $v_o = 4.41 \ m/(s \cdot mm^{0.5})$. The maximum horizontal speed was obtained by solving for hailstone velocity after being exposed to the wind force for the amount of time it takes a hailstone to travel from the cloud to the ground, or approximately 1,000 meters.

By integrating hailstone number concentrations (hailstones/m^3), terminal fall speeds or maximum horizontal speeds, and hailstone size, the total kinetic energy formulation and its components can account for hail impact energy variability within a single hail swath. This variability is due to the differences in hailstone shapes and sizes (which reach different maximum velocities and result in different hail impact energies) present in a hail swath.
To compare the modeled kinetic energy calculation to those from published studies (e.g., the Tornado and Storm Research Organization (TORRO) Hailstorm Intensity Scale), the results from Equation 1 are multiplied by a time factor such that the resulting values have units of J/m^2. The values for time are obtained by drawing from a log-normal distribution that represents the full range of possible durations a single point within a hail swath could experience from hailstones of various sizes.

For the Verisk Severe Thunderstorm Model for the United States, Verisk researchers developed hailstone number concentration distributions very similar to the Marshall-Palmer distributions, which use inverse exponential relationships to accurately represent various rainfall rates (Marshall and Palmer, 1948). The Marshall-Palmer distribution is represented in general form as follows:

$$n(\mathrm{D}) = n_0 e^{-\Lambda D} \quad (3)$$

The distributions are parameterized by the y-intercept, n_0 (number of raindrops with a diameter of 0 mm), and the slope, $-\Lambda$.

According to the Marshall-Palmer distribution equation, as the rainfall rate increases, so does the number of large diameter raindrops. For example, given a rainfall rate of 1 mm/hr, the concentration of 2 mm raindrops is roughly 10^0, or 1 raindrop/m^3, whereas it increases to about 10 drops/m^3 for a rainfall rate of 5 mm/hr. Thus, the distributions implemented for the simulated hail swaths are based upon the maximum reported hail size for the clustered reports. The choice of maximum hail size as opposed to average hail size is further justified by previous studies in both the meteorological and engineering communities that have typically focused on maximum hail size in relation to damage estimation due to hailstorms.

The final equation for the vertical kinetic energy that results from substituting Equations 2 and 3 into Equation 1 is as follows:

$$KE \;=\; \frac{(v_o^3 \times \pi \times \rho)}{(12 \times 10^6)} \times t \int_{0.022}^{\infty} n_o exp(-\Lambda D) \times D^{9/2} \, \mathrm{d}D \quad (4)$$

Notice that the integral is bounded on the lower end by a diameter size of 22 mm (0.86 in.). Even though the minimum hailstone size assigned for each microevent in the stochastic catalog is one inch in diameter (i.e., consistent with SPC's definition of a severe hail event), hailstones smaller than this diameter can cause damage, especially in the presence of high wind gusts. The model takes this fact into consideration in its hail energy calculation by integrating over all hailstone sizes (i.e., 0.86 in. or greater) capable of producing damaging energy.

The value of Λ is obtained from a mathematical relationship of the form: $\Lambda = aD_{max}^{b}$. This relationship was obtained by iteratively calculating Λ to match energies from the TORRO Hailstorm Intensity Scale shown in Table 5.

Table 5. TORRO hailstorm intensity scale

Intensity Category	Typical Hail Diameter[68] (mm)	Probable Kinetic Energy (J/m^2)	Typical Damage Impacts
H0 Hard Hail	5	0 - 20	No damage
H1 Potentially Damaging	5-**15**	> 20	Slight general damage to plants, crops
H2 Significant	10-**20**	> 100	Significant damage to fruit, crops, vegetation
H3 Severe	20 - **30**	> 300	Severe damage to fruit and crops, damage to glass and plastic structures, paint and wood scored
H4 Severe	25 - **40**	> 500	Widespread glass damage, vehicle bodywork damage
H5 Destructive	30 - **50**	> 800	Wholesale destruction of glass, damage to tiled roofs, significant risk of injuries
H6 Destructive	40 - **60**		Bodywork of grounded aircraft dented; brick walls pitted
H7 Destructive	50 - **75**		Severe roof damage, risk of serious injuries
H8 Destructive	60 - **90**		(Severest recorded in the British Isles) Severe damage to aircraft bodywork
H9 Super Hailstorms	75 - **100**		Extensive structural damage. Risk of severe or even fatal injuries to persons caught out in the open
H10 Super Hailstorms	> **100**		Extensive structural damage. Risk of severe or even fatal injuries to persons caught out in the open

Verisk-modeled hail ellipses have an intensity profile, which is generated by applying a scaling factor to the maximum hail impact energy. This intensity profile was developed based on Verisk researchers' analysis of both IBHS Hail Study and Verisk Weather Solution's RESPOND® data as well as results from published studies. The resulting hail energy profile is shown in Figure 37.

[68] **Bold**: Typical maximum reported diameter

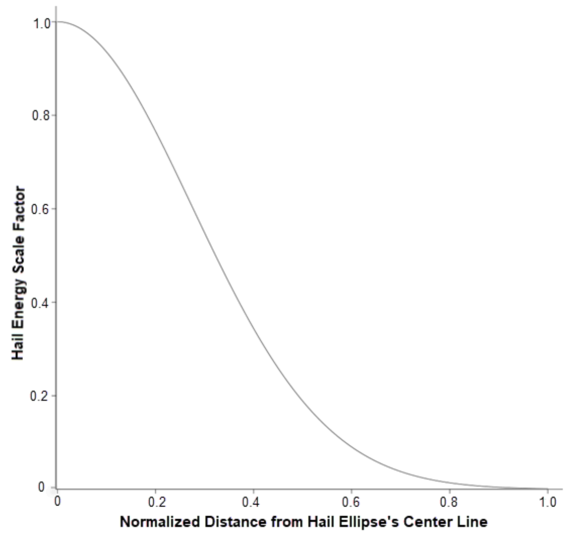

Figure 37. Hail energy swath profile

See Also
Event Definition

4.3 Straight-Line Wind Speeds

Wind speeds assigned to stochastic straight-line wind events are drawn from an empirical CDF derived from the clustered SPC reports. These wind reports can either be measured with instrumentation (e.g., anemometer) or estimated by trained storm spotters, emergency management, NWS employees, or the general public. Research has shown that estimated wind gusts are biased high when compared to wind tunnel experiments (Edwards et al., 2018) or actual measured reports. In some cases, these overestimations can be on the order of 20 - 30% higher than actual wind speeds. Moreover, estimated wind speeds comprise the majority (90%) of the SPC severe wind speed database (Edwards et al., 2018). This value closely matches the percentage of wind speed reports that are estimated (approximately 89%) in the Verisk database beginning in 2006.

To account for the high estimated wind speed bias in SPC's clustered wind speed values, Verisk researchers reduce the SPC wind report values that are labeled or assumed to be estimated by 30%. This procedure is completed for wind bin values of 1 mph for each state in the following steps:

1. Compute the percentage of estimated versus total wind speed report values (i.e., estimated plus measured) from post-2006 SPC data, by state and by wind speed (bin values of 1 mph).
2. Use the corresponding calculated percentage to randomly sample that amount of pre-2006 wind reports that are flagged (i.e., assumed) to be estimated for each state and wind speed.

3. Apply a 30% reduction to the wind speed magnitude for reports that are flagged as estimated.

An example of Verisk's wind speed reduction procedure for the state of Illinois is shown in Figure 38 and Figure 39. Figure 38 shows the relative frequency distributions of the original observed SPC estimated and measured wind speed reports from 2006 to 2018. Figure 39 shows the relative frequency distributions of the 1955-2018 original and resulting Verisk-adjusted observed SPC wind speed reports for the state of Illinois. The original and adjusted mean wind speeds are 54 kts and 46 kts, respectively.

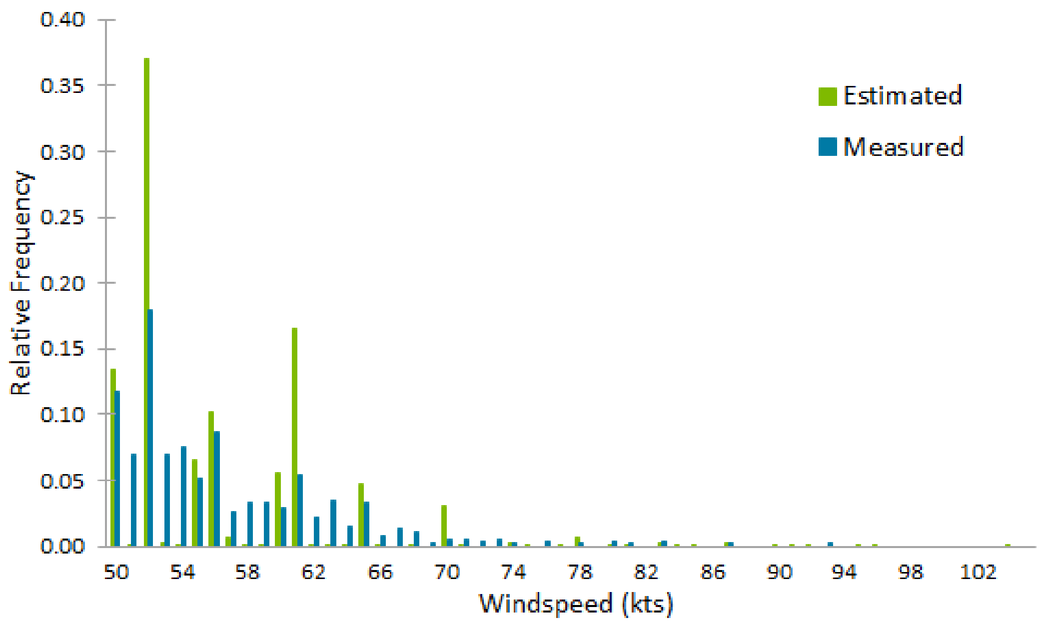

Figure 38. Relative frequency distributions of the 2006-2018 estimated (green) and measured (blue) SPC observed wind speed reports (grouped into 1-kt bins) for the state of Illinois

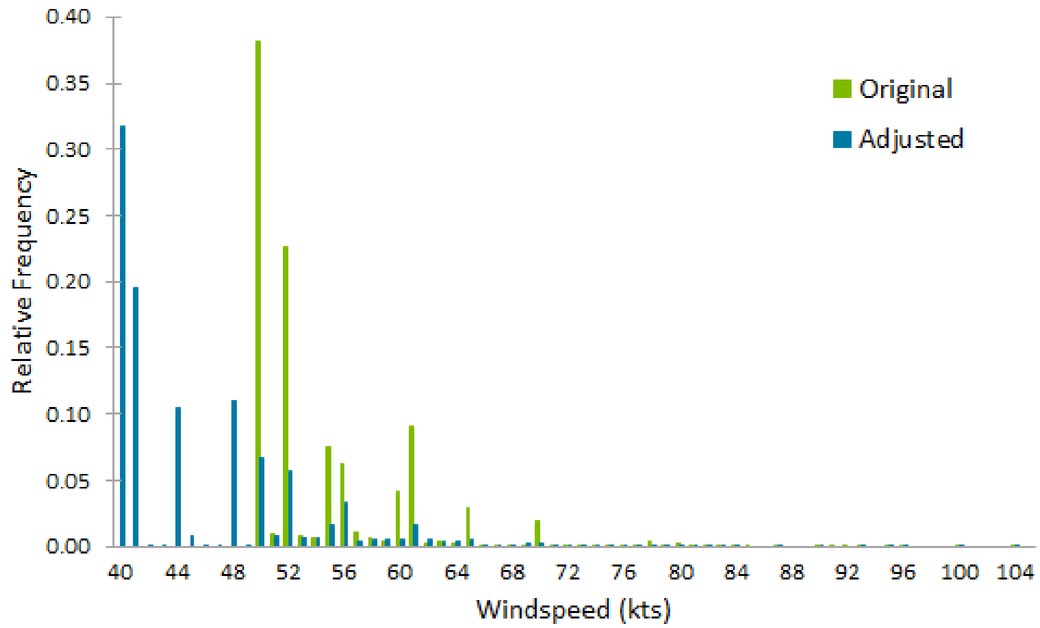

Figure 39. Relative frequency distributions of the 1955-2018 original (green) and adjusted (blue) SPC observed wind speed reports (grouped into 1-kt bins) for the state of Illinois

The following assumptions are made with this wind speed reduction process:

- If a wind bin has less than four reports, the average ratio of the overall estimated to measured wind speed values is used
- If a wind bin has a probability of 0 or 1.0, the calculated rolling mean probability (with a 5-mph window) is used for the wind speed's adjustment probability
- If a wind bin has a rolling mean probability less than 0.02, then the average of the adjacent rolling mean bins is used

To determine the wind speed assigned to a given wind speed swath, the average straight-line wind speed of all reports that fall within a given swath is used. This average wind speed is used because the clustered wind footprints tend to be quite large, but only a small fraction of the area experiences the highest of wind speeds. Using the average reported wind speed allows for the areal coverage of these footprints to be realistically large (as with a derecho, for example) but still produce reasonable loss estimates.

While Verisk considers all SPC wind reports of 58 mph (50 knots) or greater, 58 mph is not, however, the minimum modeled intensity threshold for straight-line winds. The reason being that if the average of the clustered SPC reports is 58 mph (i.e., all the SPC reports within the cluster are 58 mph), it is more than likely, especially given the heterogeneous nature of severe thunderstorm wind fields, that many exposures within the microevent footprint experience wind speeds less than the maximum wind speed. Considering how large the clustered wind footprints can be, particularly in a derecho, for example, the losses would be unrealistically inflated if the modeled intensity threshold was set equal to the SPC minimum intensity threshold. Therefore, when assigning wind speeds to microevents, the intensities can fall below the severe wind speed threshold.

See Also
Event Definition

4.4 Validating Local Intensity

Verisk researchers have extensively validated the local intensity module of the Verisk Crop Hail Model for the United States against historical observational data. Comparisons of Verisk-modeled hail size and convective straight-line wind speed intensity distributions to observational data demonstrate the robustness and reliability of the Verisk model.

Validating Hail Distribution

Figure 40 compares the Verisk-modeled (green) with 2000-2018 SPC-observed (light blue) and 1996-2017 (minus missing data during 2003-2004) radar-derived (dark blue) 1-in. or greater hail diameter size distribution for the conterminous U.S. The Verisk model was run using the 10K all-events catalog. As evident in the figure, the SPC-observed distribution of hail sizes has notable peaks around common objects (e.g., golf ball), while the Verisk-modeled distribution shows a smoother and more realistic distribution that decreases monotonically from its peak occurrence frequency of one inch. The Verisk-modeled hail distribution more closely matches the observed radar-derived distribution than the SPC-observed distribution.

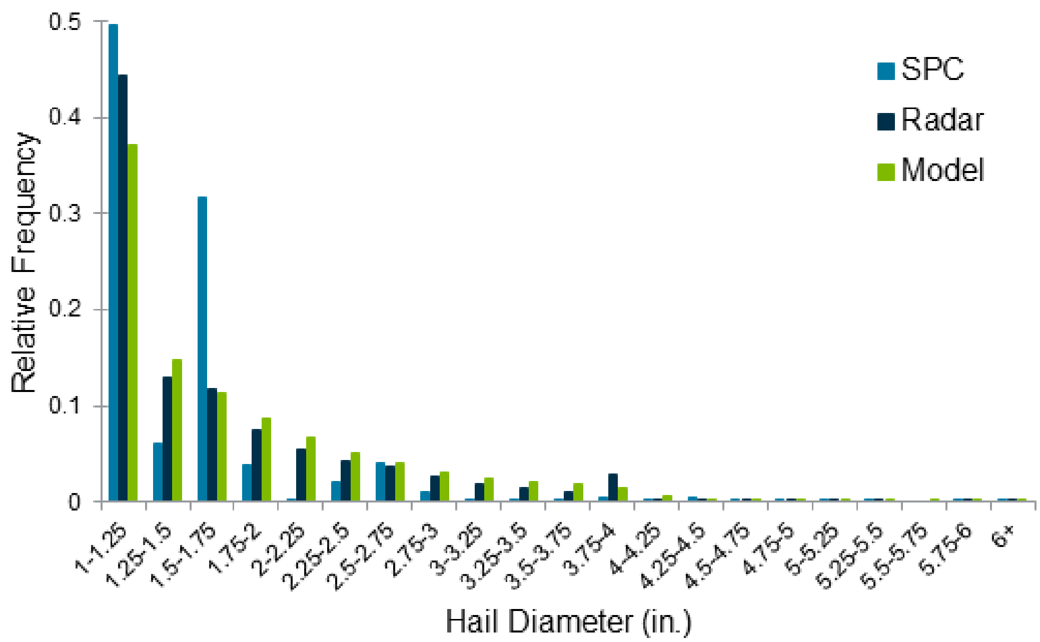

Figure 40. Relative frequency distribution of Verisk-modeled (10K all-events catalog; green), SPC-observed (2000-2018; light blue), and radar-derived (1996-2002 and 2004-2017; dark blue) 1-in. or greater hail diameters across the conterminous U.S.

Validating Straight-Line Wind Speed Distribution

Figure 41 compares the Verisk-modeled (green) and 2000-2018 SPC-observed (light blue) severe convective straight-line wind speed distributions for the conterminous U.S. The Verisk model was run using the 10K all-events catalog. As evident in the figure, the Verisk-modeled and SPC-observed wind speed intensity distributions closely match.

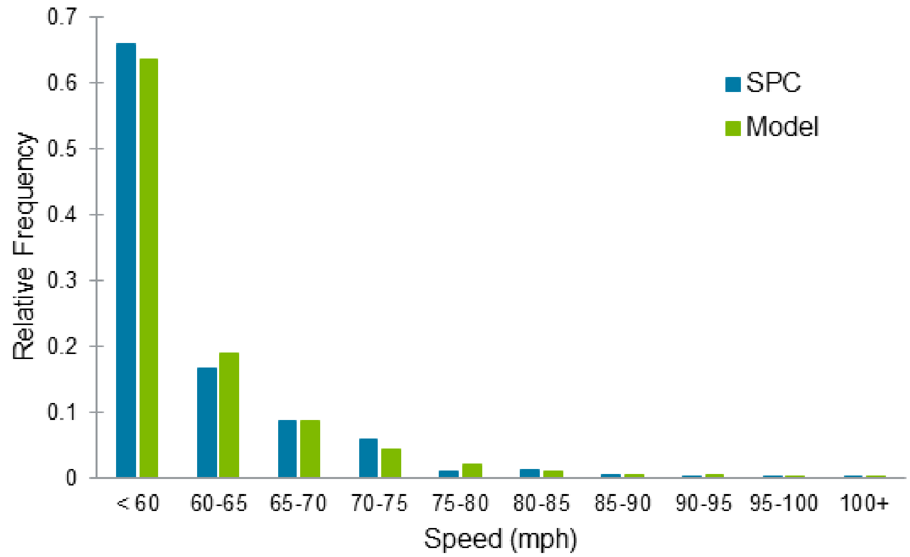

Figure 41. Relative frequency distribution of Verisk-modeled (10K all-events catalog; green) and SPC-observed (2000-2018; light blue) severe convective wind speeds (mph) across the conterminous U.S.

5 Damage Estimation

The Verisk Crop Hail Model for the United States estimates hail damage to crops utilizing crop hail damage functions, which relate the intensity of simulated hail events on an 8-km exposure grid to the percentage of a crop damaged by the hail events. Hail intensity is quantified by the hail total kinetic energy derived from Verisk's 10,000-year all-events stochastic catalog.

Damage functions translate the total kinetic energy of a hail event affecting a crop portfolio into the damage percentage independently of any risk sharing (insurance contracts). Each explicitly modeled crop has several damage functions based on the crop's developmental stage at the time of the hail event. Losses from crops that are not explicitly modeled, such as tobacco and fruits, are added based on the observed county-level statistical relationship with the losses for modeled crops.

Crop exposure that lies in regions of frequent hail activity may experience multiple hailstorms during the growing season. This is reflected in the stochastic hail catalog where, for example, grid cells in Kansas and Nebraska may be impacted by multiple events during a single simulation year. The model accounts for this behavior by assuming that each storm that impacts a grid cell destroys a fraction of the crop exposure that it impacts. This fraction of the exposure is removed from the available crop area that can be damaged by subsequent storms during the same simulation year.

See Also

Effects of Hail on Crops
Covered Crops
Crop Hail Loss Calculation

5.1 Damage Functions by Crop Type

Overall, crop damage increases as the kinetic energy of hail increases. The mean damage ratio (MDR) represents the mean of a probability distribution of possible damage ratios for a given crop and developmental stage. The damage ratio probability distributions were derived from several years of available claims data that included damage from all hail stone sizes, including hail stones smaller than 0.75 inches in diameter.

See Also

Variables Affecting Hail Damage

5.2 Damage Functions by Crop Type and Developmental Stage

The extent of crop damage from hail depends not only on the type of crop, but also on the developmental stage of the crop at the time of the hail event.

For example, as shown in Figure 42, during the fourth developmental stage barley is most vulnerable to hail damage and therefore exhibits the steepest damage function, and rice is least vulnerable and therefore has the shallowest damage function.

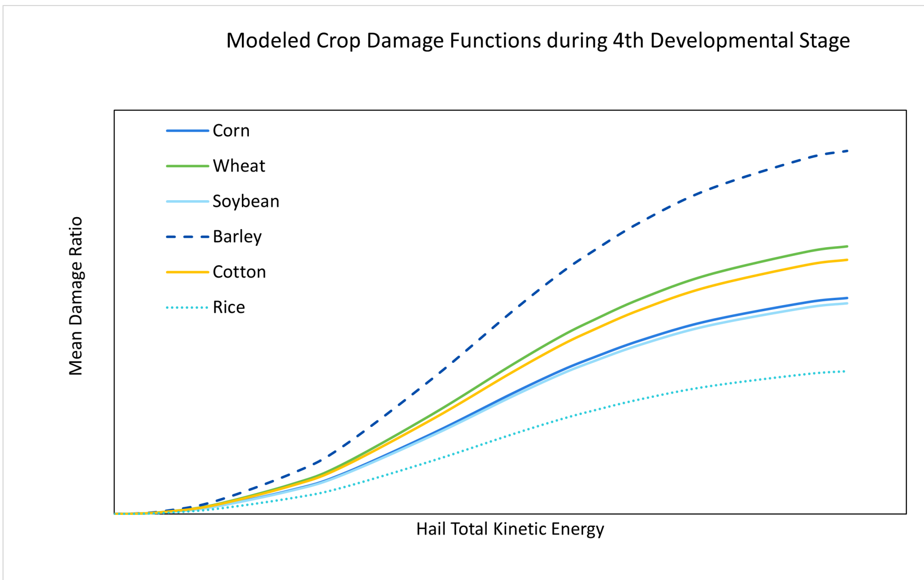

Figure 42. Damage functions for each explicitly modeled crop during the fourth developmental stage

The developmental stages for each crop are determined from typical planting and harvest dates for each crop by state. The growing season for each crop varies geographically; planting dates are generally earlier further south. For example, the variability in corn planting dates and timing of the tasseling stage across the United States are shown in Figure 43.

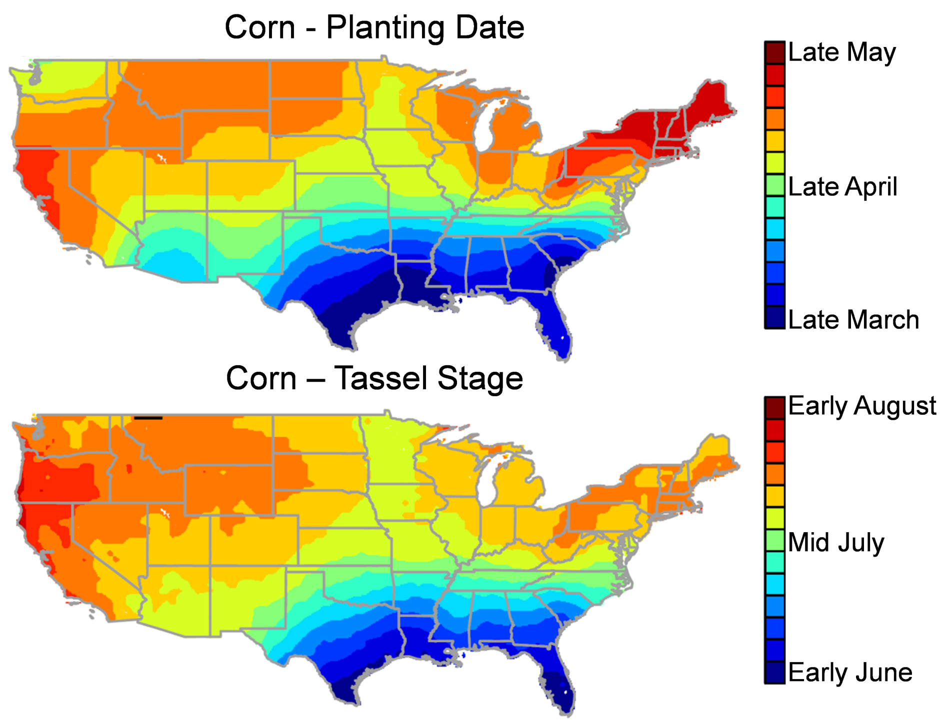

Figure 43. Planting date of corn, based on USDA typical planting dates by crop and state (top); Beginning date of tassel stage of corn, based on USDA typical planting and harvest dates by crop and state, and growing degree days (bottom)

Damage Functions by Developmental Stage for Each Modeled Crop

Damage functions by developmental stage are shown for each modeled crop in the figures below.

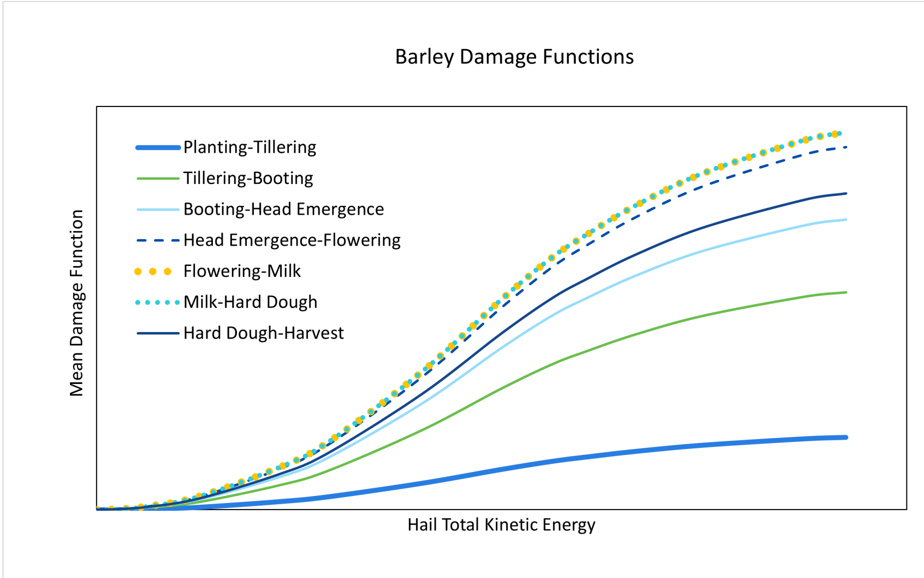

Figure 44. Damage Functions for Barley by Developmental Stage

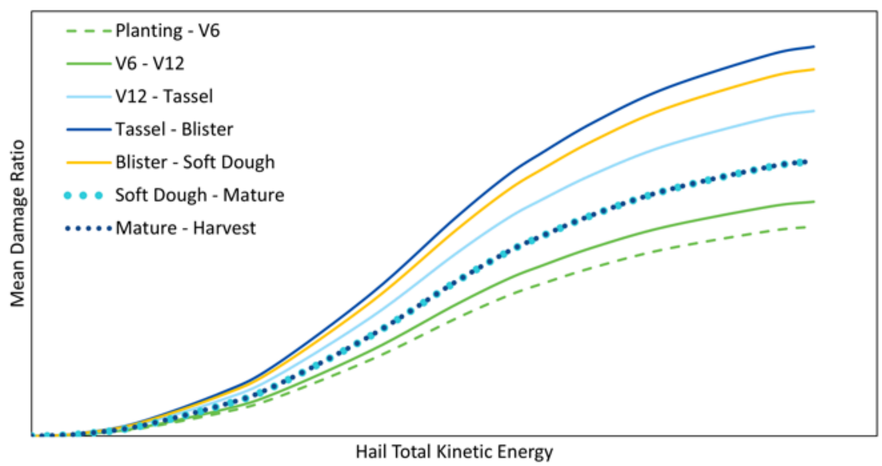

Figure 45. Damage Functions for Corn by Developmental Stage

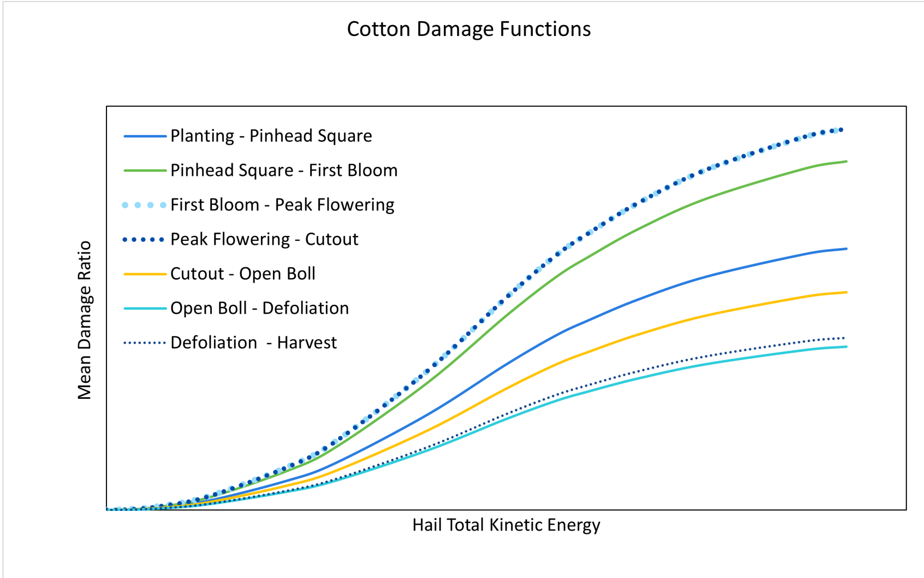

Figure 46. Damage Functions for Cotton by Developmental Stage

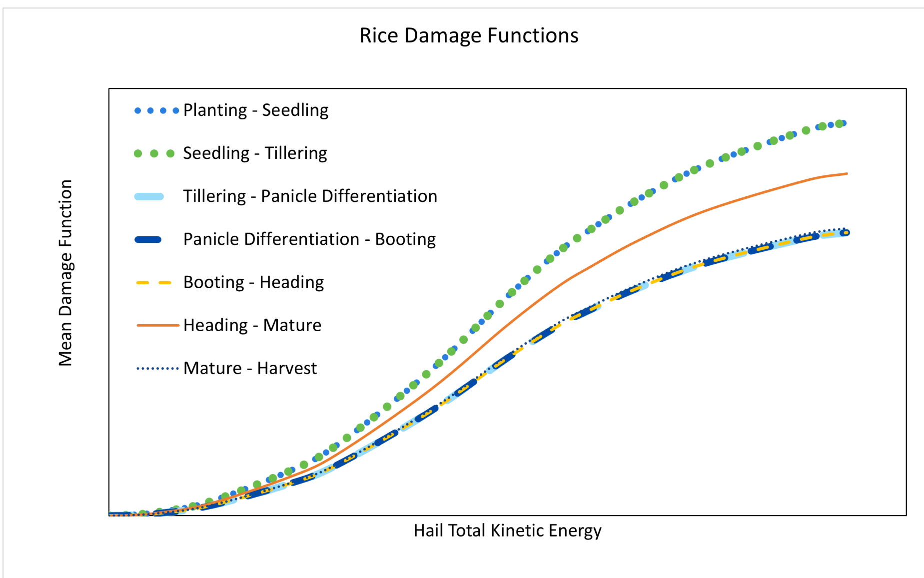

Figure 47. Damage Functions for Rice by Developmental Stage

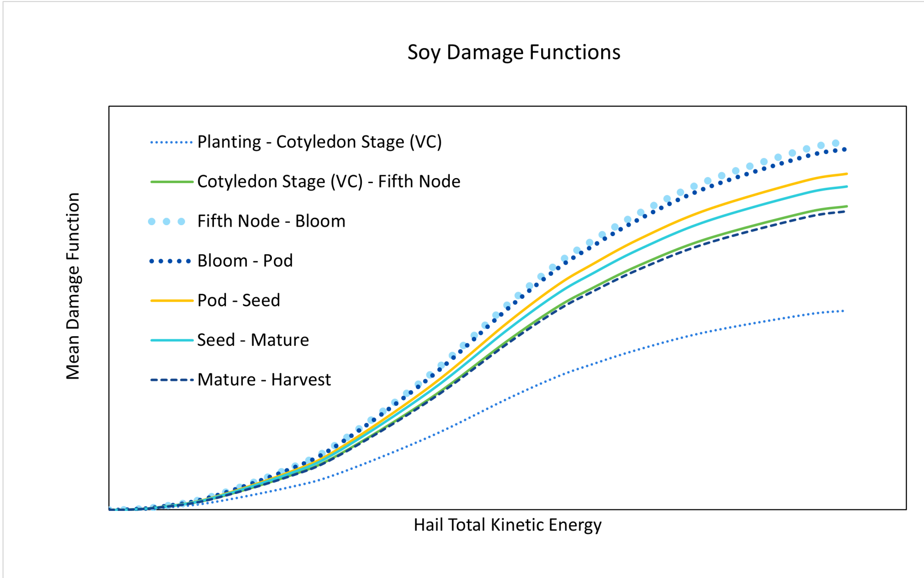

Figure 48. Damage Functions for Soy by Developmental Stage

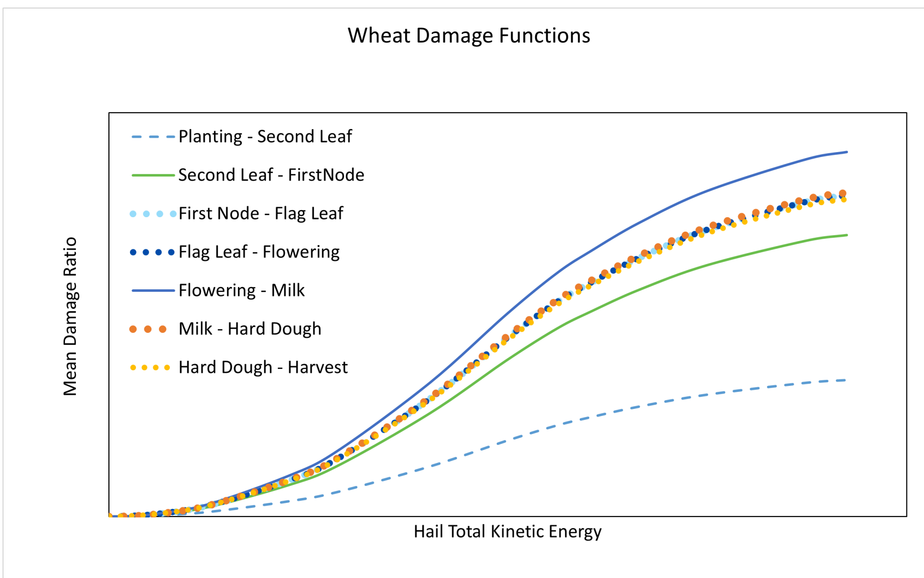

Figure 49. Damage Functions for Wheat (all varieties) by Developmental Stage

5.3 Calculating Crop Areas Damaged by Hail

Damaged areas are defined as the regions where the MDR is greater than zero. The intersection of each stochastic hail swath with the 8-km exposure grid is used to calculate the damaged area by crop type and developmental stage (the planted acreages of each of the eight explicitly modeled crops on the 8-km exposure grid are determined from the NASS Cropland Data Layer). The crop exposure in a grid cell is reduced following each simulated hailstorm to avoid the same crop acreage being damaged several times throughout a growing season.

The damaged area is then aggregated to county and state levels for each modeled crop for each simulation year.

See Also

Model Resolution
Crop Hail Loss Calculation

5.4 Validating Damage Functions

The crop hail damage functions developed by Verisk researchers are similar to the relationships between crop damage and total kinetic energy described in scientific literature.[69, 70]

For example, Figure 50 shows damage functions for several crops based on observations of crop damage resulting from a hailstorm in central Switzerland.

The damage functions shown in Figure 50 are similar in shape to the damage functions used in the Verisk Crop Hail Model for the United States. In addition, the variation between the damage functions for each crop type reported by Schiesser[71] indicates that barley (both spring barley and winter barley) and wheat, when mature, are the most vulnerable of the modeled crops to hail damage; this is consistent with the barley and wheat damage functions derived by Verisk researchers. The observations of damage to corn shown in Figure 50 (left panel) also illustrate the range of crop damage for a single hail impact energy value; the damage function probability distributions used in the Verisk Crop Hail Model for the United States capture this variability.

69 Schiesser, H. H. "Hailfall: the relationship between radar measurements and crop damage." Atmospheric Research. Science Direct, 01 Jan. 1990. Web. 23 May 2017. http://adsabs.harvard.edu/abs/1990AtmRe..25..559S.

70 Hohl, Roman Marco. "Relationship between hailfall intensity and hail damage on ground, determined by radar and lightning observations - RERO DOC." Rero Doc Digital Library. N.p., Nov. 2001. Web. 23 May 2017. https://doc.rero.ch/record/5136/files/1_HohlRM.pdf.

71 Ibid

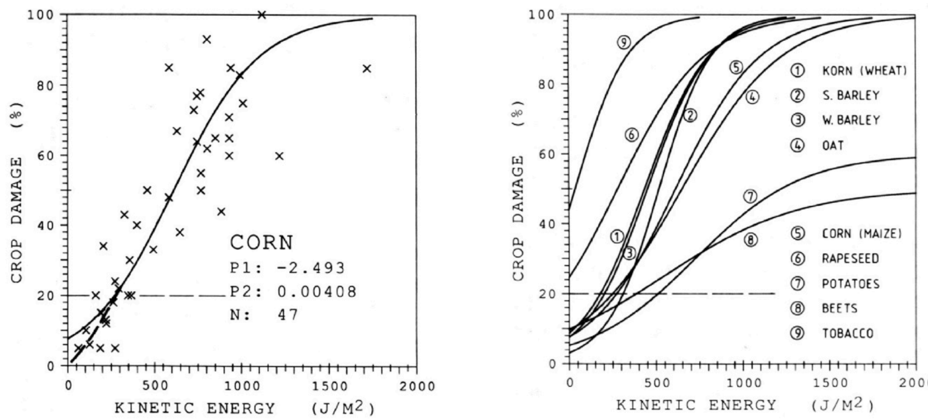

Figure 50. Damage functions derived for corn (left panel), and for wheat (labeled korn), spring barley, winter barley and 6 other crops (right panel) derived from damage observations from the severe "Ruswil" hailstorm of central Switzerland, July 15, 1982

The left panel shows the raw data points for corn (each point shown with an X), along with the derived damage function (solid line). The right panel compares the derived damage functions for nine different crops, all near maturity: wheat (labeled "korn"), spring barley, winter barley, oats, corn, rapeseed, potatoes, beets, and tobacco. The figure indicates that barley (both spring barley and winter barley) and wheat, when mature, are the most vulnerable of the modeled crops to hail damage

6 Insured Loss Calculation

In this component of the Verisk Crop Hail Model for the United States, ground-up damage is translated into financial losses. Insurable losses are calculated at the 8-km exposure grid by applying policy conditions to the damage estimates resulting from the damage estimation module. The policy conditions include various deductibles and limits. Insurable losses are then aggregated to the county and state resolutions and reported by year.

6.1 General Structure of Loss Estimation

Insurable losses are calculated for two lines of business: crop hail and production plan. Crop hail policies pay when crop damage occurs from a hailstorm regardless of the final production outcome at harvest. Production plan policies pay when the actual yield at harvest is below a guaranteed yield. Production plan policies cover the portion of the crop not insured under an MPCI policy and pay out the lesser of the hail loss or production loss. Crop Hail is supported in the entire model domain, production plan policies are supported in the following states: Colorado, Iowa, Idaho, Illinois, Indiana, Kansas, Minnesota, Missouri, North Dakota, Nebraska, Ohio, South Dakota, Texas and Wisconsin

See Also

Supported Lines of Business

Crop Hail Loss Calculation

Loss is estimated for crop hail policies based upon the damage ratio and damaged area of the eight explicitly modeled crops for each simulated hailstorm in the catalog. Insurable losses are calculated by applying the appropriate policy conditions to the damaged area and damage ratio on the 8-km exposure grid.

For each simulated hailstorm, the model gives a damaged area (*DA*) and mean damage ratio (*DR*) . *DR* is a function of crop type, developmental stage, and hail impact energy. The crop hail loss (*CH loss*) for each simulated storm is the product of *sums insured*, the *policy condition proportion* (the proportion of liability written in a policy), *DA,* and *DR*:

$$CH\ loss = sums\ insured * policy\ condition\ proportion * DA * DR$$

Loss is summed for all appropriate policy conditions. Loss is further aggregated by summing the various damage ratios around the mean damage ratios to find the total insurable loss for each simulated storm. Losses for all non-modeled crops are added based on the observed statistical relationship (at the county level) with losses for modeled crops; total losses for all crops are then aggregated and reported by year.

See Also

Model Resolution
Damage Estimation
Policy Condition Assumptions
Calculating Crop Areas Damaged by Hail

Production Plan Loss Calculation

The Verisk Crop Hail Model for the United States uses yield scenarios from the Verisk Multiple Peril Crop Insurance (MPCI) Model for the United States to estimate production loss for Production Plan policies, see (Figure 51) as an example. The yield estimates by county are applied with the industry Production plan policy conditions to determine production loss.

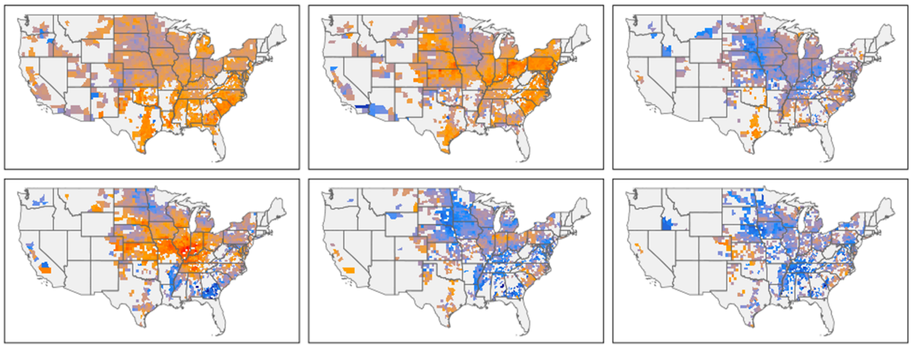

Figure 51. Examples of corn yield scenarios from the Verisk MPCI Model for the United States (light blue/dark blue = above normal yield; yellow/orange/red = below normal yield)

When the final yield at harvest is below the guaranteed yield under a production plan policy, production loss is calculated as the difference between guaranteed yield and actual yield, times sums insured:

$$Production\ loss = (guaranteed\ yield - actual\ yield) * sums\ insured$$

Hail loss is calculated as the product of guaranteed yield, sums insured, and the damage ratio (*DR*):

$$Hail\ loss = guaranteed\ yield * sums\ insured * DR$$

The calculated production loss is compared to the hail loss, and the insurable loss on the production plan policy is the smaller of the two values If the damage ratio is below the minimum loss on the policy, no loss is paid.

See Also

Policy Condition Assumptions

Loss Calculation in the Wind Module

The Wind Module in the Verisk Crop Hail Model for the United States is designed to calculate the potential value of crop loss due to damaging winds for states in which wind endorsements in crop hail policies are popular. In these states, loss from wind damage can account for a substantial portion of the yearly loss. As shown in Figure 52, the fraction of losses and liability due to wind alone vs hail varies considerably across states; notably, in some states the loss due to winds can be higher than the loss due to hail.

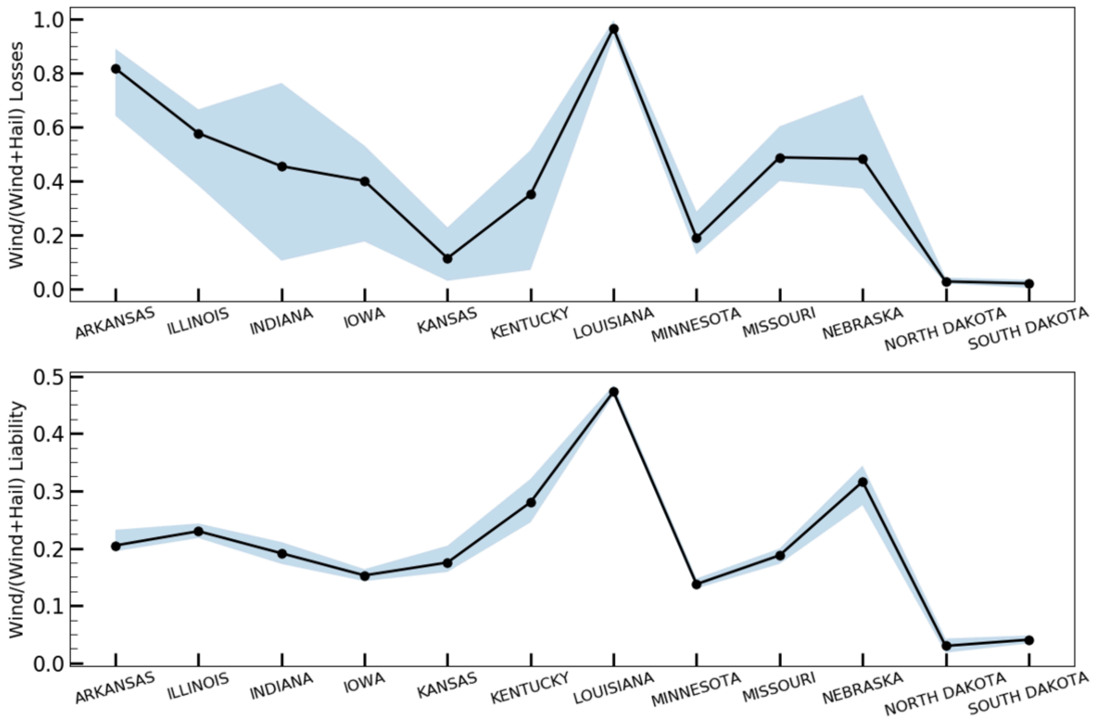

Figure 52. Mean ratios of wind to wind plus hail losses (top figure) and liability (bottom figure), for all crops
The shading indicates the maximum and minimum ratios between 2017 and 2020

Table 6 shows the states and insurance products processed by the wind module. For those states,[72] the wind module calculates – at the state level – total wind loss, straight wind loss and production plan loss as functions of:

- total state-level NCIS loss cost data (using years 2011-2020)
- the number of wind-based local storm reports per month at the state level (for the months of May, June, July and August)
- data from crop exposure database
- ratios between the total crop-hail (and production plan, as applicable) liability and the wind-only liability at the state level

Verisk researchers calculated an ordinary least square (OLS) regression between reported NCIS loss cost (using years 2011-2020) and the number of wind-based local storm reports per month at the state level for the months of May, June, July and August. To calculate the wind loss catalog, Verisk researchers:

- disaggregated the wind events in the 10,000 year all-events stochastic catalog from the Verisk Severe Thunderstorm Model for the United States into state-level catalogs

[72] Arkansas, Iowa, Illinois, Indiana, Kansas, Kentucky, Louisiana, Minnesota, Missouri, North Dakota, Nebraska, South Dakota – these states comprise more than 85% of total industry wide wind endorsement liability (2017-2020 average)

- processed the state-level catalogs to mimic the number of SPC Local Storm Reports per day per event for the months of April-October (these local storm reports are available starting in 2004)
- filtered out events with wind speeds below the NWS severe weather threshold of 58 mph (50kt)

Once the wind module calculates the loss values for wind, they are incorporated into the final industry loss values for the entire model for each year of the 10K catalog. The annual losses at the state-level for straight wind and for production plan are split equally among counties.

The wind module calculates the loss independent of crop type. Exposure data only includes corn because wind endorsements target corn; using exposure data for other crops overestimates the potential exposure and losses in each state.

Table 6. States and insurance products that are modeled within the wind module

State	Product
Arkansas	Crop Hail Wind
Iowa	Crop Hail Wind, Production Plan Wind
Illinois	Crop Hail Wind, Production Plan Wind
Indiana	Crop Hail Wind, Production Plan Wind
Kansas	Crop Hail Wind, Production Plan Wind
Kentucky	Crop Hail Wind, Production Plan Wind
Louisiana	Crop Hail Wind
Minnesota	Crop Hail Wind, Production Plan Wind
Missouri	Crop Hail Wind, Production Plan Wind
North Dakota	Crop Hail Wind, Production Plan Wind
Nebraska	Crop Hail Wind, Production Plan Wind
South Dakota	Crop Hail Wind, Production Plan Wind

See Also
Model Resolution

6.2 Validating Insured Losses

The loss module of the Verisk Crop Hail Model for the United States was validated by comparing modeled losses with industry experience and claims data. Validation was conducted separately for both lines of business (crop hail and production plan), as described in the following subsections.

Crop Hail Loss Validation

Crop hail losses were validated using 1999-2020 NCIS industry data. Figure 53 shows the average annual loss cost from NCIS and the Verisk model, by county. The Verisk model captures the large-scale spatial pattern of loss cost seen in the observations, specifically reflecting the area of large loss cost in the Midwest and Great Plains with decreasing loss cost to the east. The model further captures the area of relatively large loss cost values in the mid-Atlantic states due to the vulnerability of tobacco to hail damage.

County-level differences between the NCIS and modeled loss cost values are due to a combination of three main factors:

- The deductibles in policy conditions have a large impact on insurable losses.
- Crop exposure varies significantly over time
- The model simulates 10,000 years of hailstorm activity and is expected to vary compared to the 22 years of available industry data

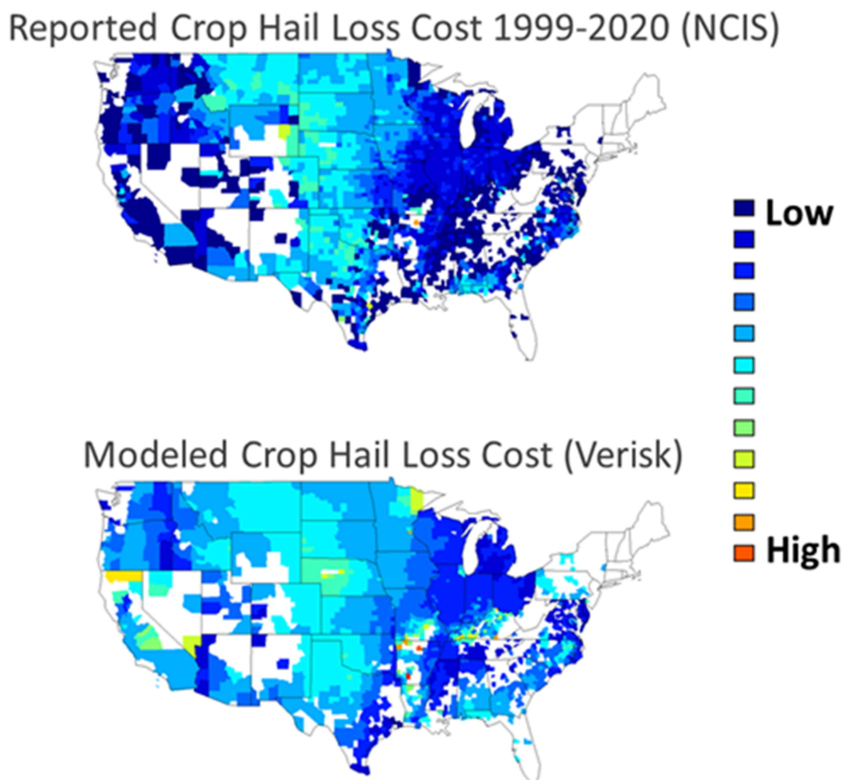

Figure 53. Reported (NCIS) and Verisk Modeled Crop Hail Loss Cost

Modeled losses were also compared to industry data on the state level. Figure 54 shows average annual modeled and NCIS loss cost by state. The crops planted in these states are predominantly made up a combination of the eight explicitly modeled crops, with non-modeled specialty crops making up a small portion of the total liability in each state. The modeled average annual loss cost agrees well with the reported average annual loss cost for each state.

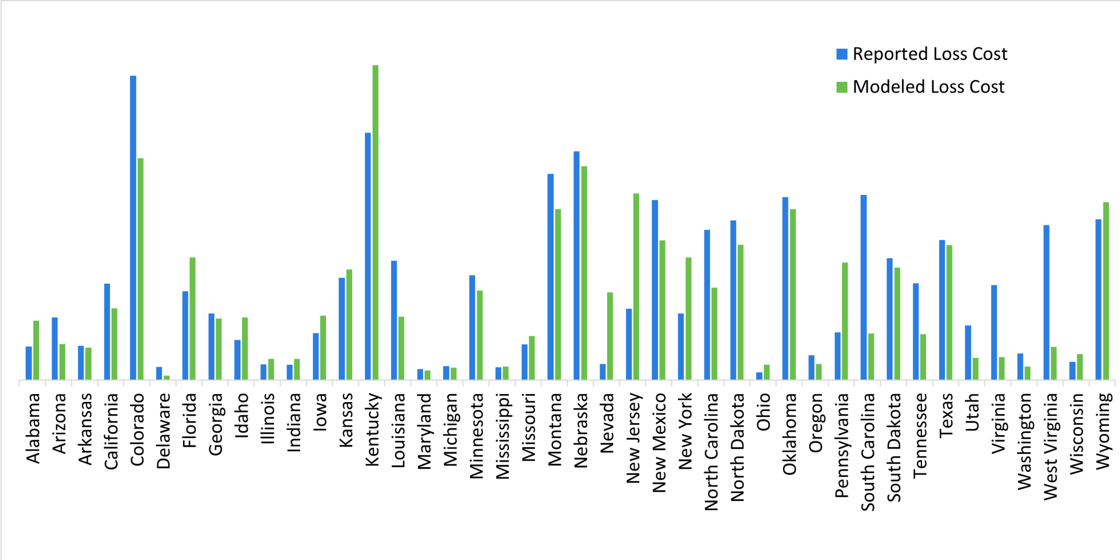

Figure 54. Comparison of average modeled annual loss cost (Modeled Loss Cost) with average 1999-2020 NCIS data (Reported Loss Cost) for crop hail policies

Production Plan Loss Validation

Validating Verisk modeled production plan losses against industry experience was challenging due to the limited amount of historical data that are available; there are 10 years (2011–2020) of available industry loss data for production plan policies. Figure 55 shows the modeled production plan average annual loss cost, as well as the loss cost reported by NCIS by state for 2011–2020. Production plan policies are available in the following states in recent years:Colorado, Iowa, Idaho, Illinois, Indiana, Kansas, Minnesota, Missouri, North Dakota, Nebraska, Ohio, South Dakota, Texas and Wisconsin.

In addition, the variability in reported production plan losses and policies in most states for these 10 years complicated the use of these NCIS data to validate the Verisk model for this line of business. Because both hailstorm activity and crop yield can significantly vary annually, the magnitude of reported production plan losses often change to a greater extent over time compared to crop hail. For example, 2011 is known to have been a high loss year for crop hail insurers and the loss cost in 2011 was quite high in most states whereas 2012 did not exhibit similarly large Production Plan hail losses, as this was a drought year. Hail activity then increased again in 2014, raising reported losses in a few states.

In addition, production plan policy terms often change more drastically leading to larger year-to-years variation in losses. In 2012, for example, the portion of production plan liability written to policies with 10% minimum loss in Colorado more than doubled from 2011 to 2012, while the portion of liability written to policies with 0% minimum loss decreased from 2011 to 2012. Higher minimum loss values act to decrease the payout on small production plan losses, as only large hail events will inflict production plan losses, whereas minimum loss values of zero would nearly always result in a production plan loss, even from small hail events. Production plan policy conditions in many of these states changed again between 2012 and 2013, with a tendency toward policies with 0% minimum loss rather than the more common 5% minimum loss seen in 2011 and 2012. Additional states including Texas and Oklahoma saw this switch from nonzero minimum loss production plan policies to 0% minimum loss policies between 2015 and 2016. In Nebraska, Minnesota, and Iowa, the top three production plan liability states, a significant percentage of the farmers have shifted from higher (80-85%) to lower (70-75%) MPCI coverage levels for their production plan policies between 2016 and 2020, which implies majority of the farmers have preferred higher crop hail production guarantee in recent years.

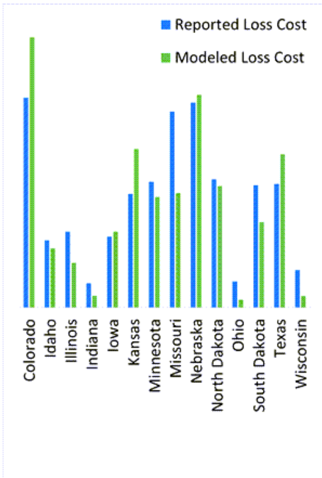

Figure 55. Comparison of average modeled annual loss cost (Modeled Loss Cost) with average 2011-2020 NCIS data (Reported Loss Cost) for production plan policies

Benchmarking Exceedance Probabilities

Figure 56 shows the modeled loss ratio (ratio of loss to premiums earned) at several return periods for the entire model domain for combined crop hail and production plan lines.

Verisk scientists benchmarked the predicted frequency of historical losses as captured in the stochastic catalog to confirm the validity of the modeled exceedance probabilities. The reported loss ratio to the U.S. crop hail industry in 2014 was the largest for any year and is shown to have an exceedance probability of 5.8%, which corresponds to a return period of just over 17 years. The industry-wide loss ratio for the 2020 growing season was also a large loss year with an exceedance probability of 8.6%, or a return period of approximately 11.5 years.

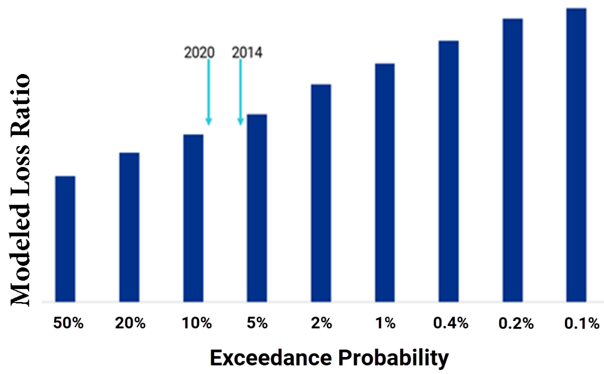

Figure 56. Exceedance probability for combined crop hail and production plan lines

7 Accounting for Climate Change

Climate change affects extreme weather events (Stott, 2016).

Detecting and attributing climate change impacts on various weather phenomena is a relatively new branch of climate science that is growing in demand and sophistication. Attribution confidence depends on many factors, including:

- how robustly climate models simulate impacts;
- whether the climate models agree with one another;
- whether there is a detectable trend in the historical data that agrees qualitatively with the modeled future result; and
- how well we can physically connect and understand the modeled or observed effect on climate.

Figure 57 shows the relative degree of confidence scientists have in ascribing climate change impacts to individual weather events. Temperature phenomena are most confidently assessed because of the direct physical connection between increasing carbon dioxide and other greenhouse gases and a warming atmosphere.

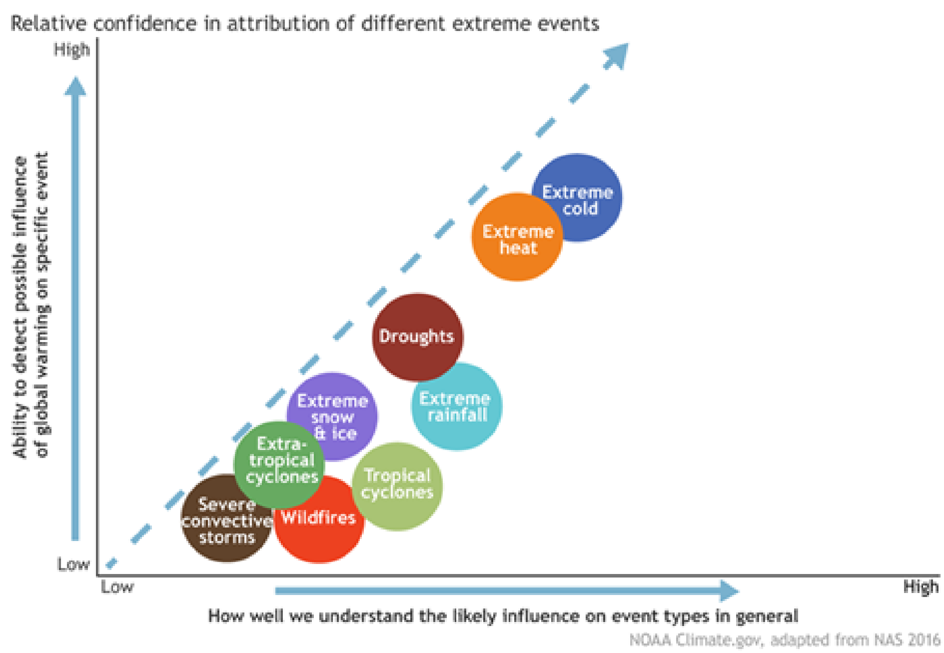

Figure 57. Relative Confidence in Attribution for Extreme Events

There is less confidence that climate change is impacting severe thunderstorms (i.e., severe convective storms) relative to other types of weather phenomena (such as extreme heat/ cold). Reasons for this low confidence include:

- their relatively small spatial scale (i.e., typically less than 1,000 km), which climate models cannot explicitly resolve;

- their dependence on subtle changes in the environment in which they grow (e.g., planetary boundary layer inversions);
- a historical record with changes in observational uncertainty over time, particularly associated with population biases in reports; and
- the inherently nonlinear physics driving these events.

Despite these challenges, the Verisk Crop Hail Model for the United States, using the 10,000K all-events catalog from the Verisk Severe Thunderstorm Model for the United States, captures changing trends in severe thunderstorm hail and straight-line winds by appropriately weighting the current and near-current climate (the last 30 years).

7.1 Global Climate Models and Reanalysis Datasets

Even though severe thunderstorms and their sub-peril components cannot be explicitly resolved, global climate models (GCMs) can resolve the larger-scale environmental conditions favorable for their development over a reasonably long time period. These environmental factors can be used as proxies for severe thunderstorm development and include temperature and moisture vertical profiles (i.e., lapse rates), the change in wind speed and direction with height (i.e., vertical wind shear), and convective triggering mechanisms (e.g., cold fronts). These favorable environments can be quantified using various parameters, including convective available potential energy (CAPE), vertical wind shear, moisture advection, and freezing level. By analyzing changes in these quantities over time, the extent to which climate change and/or natural variability may be playing a role in these trends can be examined. However, it is important to keep in mind that even with increasingly favorable environmental conditions, these conditions are only proxies for severe thunderstorm development. Thus, changes in these parameters do not necessarily imply the same changes in severe thunderstorm characteristics over time. In addition, reanalysis datasets have their own uncertainties due to their numerical modeling component as well as the temporal evolution of the data used to produce these datasets (e.g., satellite-derived data used in reanalyses began in 1979). Nonetheless, many studies use GCMs to examine the potential impact climate change may have on U.S. severe thunderstorm frequency and intensity.

Using GCMs and a high-resolution regional climate model to compute CAPE and 0-6 km vertical wind shear, Trapp et al. (2007) examined the potential change in U.S. severe thunderstorm frequency due to climate change. They concluded that the number of days with severe thunderstorm environments (NDSEV) throughout the continental U.S. by the late 21st century is projected to increase. Large increases in CAPE, which are favorable for severe thunderstorm development, are found across much of the eastern two-thirds of the country, with the greatest increases (by as much as 500 J/kg) occurring across the Southeast during the summer months. Decreases in vertical wind shear, which are unfavorable for organized severe thunderstorms, are greatest across the central latitudes of the U.S., with increases seen over the northern Great Plains and along the U.S.-Mexico border. While this reduction in vertical wind shear is evident, the authors conclude that the large increase in CAPE far outweighs the amount of decreased shear in this study. The net result is a predicted increase in the NDSEV across much of the continental U.S., with the greatest increase evident across the southern and eastern U.S. during the summer months.

While regional reanalysis datasets provide insight into past environments favorable for severe thunderstorm development, and global climate modeling studies provide the best estimates of future impacts on severe thunderstorm activity, the more relevant challenge for catastrophe risk modeling is quantifying the effects of climate change that has occurred already on current severe thunderstorm risk. Given the magnitude of the GCM-simulated changes expected by late this century, one may expect that non-negligible changes are already occurring. As a result, many studies have analyzed trends in severe thunderstorms thus far. The noted limitations in observational records, including regional variations in observational quality and quantity, make it difficult to determine whether any observed trends are robust or meaningful. As a result, trends in both environmental and observational sources are discussed in this chapter to provide a comprehensive analysis of the extent to which climate change may be impacting U.S. severe thunderstorm activity.

More recently, Diffenbaugh et al. (2013) used daily CAPE and both low-level (0-1 km) and deep-layer (0-6 km) vertical wind shear output from the Coupled Model Intercomparison Project, Phase 5 (CMIP5) General Circulation Model ensemble to analyze NDSEV across the continental U.S. Their results (Figure 58) show appreciable increases in the NDSEV across the eastern half of the U.S. and significant increases in CAPE across the continental U.S. during all seasons by the late 21st century under a Representative Concentration Pathway 8.5 (RCP8.5) greenhouse gas concentration trajectory scenario. A large percentage of the NDSEV in their study is associated with high CAPE coupled with strong low-level vertical wind shear and low convective inhibition. In contrast, weak vertical wind shear days are often coupled with low CAPE days. These findings support the theory that increased CAPE likely results in increased NDSEV, despite decreased vertical wind shear, due to surface heating and increased moisture having a significant impact on increasing the thermal instability of air parcels near the ground.

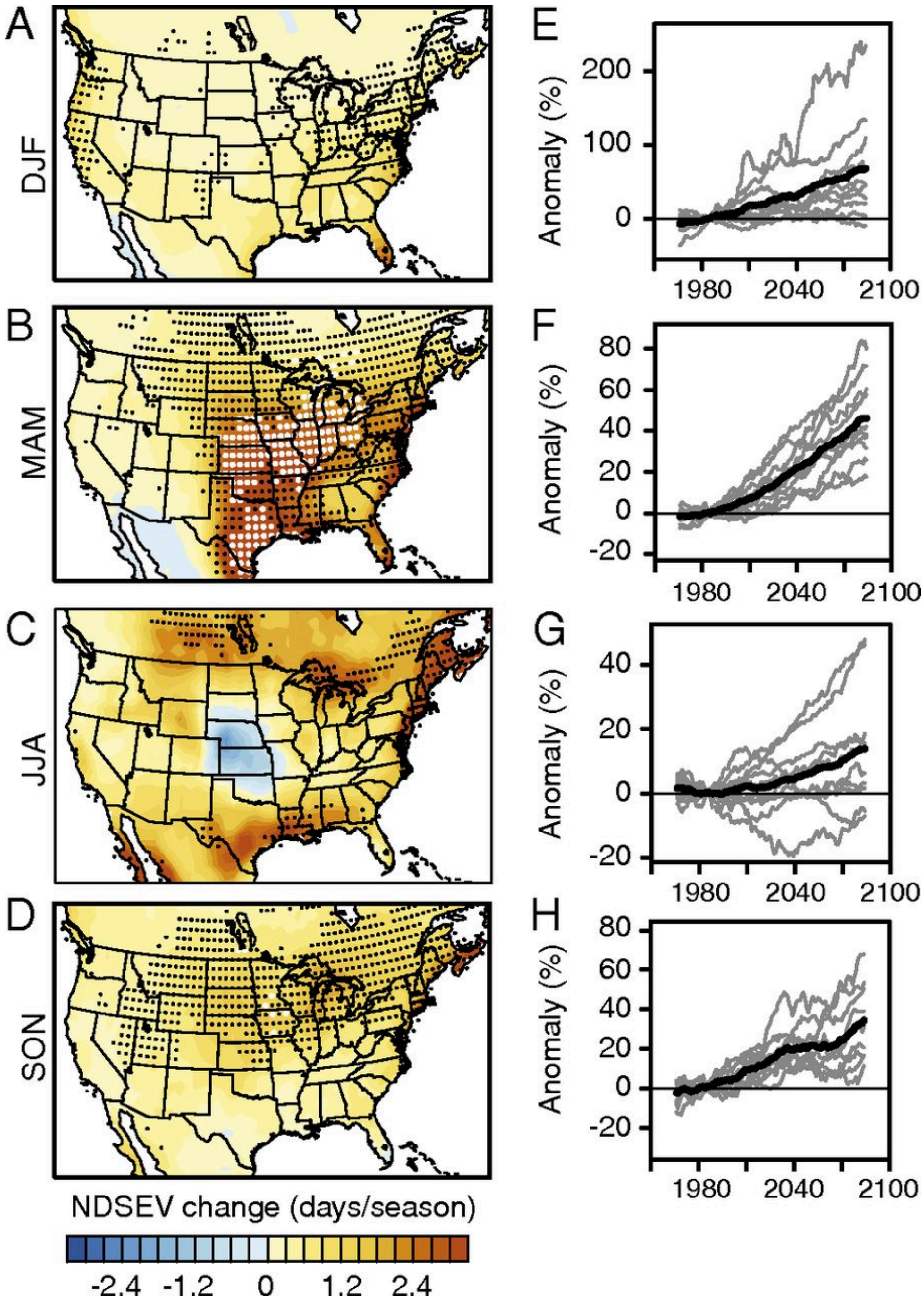

Figure 58. Projected change in NDSEV by the late 21st century using an RCP8.5 scenario during A) winter (December - February; "DJF"), B) spring (March - May; "MAM"), C) summer (June - August; "JJA"), and D) fall (September - November; "SON").
The warm (cool) colored areas for the panels on the left (A-D) represent an ensemble model mean positive (negative) NDSEV change between RCP8.5 period 2070-2099 and the baseline period 1970-1999. Robust (highly robust) changes (i.e., areas where the ensemble signal is >1 (>2) standard deviation(s) above the ensemble noise) are indicated by the black (white) dots. The anomaly (as a percent of the 1970-1999 baseline mean value) in the eastern regional (i.e., land area within a 105–67.5°W, 25–50°N box) average NDSEV value is plotted for each

individual model run as gray lines in the panels on the right (E-H). The black line in these plots represents the mean value of the individual model runs (Source: Diffenbaugh et al., 2013).

In addition to using GCMs to predict future changes, other studies use reanalysis datasets to assess changes in severe thunderstorm activity that have occurred to date using relevant environmental parameters. For example, Koch et al. (2021) used the North American Regional Reanalysis (NARR) dataset to examine changes in CAPE, 0-3-km storm relative helicity (SRH), and PROD (i.e., a parameter based on CAPE and SRH, where PROD = $(CAPE)^{1/2}$ x SRH (in m^3/sec^3)) maxima from 1979 to 2015 within an area spanning from -110° to -80° longitude and from 30° to 50° latitude. Since large/extreme values of CAPE, SRH, and PROD represent environments favorable for severe thunderstorm development, the authors examined extreme CAPE, SRH, and PROD values to see if any temporal trends in these data exist. Their results show that severe thunderstorm risk is increasing across portions of the central U.S., an area already particularly prone to severe thunderstorms, during April and May. They found non-negligible increases in PROD maxima in April, May, and August, in CAPE maxima in April, May, and June, and in SRH maxima in April and May. The April PROD spatial and temporal maxima trends are shown in Figure 59. (Note that a subsetted geographical area encompassing northeast Texas, northern Louisiana, southern Nebraska, southern Iowa, and much of Kansas, Oklahoma, Missouri, and Arkansas was used to calculate the region-averaged April PROD maxima time series plot in the figure).

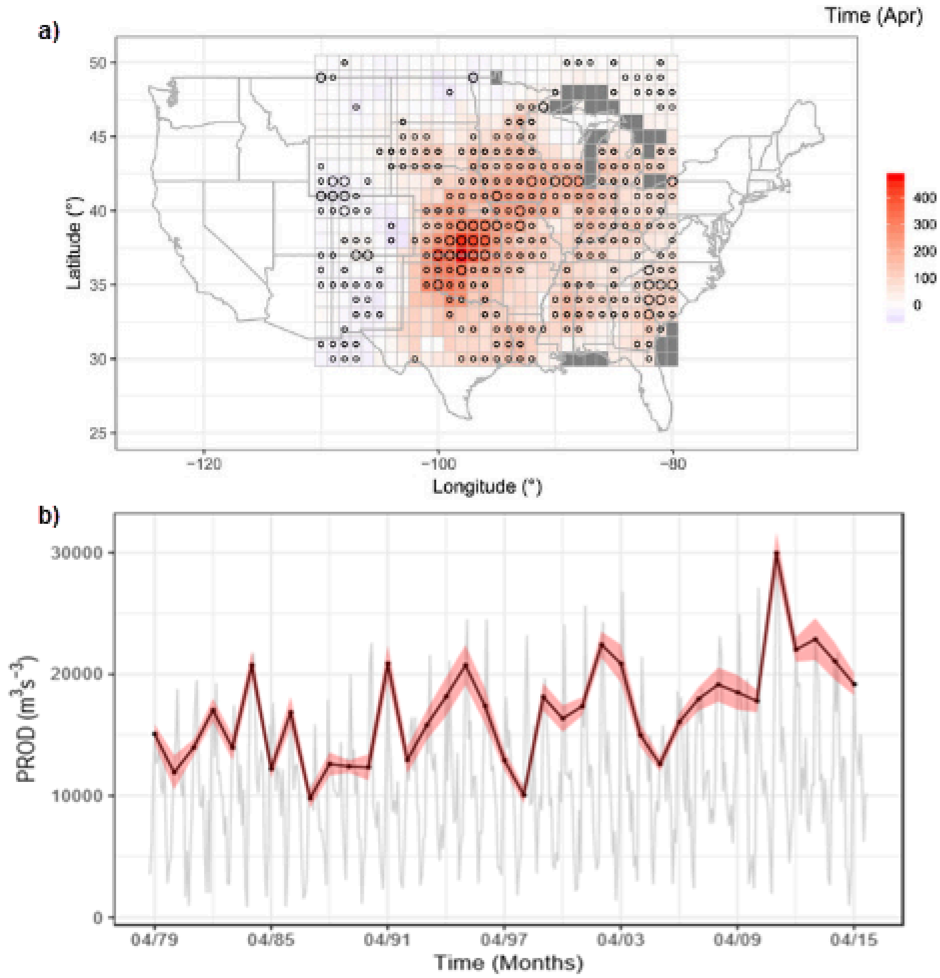

Figure 59. April PROD a) spatial and b) area-averaged temporal maxima trends from 1979 to 2015 using the NARR dataset.
The shading in the top figure indicates the magnitude of the slope over the analysis period, and the large (small) circles indicate statistical significance at a p=0.05 (p=0.20). The black line in the bottom figure represents the area-averaged April maxima time series, the red shaded region indicates its 95% confidence interval bounds, and the gray lines represent the area-averaged monthly maxima time series for all 444 months (Adapted from: Koch et al., 2021; CC BY-SA 4.0).

While regional reanalysis datasets provide insight into past environments favorable for severe thunderstorm development, and global climate modeling studies provide the best estimates of future impacts on severe thunderstorm activity, the more relevant challenge for catastrophe risk modeling is quantifying the effects of climate change that has occurred already on current severe thunderstorm risk. Given the magnitude of the GCM-simulated changes expected by late this century, one may expect that non-negligible changes are already occurring. As a result, many studies have analyzed trends in severe thunderstorms thus far. The noted limitations in observational records, including regional variations in observational quality and quantity, make it difficult to determine whether any observed trends are robust or meaningful. As a result, trends in both environmental and observational sources are discussed in this chapter to provide a comprehensive analysis of the extent to which climate change may be impacting U.S. severe thunderstorm activity.

7.2 Historical Trends

See Also

Data Sources for the Verisk Crop Hail Model for the United States
Data Sources for Event Generation

Historical Trends in Hail Activity

The effect of climate change on hail frequency has received much attention, not just in the U.S. but also globally, due to hail's high frequency of occurrence and the resulting amount of hail damage sustained worldwide. Unfortunately, observed hail report data are adversely affected by significant population biases and suffer from a relatively short observational record. Thus, the extent to which climate change plays a role in any temporal trends seen in the observed data is difficult to determine. To minimize these population biases and isolate temporal trends due to climate change and/or natural variabilities, many studies analyze temporal trends in hail days (i.e., days containing at least one report of hail) instead of the raw hail reports themselves. Results from these studies have generally found no overall trend in U.S. hail frequency over time but, on a regional level, some statistically-significant increases in hail frequency may exist.

As seen in Figure 60 and Figure 61, Verisk researchers analyzed time series of annual 1-inch or greater and 2-inch or greater hail days, respectively, across the contiguous U.S. along with U.S. population from 1955 to 2018. It is evident from both plots that there is an upward (i.e., increasing) trend in hail days until around 1990, after which the total hail days are relatively stable. Plotting a ratio of the two (not shown) indicates that the proportion of 2-inch or greater hail days to 1-inch or greater hail days has increased slightly since 1990. The stability of the hail day frequency record since 1990 is consistent with other studies (e.g., Allen and Tippett, 2015) and suggests there is no observed temporal trend in the overall U.S. hail frequency.

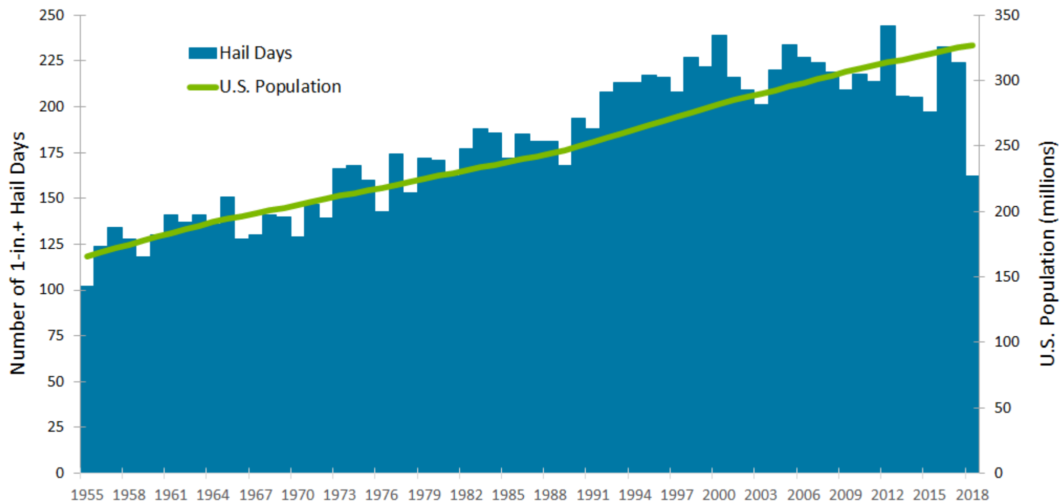

Figure 60. Number of 1-inch or greater hail days (blue bars) and population (green line) across the contiguous U.S. from 1955 to 2018 based on SPC's Storm Reports database

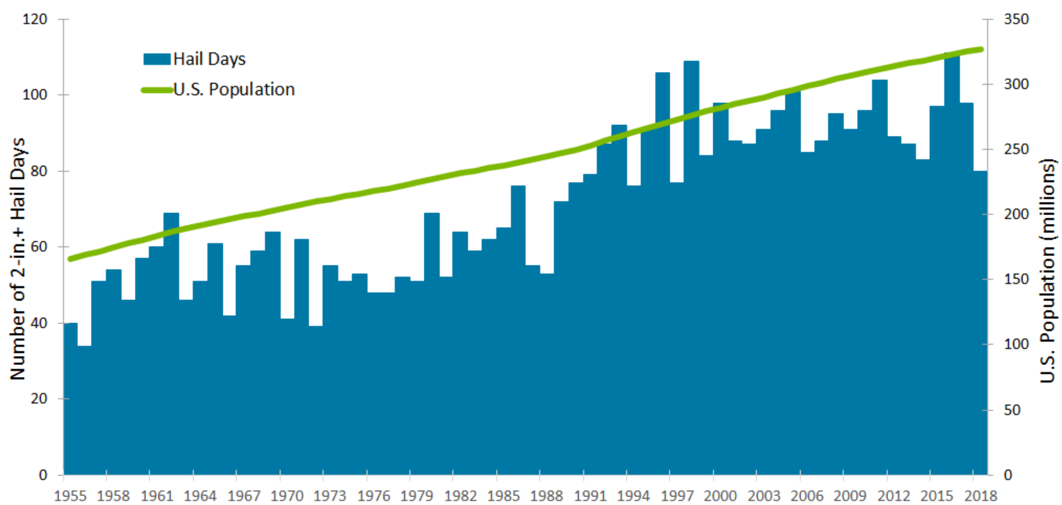

Figure 61. Number of 2-inch or greater hail days (blue bars) and population (green line) across the contiguous U.S. from 1955 to 2018 based on SPC's Storm Reports database

On a regional level, Verisk researchers have found hail frequency trends unrelated to population biases, which is consistent with other studies (e.g., Tang et al. 2019). For example, Verisk researchers compared the mean annual number of 1-inch or greater hail days in 1990 to the mean annual number of hail days in 2018, by state, (Figure 62 and Figure 63, respectively), which were calculated using a best-fit curve through the 1990-2018 time series of SPC reports in each state. Hail days were once again used instead of hail reports to reduce population biases in the observed data. The numbers in red in Figure 63 represent statistically-significant changes from 1990 to 2018, as determined by a two-sided t-test with a confidence of 95%. As seen in Figure 62 and Figure 63, relative changes are largest in states along the west and east coasts; some of these changes are primarily a result of the low overall numbers in these states. Four southern states (Texas, Oklahoma, Louisiana, and Florida) show a decrease in hail days from 1990 to 2018 but, apart from Louisiana, these changes are statistically insignificant. Due to the relatively short observational record, it is difficult to draw any conclusions in longer-term regional severe hailstorm trends based on these results alone.

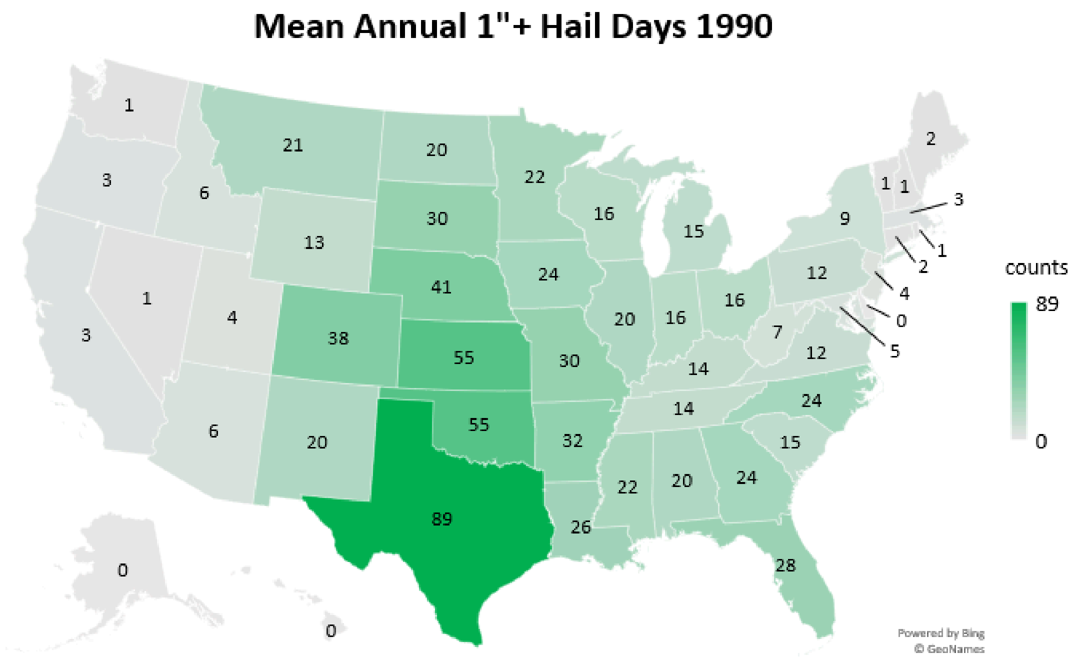

Figure 62. Mean annual number of 1-inch or greater hail days in 1990 based on values along a best-fit line through the 1990-2018 times series of SPC reports in each state.

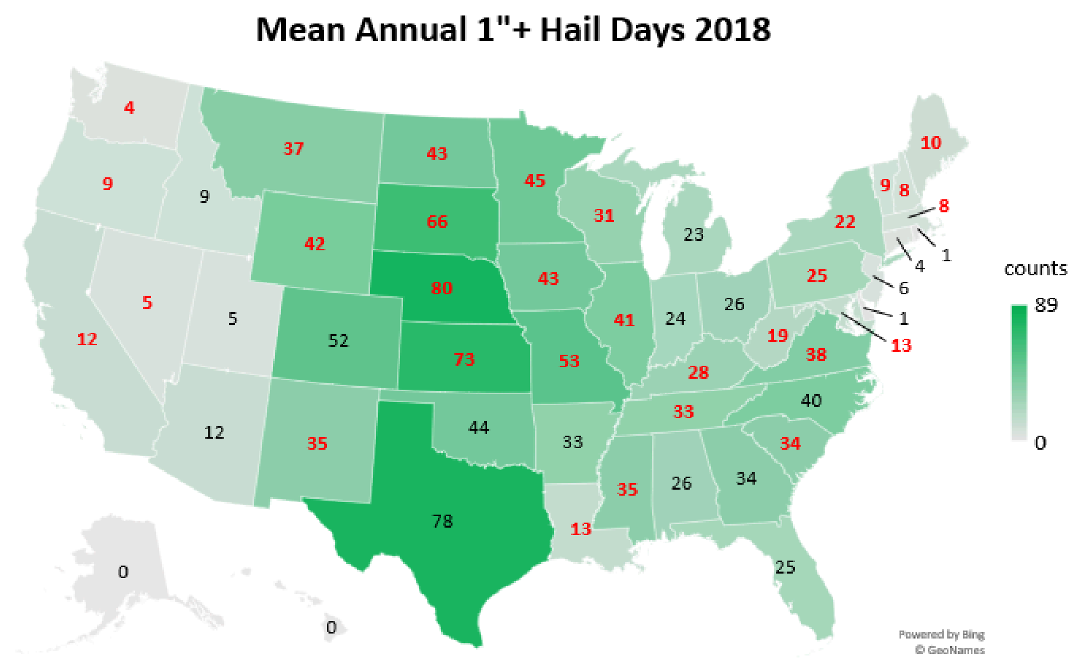

Figure 63. Mean annual number of 1-inch or greater hail days in 2018 based on values along a best-fit line through the 1990-2018 times series of SPC reports in each state. The red numbers represent statistically-significant changes from 1990 to 2018, as determined by a two-sided t-test with a confidence of 95%.

Many studies have attempted to circumvent the relatively short stable hail report record by analyzing environmental conditions favorable for hail development over longer historical periods. For instance, Allen et al. (2015a) evaluated various environmental parameters within the NARR dataset to develop a four-parameter model that correlates best with observed hail activity from 1979 to 2012. These four parameters include: convective precipitation, CAPE, storm relative helicity, and 0-1 km specific humidity. In comparing the model-simulated mean monthly values across the continental U.S. to observed interannual activity, they found that while the model captured the year-to-year changes in sign, it did not reveal an increasing frequency trend over the entire period like seen in the observations. Allen et al. (2015a) hypothesized this lack of a nationwide trend may be a result of the NARR data not capturing the individual component trends of the environmental factors used in the model, and/or not capturing regional behavior well, as evidenced by the model underestimating warm season events in the eastern U.S. in their study.

Tang et al. (2019) examined environmental conditions conducive for hail activity using a combination of NARR data, SPC reports, and radar data and found significant increasing trends in large hail (≥2 in.) parameter (LHP) days[73] in the eastern two-thirds of the U.S. since 1979. These LHP days were identified in the NARR by evaluating environmental conditions that correlate strongly with large hail production. Specifically, they found LHP-day and SHiP-day time series strongly correlate with large hail reports and radar-derived maximum

[73] The LHP is defined similarly to SHiP, as a nonlinear combination of six variables: MUCAPE, hail growth zone (−10 °C to −30 °C) thickness, the 700–500 hPa lapse rate, bulk wind difference between the surface and parcel equilibrium level, wind direction difference between the equilibrium level and the 3–6 km layer, and the storm-relative wind difference between the 3–6 km and the 0–1 km layers.

estimated size of hail (MESH) signatures in the Midwest and in the Northeast, and good correlations are also seen in portions of the Southeast. As seen in Figure 64 and Figure 65, significant correlations between NARR parameters and SPC reports are evident everywhere except for the Rocky Mountain Region, where slight decreasing trends in LHP days and SHiP days are noted. Of particular interest are the statistically-significant correlations between the Midwest and Northeast annual large hail environmental areas and the radar-derived MESH areas, as well as weak (i.e., not statistically significant) correlations in other regions. While radar-indicated hail is still another proxy for severe thunderstorm development, it is more closely related to the occurrence of actual severe hail than other environmental proxies. However, due to the limited radar dataset available (1995-2016), it is difficult to draw any conclusions in longer-term severe hailstorm trends based on these MESH signatures alone.

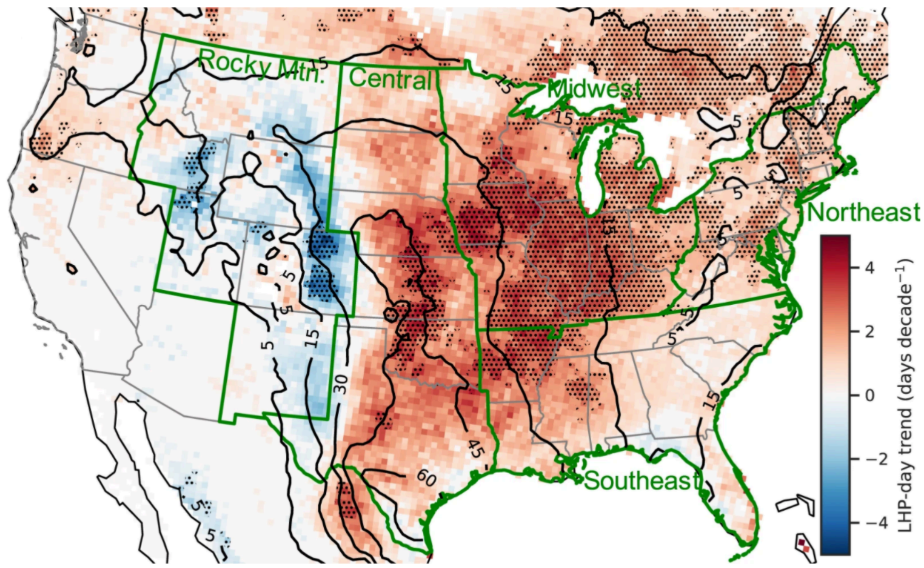

Figure 64. 1979-2017 LHP days trend (shaded) and annual mean number of LHP days (contoured) using NARR data.
The 95% confidence level statistically-significant trends are indicated by the green dotted regions. The green outlines define the regions used in the study (Adapted from: Tang et al., 2019; CC BY-SA 4.0).

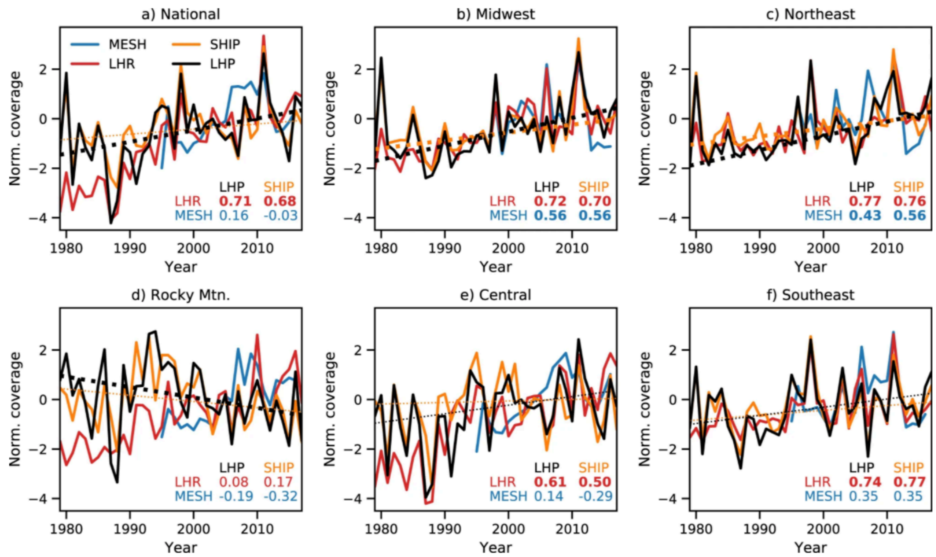

Figure 65. National (a) and regional (b-f) normalized annual trends in 1979-2017 LHP-day area (solid black line), SHiP-day area (solid orange line), large hail report-day area (LHR-day area; solid red line), maximum radar-estimated size of hail-day area (MESH-day area; limited to 1995-2016; solid blue line), and annual mean number of LHP days (contoured). Annual LHP-day area and annual SHiP-day area linear trends are represented by the black and orange dotted lines, respectively. Bold/thick dotted lines indicate these trends are statistically significant. The linear correlation values are presented in the lower right portion of each graph, with the 95% confidence level statistically-significant correlation trends emphasized using bold text (Source: Tang et al., 2019; CC BY-SA 4.0).

Historical Trends in Straight-Line Wind Activity

Similar to hail, convective straight-line wind reports are skewed by population biases. Some of these biases can be removed by analyzing wind days instead of individual wind reports. In addition, although damaging winds can be identified by Doppler weather radar, the U.S. nationwide archived data from these radars are only available for a relatively short historical time period. This time period is too short to be able to identify with certainty if and to what extent climate change plays a role in any temporal trends in straight-line wind frequency and/or intensity seen in the observed data. In addition, widespread severe straight-line wind events are rare. As a result, there are far fewer published studies about potential climate change impacts on convective straight-line wind temporal and spatial trends than on potential hail climate-related changes (Gensini et al., 2020).

Verisk researchers analyzed a subset of extreme straight-line wind events produced by severe thunderstorms in the U.S. that were officially classified as derechos (i.e., straight-line winds that produce over a 240-mi damage swath with wind gusts of at least 58 mph (50 kts) along most of its length) in SPC's Storm Reports database from 1990 to 2019. As evident in Figure 66, results show that U.S. nationwide derecho frequency has increased over the last three decades. However, the criteria for classifying a derecho is heavily dependent on the number and density of severe straight-line wind reports. Any non-meteorological changes in reporting will likely impact derecho identification, so it is not clear if this trend has a meteorological cause.

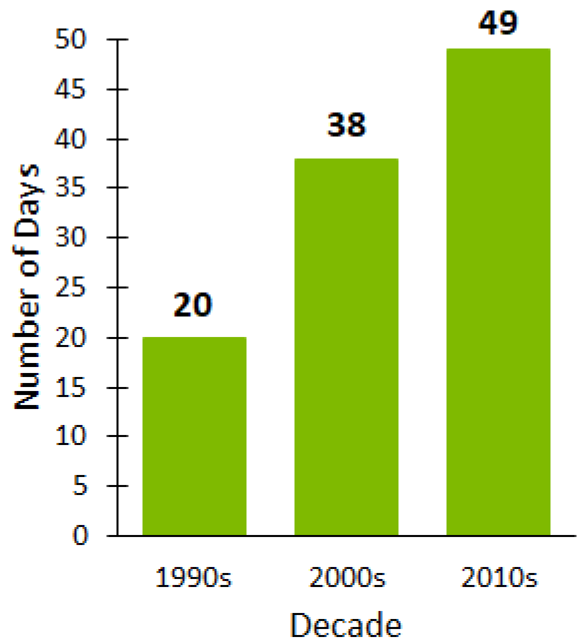

Figure 66. Number of days per decade in which a derecho occurred in the U.S. based on SPC's Storm Reports database

In addition, Verisk researchers analyzed a time series of annual 58-mph (50-kt) or greater convective straight-line wind gust days in the U.S. (i.e., number of days when at least one straight-line wind gust report of 58 mph or greater was reported in the U.S.) based on SPC's Storm Reports database along with U.S. population from 1979 to 2018 (Figure 67). Wind gust days were once again used instead of individual wind reports to reduce population biases in the observed data. Results show that annual severe straight-line wind days have been fairly stable despite the increase in U.S. population during this 40-year time period. These results suggest that 1) by using wind days instead of individual wind reports, population biases in the data have been greatly reduced, and 2) no statistically-significant trends in severe straight-line wind frequency have occurred on a countrywide level between 1979 and 2018.

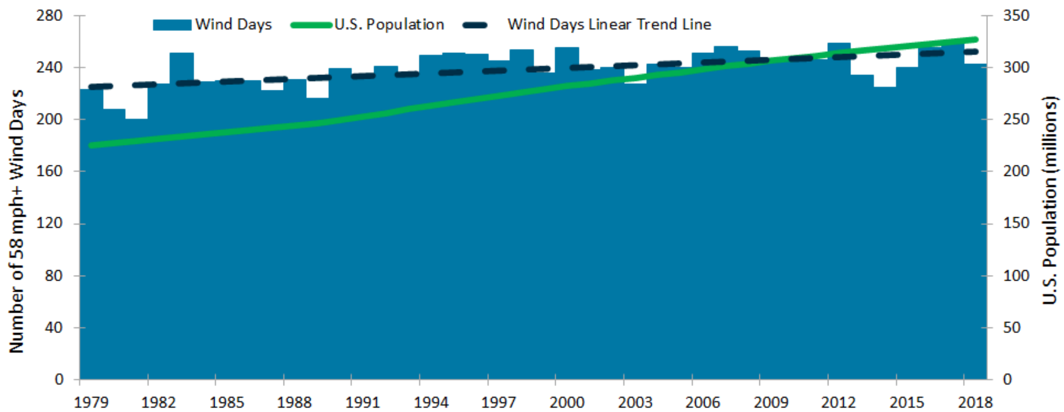

Figure 67. Number of 58-mph or greater straight-line wind gust days across the contiguous U.S. based on SPC's Storm Reports database (blue bars), linear best fit straight-line wind trend line (dark blue dashed line), and U.S. population (green line) from 1979 to 2018.

Next, Verisk researchers used a slightly higher wind threshold to analyze the mean annual number of 63-mph (55-kt) or greater convective straight-line wind gust days in 1990 and in 2018, by state (Figure 68 and Figure 69, respectively), which were calculated using a best-fit curve through the 1990-2018 time series of SPC reports in each state. Comparing the two figures, notable statistically-significant increases are seen, especially across New Mexico, Oklahoma, Minnesota, Wisconsin, Illinois, and much of the Southeast U.S., where straight-line wind days have increased severalfold. It is difficult to attribute these increases entirely to population increases, although some states (e.g., Mississippi and Georgia) exhibit a more significant population bias beginning in the early 2000's (not shown). However, it is equally difficult to quantify the extent to which climate change has impacted severe straight-line wind activity in this area (Gensini et al, 2020).

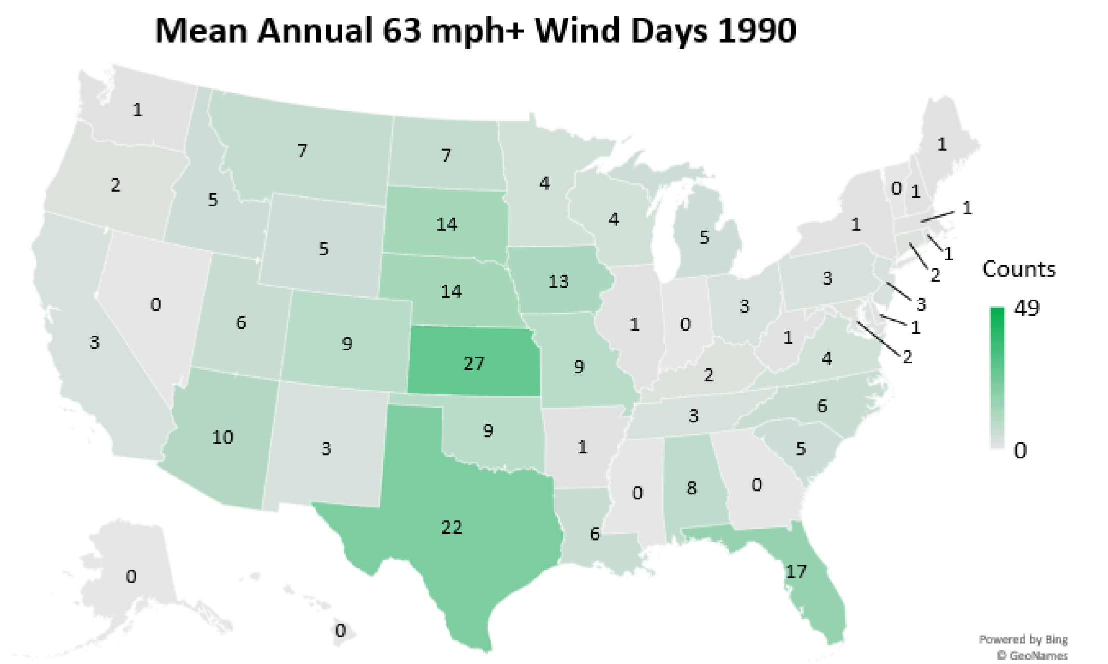

Figure 68. Mean annual number of 63-mph or greater straight-line wind days in 1990 based on values along a best-fit line through the 1990-2018 times series of SPC reports in each state.

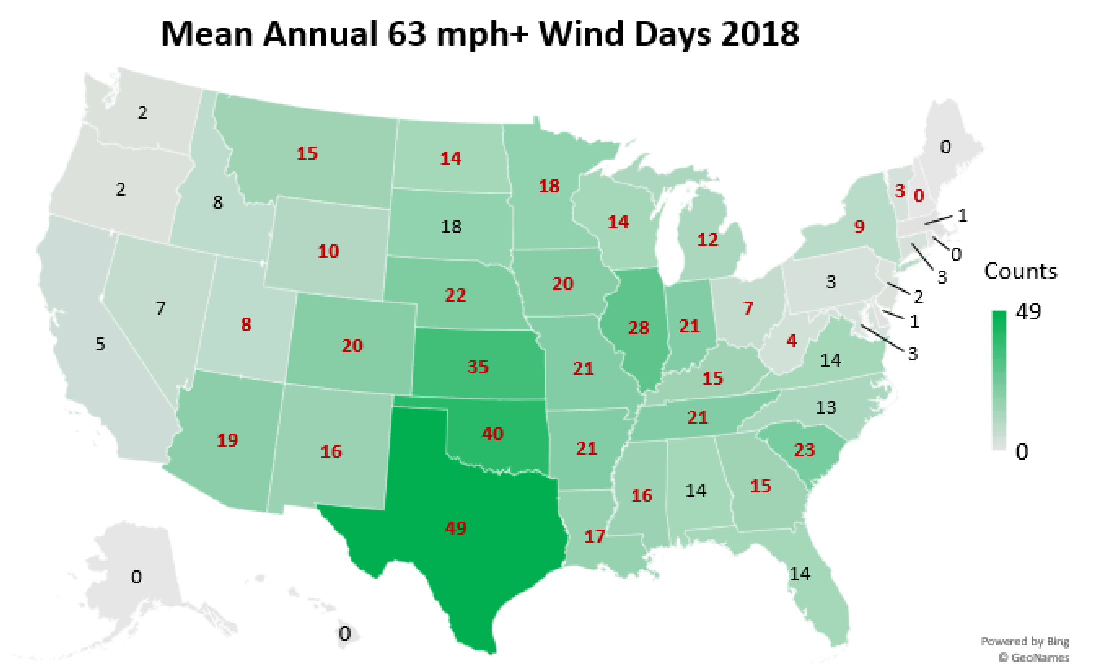

Figure 69. Mean annual number of 63-mph or greater straight-line wind days in 2018 based on values along a best-fit line through the 1990-2018 times series of SPC reports in each state.
The red numbers represent statistically-significant changes from 1990 to 2018, as determined by a two-sided t-test with a confidence of 95%.

Summary of Historical Trends

While Verisk researchers and various other studies have found no nationwide statistically-significant temporal trends in severe thunderstorm frequency attributable to climate change in the U.S. overall, they have identified statistically-significant regional trends in the occurrence frequency of both severe thunderstorms and the environmental conditions favorable for severe thunderstorm development. Both occurrence frequencies have increased across much of the eastern half to two-thirds of the U.S. and have decreased across much of the western third to one-half of the U.S. The extent and amount of these changes vary by season. Looking forward, various GCMs project the frequency of favorable severe thunderstorm environments will increase by the late 21st century, especially across the eastern half to two-thirds of the U.S. Similar to observed trends, this increase is projected to vary by season.

Despite these noted trends in severe thunderstorm activity and a physically-plausible explanation as to why climate change would increase severe convective weather activity (i.e., a warming climate would add more moisture to the air and enhance instability needed for thunderstorm development), other factors limit our ability to isolate the amount to which these changes can be attributed to anthropogenic climate change alone. These factors include a limited historical dataset affected by population and reporting biases, inherent uncertainties associated with the numerical modeling component of GCMs, and the amount of influence other recurring climate patterns (e.g., ENSO) have on severe thunderstorm development. As a result, researchers express modest confidence that the noted severe thunderstorm activity changes can be attributed to anthropogenic climate change.

Verisk's overall assessment is that climate change may be impacting U.S. severe thunderstorm activity and more attention should be given to the recent climatology (e.g., last 20 years) than to the climatology of the distant past (e.g., prior to 1998). Observed data from the last century should not be completely ignored but, rather, these data should be used to define aspects of interannual variability rather than conveying absolute numbers for frequency and intensity. Verisk's assessment is supported by existing literature, Verisk's own analyses, a physically-plausible explanation for changes in some aspects of severe convective weather, changes observed in SPC's Storm Reports database, and historical resimulations from many GCMs.

7.3 Accounting for Current Climate in the Model and Catalog Development

The Verisk Severe Thunderstorm Model for the United States' stochastic catalog is built based on detailed information from NOAA's SPC and NCEI storm reports, NCEP's CFSR, and NOAA's Next Generation Radar (NEXRAD) Level III radar data. Verisk's stochastic catalog was last updated in 2020 to leverage 8 years of additional data along with new datasets available since the catalog was previously updated. Particular focus was given to more closely match hailstone frequency and intensity climatology by incorporating additional historical data and geographically-varying hailstorm event generation methodologies.

Verisk researchers correct for reporting biases in the SPC data by employing a combination of statistical and physical methods (e.g., additional observational datasets, atmospheric severe weather indices, smart smoothing, population growth detrending, and generalized additive models). Stability is an important aspect of any catastrophe model, as well as its ability to reflect the current climate. Thus, Verisk researchers focus on implementing a robust stochastic catalog that reflects both the 1979-2018 mean and the longer-term variability about the mean, adjusted to account for climate-based trends so it represents the current climate, as discussed below. The stochastic catalog includes severe thunderstorm-modeled event frequency, starting location, storm track direction, storm length and width, and intensity information specific to the sub-peril (i.e., hail, straight-line wind).

One of the most important data sources for developing the model is the local storm reports database maintained by the SPC. These reports represent point observations of severe weather by trained storm spotters, emergency management, and the general public. While this dataset contains valuable information about severe thunderstorm events, there are also several types of reporting biases in these data. Since this dataset is composed of observed reports, these reports tend to be clustered around population centers and major roads. There is also a general noticeable increase in the number of reports with time. Potentially contributing non-meteorological factors to this increase include population growth (more possible observers), metropolitan expansion into previous rural areas, greater interest in severe weather, storm chasing, and expansion of cell phone networks and social media, making reporting easier. Climate variability and change may also be contributing factors. Since these potential signals contributing to the trend are inseparable from each other, Verisk researchers take an agnostic approach to detrend the historical storm reports data. This approach corrects any under-reporting in early years of the record and accounts for climate-related impacts to create a near-present view of the hazard.

The first step in detrending SPC data is to correct for over-reporting. For example, two reports separated by only a few miles and minutes are likely to be separate observations of the same storm. Hail and windstorm reports are spatially-clustered on a daily time scale to create a set of reported storms from the storm reports. After the over-reporting is accounted for by clustering, the second step corrects the upward trend in annual reported severe days. A severe day is a day that results in one or more severe storm reports. This upward trend in severe days appears to level off around 1998. The earlier years likely had severe weather on more days than were reported. A piecewise model is fit to the observed data that assumes a positive linear trend in early years and no trend in more recent years. Then, this model is used to make the mean severe day frequency consistent with recent years. Even after accounting for the upward trend in severe days, there is still a positive trend in the annual count of severe storm reports. The annual counts are detrended in the same manner as the annual severe days, using the mean of years 2010 and later as the baseline. The mean frequency of the model is based on the most recent years, removing any non-meteorological trends and accounting for the current climate. This process is performed for the hail and wind sub-perils.

The Verisk model employs a daily simulation method where stochastic days are based on historical days. Each stochastic day has a similar number and location of storms as the respective historical day. The annual detrending factors developed for the SPC reports are used to inflate the historical number of microevents (storms) to produce a modeled frequency that has a consistent frequency, no matter the historical year used as the basis for simulation.

Simulated microevents have unique attributes describing their footprints: length, width, and intensity. In creating the stochastic catalog, each microevent's attributes are randomly drawn from probability distributions. The wind distributions are created from storm reports, and hail distributions are from a blend of storm reports and radar-based storm footprints. Due to the growth in storm reports over time, distributions are implicitly weighted toward more recent years. Additionally, the radar data used is from 1996 and later, so the same implicit weighting is present there as well. While there is no clear signal in storm attributes over time, any potential changes would be mostly accounted for by using more recent data.

See Also

Data Sources for Event Generation

8 US Crop Hail Model in Touchstone-Re

8.1 Available Catalogs in Touchstone Re

Touchstone Re supports the all-events 10,000-year stochastic hazard catalog used by the Verisk Crop Hail Model for the United States (also used by the Verisk Severe Thunderstorm Model for the United States), which contains more than 2.2 million simulated macroevents consisting of more than 77 million simulated hail microevents and more than 47 million simulated straight-line wind microevents.[74] The peril-specific microevents leveraged by the Verisk Crop Hail Model for the United States are specific to the model domain.[75]

For the Verisk Crop Hail Model for the United States, events are aggregated by year to yield a single annual event.

Note that a historical event set is not included for the Verisk Crop Hail Model for the United States in the current version of Touchstone Re.

See Also

Stochastic Hazard Catalog
Data Sources for Event Generation

8.2 Resolution of Analysis Results

Touchstone Re industry loss files are developed using an 8-km exposure grid. Users can generate losses using sums insured, premiums, or user-specified market shares for all modeled lines of business. Number of risks is not supported as an exposure type in the model; however, company-specific premium rates may be entered. Losses are aggregated to the county and state levels in Touchstone Re.

8.3 Verisk Industry Exposure Database

The Industry Exposure Database for the Verisk Crop Hail Model for the United States consists of estimates of the total insurable value of the covered crops (sums insured) and premium

74 Events are categorized as *microevents* or *macroevents*. A microevent is a single simulated convective straight-line wind or hail event. A macroevent represents a large-scale atmospheric system that causes outbreaks of severe weather. The Verisk Crop Hail Model for the United States uses the hail and straight-line wind *microevents* from the 10-K all-events catalog.

75 The wind module processes the straight-line wind hazard data for the following states only: Arkansas, Iowa, Illinois, Indiana, Kansas, Kentucky, Louisiana, Minnesota, Missouri, North Dakota, Nebraska, South Dakota.

rates at the state and county levels by modeled line of business (crop hail and production plan) and include planted acreages averaged over 2017-2020. Only insurable exposures are included in the Industry Exposure Database. Verisk does not provide take-up rate assumptions for the Verisk Crop Hail Model for the United States in Touchstone Re.

The crop exposure database was developed using the National Agricultural Statistics Service's (NASS) Cropland Data Layer 30-meter land use/land cover dataset. Because of annual variations (e.g., due to crop rotations), Verisk researchers calculated grid-specific crop areas by averaging NASS crop data layers from 2017 to 2020.

First, the land use/land cover data for each crop (barley, corn, cotton, rice and soybeans, and durum, spring and winter wheat) was aggregated to an 8-km grid by 30-meter centroid. Next, the grid was mapped to the county level (assuming a uniform distribution of crops in each grid cell) to make the planted crop area and the loss allocation area spatially consistent. Finally, the Industry Exposure Database was checked to ensure that the exposure database was consistent with NASS survey data.

See Also

Data Sources for the Verisk Crop Hail Model for the United States
Model Resolution
Industry Exposure Database

Verisk Insurable Crop Industry Exposure Database Maps

The following maps show the Verisk Industry Exposure Database for crops at the county level.

See Also

2019 Crop Exposure to Hail in the United States

Industry Exposure Database Barley Exposure (Acres Per County), 2017-2020 average

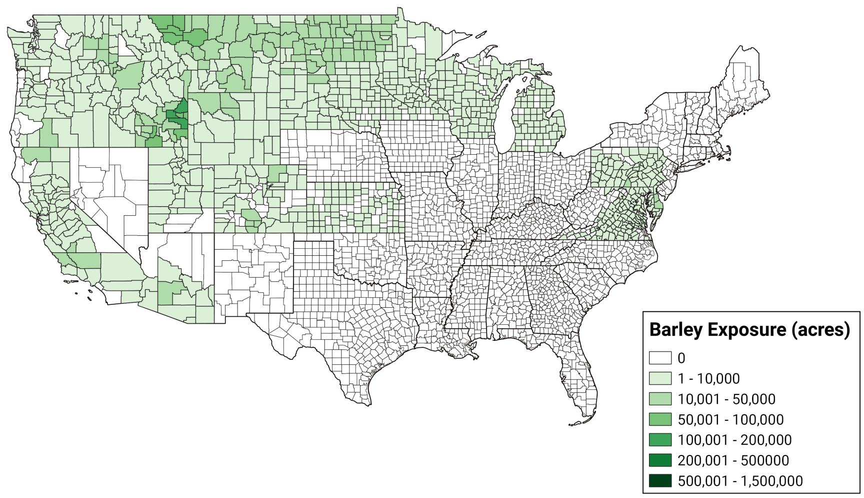

Figure 70. Barley Exposure

Industry Exposure Database Corn Exposure (Acres Per County), 2017-2020 average

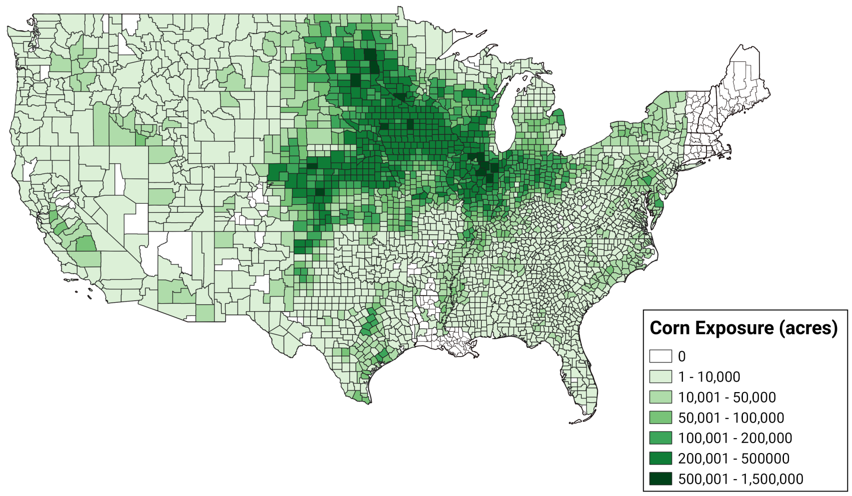

Figure 71. Corn Exposure

Industry Exposure Database Cotton Exposure (Acres Per County), 2017-2020 average

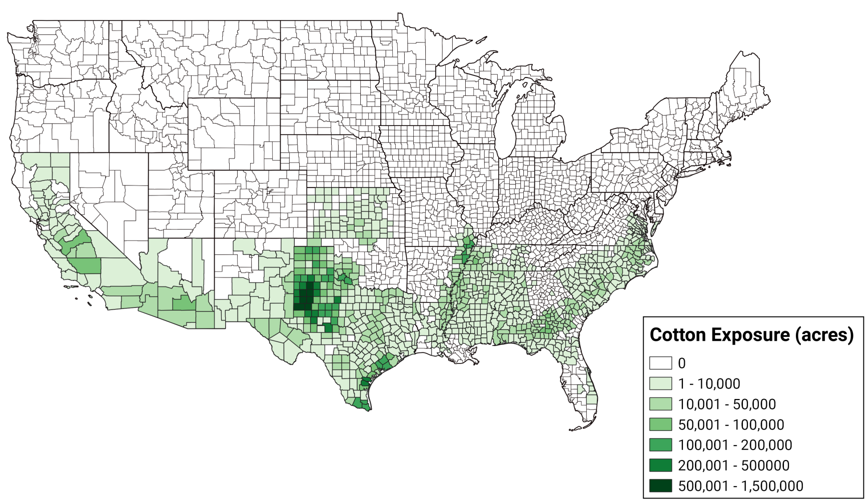

Figure 72. Cotton Exposure

Industry Exposure Database Durum Wheat Exposures (Acres Per County), 2017-2020 average

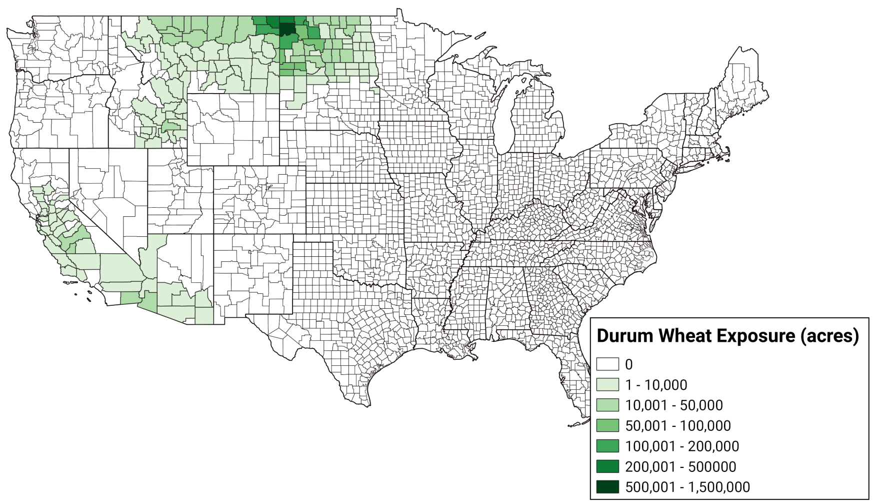

Figure 73. Durum wheat exposures (acres per county)

Industry Exposure Database Spring Wheat Exposures (Acres Per County), 2017-2020 average

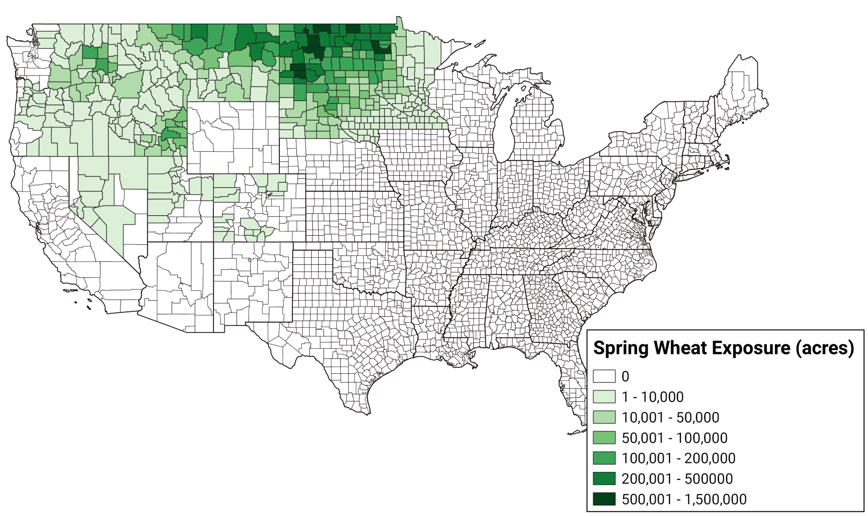

Figure 74. Spring wheat exposures (acres per county)

Industry Exposure Database Winter Wheat Exposures (Acres Per County), 2017-2020 average

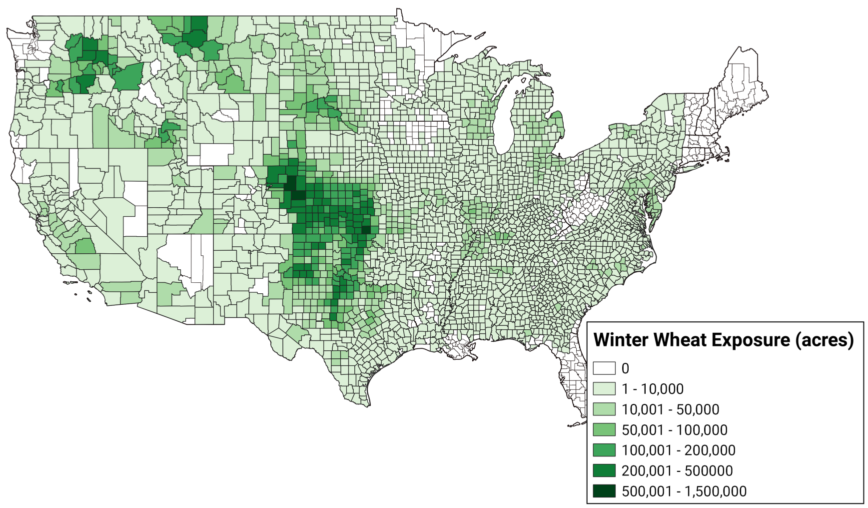

Figure 75. Winter wheat exposures (acres per county)

Industry Exposure Database Rice Exposures (Acres Per County), 2017-2020 average

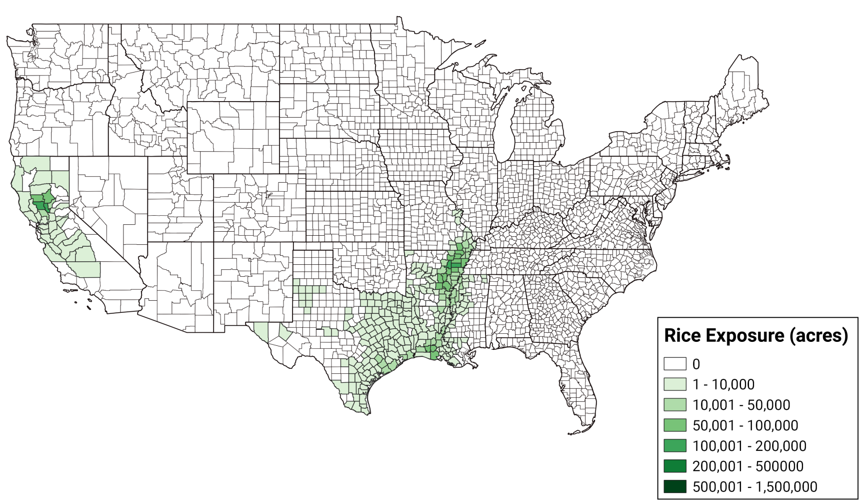

Figure 76. Rice exposures (acres per county)

Industry Exposure Database Soybeans Exposures (Acres Per County), 2017-2020 average

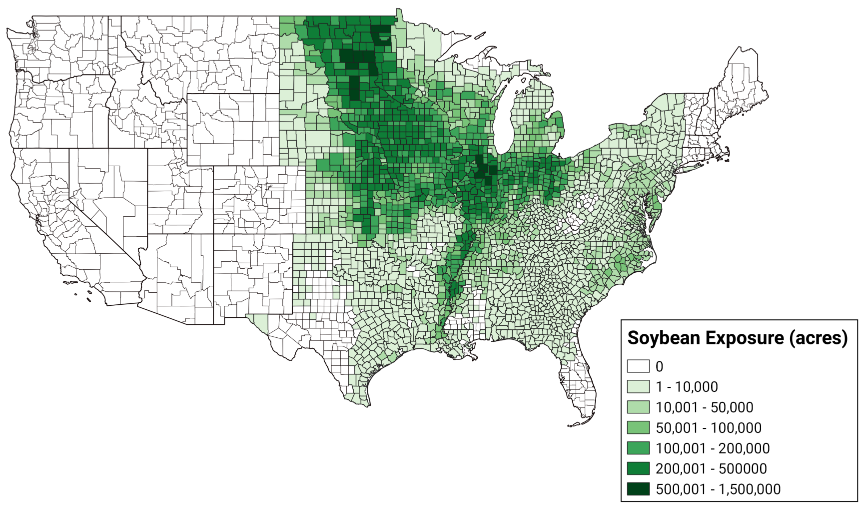

Figure 77. Soybeans exposures (acres per county)

Insurable Value of Crop Exposure

In the model's financial module, which translates the simulated crop hail damage to losses, crop hail policy information was updated with 2020 state-specific policy distributions and the 2021 harvest prices were used to estimate production plan losses.

The total insurable value of the modeled crops in the Industry Exposure Database (insurable sums insured) is shown in Table 7 at the state level for the Crop Hail line of business.

Table 8 shows the total insurable value of the modeled crops in the Industry Exposure Database (IED) (insurable sums insured) at the state level for the production plan line of business.

Table 7. Total insurable value (USD millions) of crop exposures in the Industry Exposure Database by state for the crop hail line of business

State	Barley	Corn	Cotton	Durum Wheat	Rice	Soybean	Spring Wheat	Winter Wheat
Alabama	-	59.6	115.4	-	-	63.1	-	22.3
Arizona	5.7	30.4	67.4	15.7	-	-	-	4.1
Arkansas	-	215.4	212.2	-	435.2	667.4	-	22.0
California	8.3	149.7	194.1	21.4	182.8	-	-	59.9
Colorado	10.7	260.9	-	-	-	-	2.5	164.4

State	Barley	Corn	Cotton	Durum Wheat	Rice	Soybean	Spring Wheat	Winter Wheat
Delaware	3.4	35.6	-	-	-	24.1	-	10.3
Florida	-	26.7	25.4	-	-	3.4	-	2.1
Georgia	-	107.4	340.9	-	-	29.1	-	19.6
Idaho	70.5	144.7	-	7.6	-	-	102.8	129.7
Illinois	-	2304.8	-	-	-	1703.5	-	90.1
Indiana	-	937.6	-	-	-	799.7	-	62.6
Iowa	-	2750.6	-	-	-	1481.9	-	2.9
Kansas	2.2	962.8	55.1	-	-	510.6	-	645.7
Kentucky	-	283.1	-	-	-	286.2	-	78.1
Louisiana	-	139.2	76.5	-	137.2	243.9	-	3.6
Maryland	6.3	99.4	-	-	-	71.2	-	59.8
Michigan	2.2	476.2	-	-	-	306.6	-	74.9
Minnesota	12.4	1810.0	-	-	-	1043.0	229.6	2.5
Mississippi	-	147.5	218.0	-	51.0	418.4	-	8.2
Missouri	-	664.6	132.9	-	67.6	910.7	-	63.8
Montana	58.9	27.7	-	57.7	-	-	177.1	117.9
Nebraska	-	2207.3	-	-	-	947.3	-	85.6
Nevada	-	3.8	-	-	-	-	5.3	3.5
New Jersey	-	16.2	-	-	-	15.5	-	3.3
New Mexico	-	48.9	27.1	-	-	-	-	17.6
New York	-	266.7	-	-	-	52.8	-	14.2
North Carolina	-	162.3	119.6	-	-	215.1	-	38.0
North Dakota	59.8	510.0	-	95.5	-	726.3	589.3	12.8
Ohio	-	641.3	-	-	-	702.9	-	75.1
Oklahoma	-	70.3	134.1	-	-	68.7	-	242.1
Oregon	4.4	36.9	-	-	-	-	15.4	108.7
Pennsylvania	7.1	287.6	-	-	-	105.8	-	30.5
South Carolina	-	66.3	69.4	-	-	45.7	-	10.0
South Dakota	5.4	1026.9	-	0.7	-	679.4	123.2	100.6
Tennessee	-	183.2	120.3	-	-	258.1	-	50.5
Texas	-	484.4	1597.2	-	55.1	24.1	-	273.4
Utah	3.3	28.7	-	-	-	-	1.8	12.6
Virginia	6.5	95.3	27.2	-	-	79.9	-	27.4

State	Barley	Corn	Cotton	Durum Wheat	Rice	Soybean	Spring Wheat	Winter Wheat
Washington	10.4	79.2	-	-	-	-	74.3	267.3
West Virginia	-	12.3	-	-	-	6.0	-	0.8
Wisconsin	4.0	808.7	-	-	-	272.6	-	26.7
Wyoming	10.2	20.2	-	-	-	-	-	5.6

Table 8. Total insurable value (USD millions) of crop exposures in the IED by state for the Production Plan line of business

State	Barley	Corn	Cotton	Durum Wheat	Rice	Soybean	Spring Wheat	Winter Wheat
Colorado	10.7	260.9	-	-	-	-	2.5	164.4
Idaho	70.5	-	-	7.6	-	-	102.8	129.7
Illinois	-	2304.8	-	-	-	1703.5	-	-
Indiana	-	937.6	-	-	-	799.7	-	-
Iowa	-	2750.6	-	-	-	1481.9	-	-
Kansas	-	962.8	-	-	-	510.6	-	645.7
Minnesota	-	1810.0	-	-	-	1043.0	229.6	2.5
Missouri	-	664.6	-	-	-	910.7	-	-
Nebraska	-	2207.3	-	-	-	947.3	-	85.6
North Dakota	-	510.0	-	95.5	-	726.3	589.3	12.8
Ohio	-	641.3	-	-	-	702.9	-	-
South Dakota	-	1026.9	-	0.7	-	679.4	123.2	100.6
Texas	-	484.4	1597.2	-	-	-	-	273.4
Wisconsin	-	808.7	-	-	-	272.6	-	26.7

8.4 Policy Condition Assumptions

Several policy conditions are implemented in Touchstone Re for crop hail and production plan lines of business based on the crop hail insurance industry 2020 data from NCIS.

Crop hail policy conditions are based on various deductibles and limits of coverage. This can range from a simple 5% deductible, where all crop damage losses over 5% are paid out, to more complicated policies that pay out differently depending on the severity of reported crop damage.

Production plan policies incorporate a minimum loss that must occur if the policy is to pay out on a claim. These policies also take into account the MPCI coverage level and a modifier factor that is applied to the MPCI approved yield (APH Modifier). The APH modifier allows a farmer to purchase additional protection beyond the yield guaranteed under an MPCI policy.

See Also

Modeled Industry Losses
Crop Hail Loss Calculation
Production Plan Loss Calculation

Policy Condition Distributions

Table 9 and Table 10 show the policy condition distributions applied by state for crop hail and production plan lines of business, based on 2020 NCIS crop insurance data.

Table 9. Policy conditions applied for crop hail policies by state based on the industry average proportion of liability written to each policy form

State	Policy Form	Liability (%)
Alabama	BASIC	100
Arkansas	BASIC	82
	XS10	5
	DXS5	5
	DXS10	4
	OTHER	4
Arizona	DXS10	85
	BASIC	13
	OTHER	2
California	BASIC	84
	XS10	16
Colorado	DXS10	23
	BASIC	21
	CP2	14
	DXS50	10
	DDA	9
	DXS20	8
	DDB	5
	XS20IP	4
	DDC	2
	OTHER	3
Delaware	BASIC	100
Florida	BASIC	83
	XS15	15

State	Policy Form	Liability (%)
	OTHER	2
Georgia	BASIC	99
	OTHER	1
Iowa	BASIC	40
	CP2+	16
	DXS5	16
	DXS10	12
	DDA	4
	DDC	3
	XS5	3
	DXS20	2
	OTHER	4
Idaho	BASIC	81
	XS10IP	9
	CP2	4
	DXS5	3
	OTHER	3
Illinois	BASIC	74
	DXS5	10
	XS5	9
	DXS10	4
	OTHER	3
Indiana	BASIC	82
	DXS5	7
	XS5	5
	XS10	4
	OTHER	3
Kansas	BASIC	56
	DXS10	20
	CP2+	10
	XS5	4
	DXS5	4
	DDB	2
	OTHER	5
Kentucky	BASIC	42

State	Policy Form	Liability (%)
	XS5	16
	DXS5	15
	XS5IP	13
	DXS10	7
	XS10IP	6
	OTHER	2
Louisiana	BASIC	100
	OTHER	0
Maryland	BASIC	100
	OTHER	0
Michigan	BASIC	94
	DXS5	4
	OTHER	2
Minnesota	CP2+	35
	BASIC	25
	DDA	17
	DXS5	7
	DDC	4
	DXS10	3
	XS5	2
	DDB	2
	XS20IP	2
	OTHER	4
Missouri	BASIC	66
	DXS10	16
	DXS5	10
	XS5	5
	OTHER	3
Mississippi	BASIC	98
	OTHER	2
Montana	DDA	41
	BASIC	30
	CPIP2F	12
	DXS20	10
	DDB	2

State	Policy Form	Liability (%)
	OTHER	5
North Carolina	BASIC	64
	XS5	16
	XS10	15
	OTHER	5
North Dakota	CPIP210	39
	DDA	19
	BASIC	15
	DDB	8
	DDC	7
	DXS30	6
	XS20IP	3
	OTHER	5
Nebraska	CPIP2F	45
	BASIC	18
	DDA	10
	DXS10	8
	DXS5	6
	DDB	5
	XS5	3
	XS20IP	3
	OTHER	3
New Jersey	BASIC	100
New Mexico	XS20IP	35
	XS20	18
	XS10	16
	XS10IP	16
	BASIC	13
	OTHER	2
Nevada	BASIC	100
New York	BASIC	97
	OTHER	3
Ohio	BASIC	97
	OTHER	3
Oklahoma	BASIC	55

State	Policy Form	Liability (%)
	DXS10	13
	XS20IP	8
	CP2+	8
	DDB	5
	XS5	5
	XS20	4
	OTHER	2
Oregon	BASIC	89
	DXS5	7
	OTHER	4
Pennsylvania	BASIC	95
	OTHER	5
South Carolina	BASIC	53
	XS15	40
	XS10	6
	OTHER	0
South Dakota	BASIC	31
	CPIP2F	21
	DDA	16
	DDB	11
	DXS20	8
	DDC	7
	DXS30	1
	OTHER	5
Tennessee	BASIC	49
	XS5	13
	DXS5	13
	XS10IP	12
	XS5IP	10
	OTHER	3
Texas	DXS20	42
	XS20IP	26
	XS10IP	23
	DXS10	3
	BASIC	2

State	Policy Form	Liability (%)
	DDB	2
	OTHER	3
Utah	BASIC	56
	XS10IP	29
	XS15	15
Virginia	BASIC	72
	XS10	20
	XS5	7
	OTHER	0
Washington	BASIC	92
	XS10	5
	OTHER	3
Wisconsin	BASIC	90
	CP2+	6
	OTHER	5
West Virginia	BASIC	100
Wyoming	BASIC	52
	DDA	14
	DXS10	13
	DDB	9
	XS20IP	4
	DXS30	2
	CPIP2F	2
	OTHER	4

Table 10. Policy conditions applied for production plan policies by state based on the industry average proportion of liability written for each set of policy conditions

State	APH Modifier (%)	MPCI Coverage Level (%)	Minimum Loss (%)	Liability (%)
Colorado	115	70	0	35
	115	50	10	15
	115	75	0	13
	115	70	5	11
	110	70	0	8
	110	70	10	7

State	APH Modifier (%)	MPCI Coverage Level (%)	Minimum Loss (%)	Liability (%)
	115	80	0	5
	120	75	0	3
	115	70	10	3
Idaho	100	75	5	48
	110	50	5	15
	110	80	10	15
	110	80	5	14
	110	75	5	9
Iowa	120	75	0	43
	120	80	0	24
	120	85	0	22
	120	85	5	12
Illinois	120	75	0	100
Indiana	120	85	0	100
Kansas	120	75	0	37
	120	80	0	17
	115	75	5	15
	115	70	5	8
	120	70	0	8
	110	70	0	7
	115	65	0	4
	120	65	0	4
Minnesota	120	75	0	43
	120	80	0	28
	120	85	0	14
	115	80	5	7
	120	75	5	4
	120	70	0	4
Missouri	120	75	0	64
	120	85	0	36
North Dakota	120	75	0	71
	120	75	10	15
	120	80	0	14
Nebraska	120	75	0	40

State	APH Modifier (%)	MPCI Coverage Level (%)	Minimum Loss (%)	Liability (%)
	120	70	0	20
	120	80	0	20
	115	75	0	9
	120	65	0	6
	115	80	0	5
Ohio	120	75	0	100
South Dakota	120	75	0	83
	120	80	0	17
Texas	110	70	10	47
	110	60	10	20
	110	75	10	17
	110	65	10	16
Wisconsin	120	75	0	50
	120	70	0	25
	120	80	0	24

8.5 Supported Lines of Business for Reporting Modeled Losses

Touchstone Re supports the following lines of business for reporting modeled losses in the Verisk Crop Hail Model for the United States:

- Crop hail for the model domain (42 states in the contiguous U.S., excluding six New England states)

- Production plan for the following states:
  - Colorado
  - Iowa
  - Idaho
  - Illinois
  - Indiana
  - Kansas
  - Minnesota
  - Missouri
  - North Dakota
  - Nebraska
  - Ohio
  - South Dakota
  - Texas
  - Wisconsin

See Also

Supported Lines of Business

Select References

Listed below are select references used in the development of the Verisk Crop Hail Model for the United States, along with references used in the preparation of this document:

Allen, J. T. (2018). Climate Change and Severe Thunderstorms. *Oxford Research Encyclopedia of Climate Science*, 67pp.

Allen, J. T., & Tippett, M. K. (2015). The characteristics of United States hail reports: 1955–2014. *Electronic Journal of Severe Storms Meteorology,* 10(3), 1-31.

Allen, J. T., Tippett, M. K., & Sobel, A. H. (2015a). An empirical model relating U.S. monthly hail occurrence to large-scale meteorological environment. *Journal of Advances in Modeling Earth Systems,* 7(1), 226-243.

Allen, J. T., Tippett, M. K., & Sobel, A. H. (2015b). Influence of the El Niño/Southern Oscillation on tornado and hail frequency in the United States. *Nature Geosciences,* 8, 278-283.

Allen, J. T., Tippett, M. K., Kaheil, Y., Sobel, A. H., Lepore, C., Nong, S., & Muehlbauer, A. (2017). An extreme value model for U.S. hail size. *Monthly Weather Review,* 145, 4501–4519.

Busch, R. H. 1969, "Simulated Hail Damage on Spring Wheat," *Farm Research* 26, 8-9.

Bunkers, M. J., Klimowski, B. A., Zeitler, J. W., Thompson, R. L., & Weisman, M. L. (2000). Predicting Supercell Motion Using a New Hodograph Technique. *Weather and Forecasting,* 15(1), 61–79.

Changnon, S. A., D. Changnon, and S. D. Hilberg 2009, *Hailstorms Across the Nation: An Atlas about Hail and Its Damages*, Illinois State Water Survey, Contract Report 2009-12.

Counce, P. A., B. R. Wells, R. J. Norman, and J. Leong 1994, "Simulated hail damage to rice: II. Effects during four reproductive growth stages," *Agronomy Journal* 86, 1113-1118.

"Crop Production: 2014 Summary." National Agricultural Statistics Service, United States Department of Agriculture, January 2015. Web. 08 February 2016. https://www.census.gov/history/pdf/cropan15.pdf

"Crops by County." National Agricultural Statistics Service, United States Department of Agriculture, 30 March 2016. Web. https://www.nass.usda.gov/Charts_and_Maps/Crops_County/

Diffenbaugh, N. S., Scherer, M., & Trapp, R. J. (2013). Robust increases in severe thunderstorm environments in response to greenhouse forcing. *Proceedings of the National Academy of Sciences of the United States of America*, 110(41), 16361-16366.

Doswell, C. A. III, H. E. Brooks, and M. P. Kay 2005, "Climatological estimates of daily local nontornadic severe thunderstorm probability for the United States," *Weather and Forecasting* 20, 577-595.

Gilbertson K. M. and E. A. Hockett 1979, "The effect of hail damage on barley," *Canadian Journal of Plant Science* 59, 1147-1152.

Gensini, V. A., Haberlie, A. M., & March, P. T. (2020). Spatial trends in United States tornado frequency. *Bulletin of the American Meteorological Society,* 101(8), E1259-E1278.

Hohl, R. M. 2001, *Relationship between hailfall intensity and hail damage on ground, determined by radar and lightning observations*, Doctoral thesis, Institute of Geography, University of Fribourg, Switzerland.

Katz, R. W. and R. R. Garcia 1981, "Statistical relationships between hailfall and damage to wheat," *Agricultural Meteorology* 24, 29-43.

Klein, R. N. and C. A. Shapiro 2011a, *Evaluating Hail Damage to Corn*, University of Nebraska-Lincoln Extension, Report EC-126. Available online: http://www.ianrpubs.unl.edu/live/ec126/build/ec126.pdf

Klein, R. N. and C. A. Shapiro 2011b, *Evaluating Hail Damage to Soybeans*, University of Nebraska-Lincoln Extension, Report EC-128. Available online: http://www.ianrpubs.unl.edu/live/ec128/build/ec128.pdf

Knowles, D. B. 1941, "The effect of hail injury on wheat and other grain crops in Saskatchewan," *Agricultural Research Bulletin* 102, University of Saskatchewan.

Koch, E., Koh, J., Davison, A. C., Lepore, C., & Tippett, M. K. (2021). Trends in the Extremes of Environments Associated with Severe U.S. Thunderstorms. *Journal of Climate,* 34(4), 1259-1272.

Lauer, J. 2013, "Hail Damage on Corn," Available online: http://corn.agronomy.wisc.edu/Management/L039.aspx

Lee, C. 2007, *Estimating Hail Damage in Corn*, University of Kentucky, College of Agriculture Extension Service. Available online: http://www2.ca.uky.edu/agc/pubs/agr/agr194/agr194.pdf

Longer, D. E. and D. M. Oosterhuis 1999, "Cotton regrowth and recovery from early season leaf loss," *Environmental and Experimental Botany* 41, 67-73.

Marshall, J. S. and W. M. Palmer 1948, "The distribution of raindrops with size," *Journal of Meteorology*, 5, 165-166.

Mason, B. 1971, *The Physics of Clouds* (2nd edition). Oxford University Press.

Morgan, G. M. Jr., and N. G. Towery 1976, "On the role of strong winds in damage to crops by hail and its estimation with a simple instrument," *Journal of Applied Meteorology* 15, 891-898.

Nielsen, R. L. 2012, *Recovery From Hail Damage to Young Corn*, Agronomy Department, Purdue University. Available online: http://www.agry.purdue.edu/ext/corn/news/timeless/HailDamageYoungCorn.html

Peacock, H. A. and B. S. Hawkins 1974, "Hail damage to upland cotton," *Agronomy Journal* 66, 100-104.

"Quick Stats." National Agricultural Statistics Service, United States Department of Agriculture, 5 April 2016. Web. https://quickstats.nass.usda.gov/

Sanchez, J. L., R. Fraile, J. L. de la Madrid, M. T. de la Fuente, P. Rodriguez, and A. Castro 1996, "Crop damage: the hail size factor," *Journal of Applied Meteorology* 35, 1535-1541.

Schiesser, H. H. 1990, "Hailfall: the relationship between radar measurements and crop damage," *Atmospheric Research* 25, 559-582.

Smith, C. W. and J. J. Varvil Jr. 1981, "Recoverability of cotton following simulated hail damage," *Agronomy Journal* 73, 597-600.

Staton, M. 2013, *Assessing Hail Damage to Soybeans in the Early Vegetative Stages*, Michigan State University Extension. Available online: http://msue.anr.msu.edu/news/assessing_hail_damage_to_soybeans_in_the_early_vegetative_stages

Stott, P. (2016). How climate change affects extreme weather events. *Science,* 352(6293), 1517-1518.

Tang, B. H., Gensini, V. A., & Homeyer, C. R. (2019). Trends in United States large hail environments and observations. *npj Journal of Climate and Atmospheric Science,* 2(45).

Thelen, M. 2013, *When to Assess Hail Damage to Crops*, Michigan State University Extension. Available online: http://msue.anr.msu.edu/news/when_to_assess_hail_damage_to_crops

Thompson, K. S. (1990). Adaptive Cluster Sampling. *Journal of the American Statistical Association,* 85(412), 1050-1059.

Towery, N. G., G. M. Morgan Jr., S. A. Changnon Jr. 1976, "Examples of the wind factor in crop-hail damage," *Journal of Applied Meteorology* 15, 1116-1120.

Trapp, R. J., Diffenbaugh, N. S., Brooks, H. E., Baldwin, M. E., Robinson, E. D., & Pal, J. S. (2007). Changes in severe thunderstorm environment frequency during the 21st century caused by anthropogenically enhanced global radiative forcing. *Proceedings of the National Academy of Sciences of the United States of America,* 104(50), 19719-19723.

"United States." CIA World Factbook. Central Intelligence Agency, 5 April 2016. Web. https://www.cia.gov/library/publications/resources/the-world-factbook/geos/us.html

Waldvogel A., W. Schmid, and B. Federer 1978, "The kinetic energy of hailfalls. Part I: Hailstone spectra," *Journal of Applied Meteorology* 17, 515-520.

About Verisk

Verisk Analytics (Verisk) provides risk modeling solutions that make individuals, businesses, and society more resilient to extreme events. In 1987, a Verisk subsidiary founded the catastrophe modeling industry and today models the risk from natural catastrophes, terrorism, pandemics, casualty catastrophes, and cyber incidents. Insurance, reinsurance, financial, corporate, and government clients rely on Verisk's advanced science, software, and consulting services for catastrophe risk management, insurance-linked securities, longevity modeling, site-specific engineering analyses, and agricultural risk management. Verisk (Nasdaq:VRSK) is headquartered in Jersey City, New Jersey with many offices throughout the United States and around the world. For information on our office locations, visit https://www.verisk.com/about/locations/.

Contact Information

Verisk Analytics
Lafayette City Center, 2nd Floor
Two Avenue de Lafayette
Boston, MA 02111
USA

Tel: (617) 267-6645
Fax: (617) 267-8284

Verisk welcomes feedback on its documentation. If you need assistance in using the software or understanding the information in this document, please email us at DocumentationFeedback@verisk.com.